A STUDY OF ROLL MOTION AND ROLL DAMPING FOR BIASED SMALL FISHING VESSELS

ZHIGUO WANG

A STUDY OF ROLL MOTION AND ROLL DAMPING FOR BIASED SMALL FISHING VESSELS

BY

©ZHIGUO WANG

A thesis submitted to the School of Graduate Studies in partial fulfillment of the degree of Master of Engineering

Faculty of Engineering and Applied Science
Memorial University of Newfoundland

May 1992

St. John's Newfoundland Canada

ISBN 0-315-78092-4

Abstract

Three sets of experiments with small fishing vessel models in biased condition were conducted at the towing tank of Memorial University of Newfoundland. A simulation of the asymmetric rolling motion of one of the models in beam waves without forward speed was also performed.

The first set of experiments was carried out with three fishing vessel models denoted by M363, M365 and M366 to measure the roll damping. Hundreds of decay curves were obtained from free roll tests for the analysis of biased roll damping coefficient. The *Energy Approach* developed by Haddara [10] was applied in the analysis. The results show that the nondimensional equivalent linear damping coefficient ζ_E increases linearly with average amplitude of roll angle. The effect of bias angle on roll damping varies from model to model. In the case of M366, ζ_E increases linearly with bias angle. The same tendency is seen for M365 when its roll amplitude is larger than ten degrees. However, ζ_E decreases with bias angle when the roll amplitude is lower than ten degrees. In the case of M363, the damping coefficient ζ_E shows a nonlinear relationship with bias angle for low roll amplitude, i.e. ζ_E decreases with bias angle first, then increases. For the large roll amplitude, ζ_E increase with bias angle almost linearly.

The second set of experiments was carried out with M363 in regular beam waves without forward speed. The model was tethered in drift and yaw but all other modes were free. The model was set under two different bias conditions and was tested both biased towards the wave source (wave maker) and away from the wave source. The results indicate that the effect of bias angle is pretty slight.

The last set of experiments was performed also with M363 in beam waves without forward speed but the model was restrained through a pivot in every mode except for roll. The pivot was placed at the model's *roll center* in the first group of tests; for the second group of tests, the pivot was transversely moved to a new position whose transverse coordinate is the model's actual center of gravity and vertical coordinate was unchanged. The results can be summarized as follows.

When the model was biased towards the wave source the roll amplitude was much larger, compared with when the model was biased away from the wave source or under no bias condition.

In the frequency domain, the roll amplitudes show a strong resonant phenomenon when the model is biased towards the wave source or under no bias condition. On the other hand, the curve of roll amplitude with respect to the wave frequency is fairly flat when the model is biased away from the wave source.

The results do not reflect any significant effect of pivot position. This is believed to be due to the very small distance between two pivot positions.

The results from the simulation of the rolling motion of the biased M363 under restrained conditions show reasonable agreement with experimental results, especially for the tendency of roll amplitudes with respect to the wave frequency. It is also indicated by the simulation that not only bias and wave direction but restraints are factors which make the roll amplitude large when the model is biased towards wave source.

Acknowledgements

First of all, I am most grateful to my supervisors, Dr. M. R. Haddara and Dr. D. W. Bass, for all their support, guidance, patience and kindness. Their help will be kept in my mind for all my life.

I would like to thank also Dr. D. Muggeridge for the use of the wave tank and for his patience and effort to help me use an alternative instrument for the measurement of ship motion.

I wish to extend my thanks and appreciation to Dr. T. Chari, Dr. N. Bose and Mrs. Moya Crocker for the consideration with respect to teaching assistantships which partly ensured the completion of this program.

I owe a lot of thanks to Mr. Andrew Kuczora, Mr. Lloyd Little and Mr. K. Gries for their help and assistance in my experiments.

Staff in the Center for Computer Aided Engineering deserve many thanks for their assistance and help in the use of computers.

I also want to thank Mr. David Cumming at I. M. D. for lending me the Gyroscope so many times.

Another lot of thanks should go to Mr. B. Zou for his help in many aspects throughout my program. Also many thanks to Mr. Kirk Leung, Mr Wenjie Zheng, Mr. Yanming Zhang, Mr. Shuimin Zhang and Ms. Xia Wu for their assistance in the experiments.

Last, but not least, I want to thank my wife Weizhong Zheng and my daughter Chao Zheng Wang for their patience, love and support.

Contents

Abstract i

Acknowledgements iii

Contents iv

List of Figures v

List of Tables ix

1 Introduction 1

1.1 General Introduction 1

1.2 Methodology 2

1.3 Methods for Identifying Roll Damping 5

1.4 Investigation of the Effect of Bias on Roll Motion and Roll Damping 9

2 Free Roll Tests for the Study of Roll Damping 13

2.1 The Models 14

2.2 Set-up of the Models 18

2.3 Arrangement for the Tests 19

2.4 Analysis of Data 23

2.5 Results and Discussions 31

3 Asymmetric Roll Tests in Beam Waves **50**

3.1 Unrestrained Roll Tests in Beam Waves 52

3.2 Restrained Roll Tests in Beam Waves 58

3.3 The Analysis Technique 64

3.4 Results and Discussions 68

3.4.1 Roll Damping and Natural Frequency 68

3.4.2 Frequency Responses of the Unrestrained Wave Tests 71

3.4.3 Frequency Responses of the Restrained Wave Tests 78

4 Numerical Simulation of the Asymmetric Motions **88**

4.1 Mathematical Model 91

4.2 Determination of the Parameters 94

4.3 Results and Discussions 101

5 Conclusions and Recommendations **114**

References **117**

List of Figures

2.1 Body plan of M363 15

2.2 Body plan of M365 17

2.3 Body plan of M366 17

2.4 GZ curve of M363 20

2.5 GZ curve of M365 20

2.6 GZ curve of M366 21

2.7 Smoothed and Unsmoothed Roll Decay Curve 30

2.8 ζ_E for Fixed Bias Angles, M363 32

2.9 ζ_E for Fixed Bias Angles, M365 32

2.10 ζ_E for Fixed Bias Angles, M366 33

2.11 ζ_E for Fixed Roll Amplitudes, M363 34

2.12 ζ_E for Fixed Roll Amplitudes, M365 34

2.13 ζ_E for Fixed Roll Amplitudes, M366 35

2.14 m and c of M363 36

2.15 m and c of M365 37

2.16 m and c of M366 37

2.17 Pressure Distribution on Skeg and Bottom of a Fishing Vessel . . . 38

2.18 Total Energy of M363 41

2.19 Dissipated Energy of M363 42
2.20 Total Energy of M366 42
2.21 Dissipated Energy of M366 43
2.22 ω_d of M363 45
2.23 ω_d of M365 45
2.24 ω_d of M366 46

3.1 Wave Amplitudes and Frequencies, *No Bias Condition* 55
3.2 Wave Amplitudes and Frequencies, Bias Angle: 4.1° 55
3.3 Wave Amplitudes and Frequencies, Bias Angle: −4.1° 56
3.4 Wave Amplitudes and Frequencies, Bias Angle: 7.99° 56
3.5 Wave Amplitudes and Frequencies, Bias Angle: −7.99° 57
3.6 Wave Amplitudes and Frequencies, *No Bias Condition*, Restrained . 61
3.7 Wave Amplitudes and Frequencies, T1 61
3.8 Wave Amplitudes and Frequencies, A1 62
3.9 Wave Amplitudes and Frequencies, T2 62
3.10 Wave Amplitudes and Frequencies, A2 63
3.11 ζ_E for Unrestrained Wave Tests 69
3.12 ω_d for Unrestrained Wave Tests 70
3.13 ζ_E for Restrained Wave Tests, Position 1 72
3.14 ζ_E for Restrained Wave Tests, Position 2 72
3.15 ω_d for Restrained Wave Tests, Position 1 73
3.16 ω_d for Restrained Wave Tests, Position 2 73
3.17 Unrestrained Roll Response in *No Bias Condition* 74
3.18 Unrestrained Roll Response, Bias Angle: 4.1° 75

3.19 Unrestrained Roll Response, Bias Angle: 7.99° 75
3.20 Unrestrained Roll Response, Bias Angle: −4.1° 76
3.21 Unrestrained Roll Response, Bias Angle: −7.99° 76
3.22 Mean Roll Angle from Unrestrained Wave Tests 78
3.23 Roll Amplitude from Restrained Wave Tests, No Bias 79
3.24 Roll Amplitude from Restrained Wave Tests, A1 79
3.25 Roll Amplitude from Restrained Wave Tests, T1 80
3.26 Roll Amplitude from Restrained Wave Tests, A2 80
3.27 Roll Amplitude from Restrained Wave Tests, T2 81
3.28 Mean Angle from Restrained Wave Tests, Position 1 82
3.29 Mean Angle from Restrained Wave Tests, Position 2 82

4.1 The Coordinate System 90
4.2 P_w, L_w and L_b of the Model 96
4.3 Roll Simulation for No Bias Condition 102
4.4 Roll Simulation for Condition A1 103
4.5 Roll Simulation for Condition A2 104
4.6 Roll Simulation for Condition T1 104
4.7 Roll Simulation for Condition T2 105
4.8 Effects of a_{42} and b_{42}, A1 106
4.9 Effects of a_{42} and b_{42}, A2 107
4.10 Effects of a_{42} and b_{42}, T1 108
4.11 Effects of a_{42} and b_{42}, T2 108
4.12 Effects of a_{43}, b_{43} and M_2, A1 110
4.13 Effects of a_{43}, b_{43} and M_2, A2 110

4.14 Effects of a_{43}, b_{43} and M_2, T1 111
4.15 Effects of a_{43}, b_{43} and M_2, T2 111

List of Tables

2.1 Particulars of Models 16

2.2 Bias Angles for Free Roll Tests 22

2.3 Comparison of Natural Frequencies 48

4.1 Coupling Coefficients 100

Chapter 1

Introduction

1.1 General Introduction

During the past twenty years, many aspects of ships' roll motions have been studied extensively. However, one aspect did not draw much attention : asymmetric roll motion and the effect of bias on roll damping. Asymmetric roll motion usually results when a ship suffers a biased condition as a result of icing, nonuniform weight distribution, etc.. This is particularly important in the case of a fishing vessel because of the ever changing loading condition. The characteristics of asymmetric roll motion are very different from that of symmetric roll motion. Under certain circumstances, an unfavourable loading condition in addition to adverse environmental conditions may result in larg asymmetric roll motion and may lead to ship loss.

Roll damping plays a significant role in both symmetric and asymmetric roll motion. In fact, it is one of the most important terms in the equation of roll motion. However, very little is known about the effect of bias angle on roll damping. This study is meant to pave the way for further study of roll damping and roll motion for a ship in a biased condition.

The present study consists of three parts. First, an investigation of roll damping for biased ship models. Details of this work will be shown in Chapter 2. Second, a series of experiments were conducted to study the effect of bias angle on roll motion of a fishing vessel model in beam waves. This will be presented in Chapter 3. Last, Chapter 4 will present a numerical simulation of the asymmetric roll motion of a biased ship model in beam waves.

1.2 Methodology

Given the appropriate information about a ship and the seaway, one can predict heave and pitch motions to a remarkable degree of accuracy without recourse to model tests or empirical data. Two moderate lateral-plane motions, sway and yaw, can also be predicted with reasonable accuracy. However, when one tries to predict roll motion, one realizes that roll motion is quite different from these motions. Heave and pitch are not sensitive to the effects of fluid viscosity. Roll motion, on the other hand, is extremely sensitive to viscosity effects, especially to viscosity-induced flow separation [1]. A major factor which contributes to the difficulty in prediction of roll motion is the lack of accurate estimates for damping parameters [2].

A biased condition of a ship makes the matter more complicated because of the complex effect of bias on roll damping and consequently on roll motion [3] [4]. For these reasons, empirical and semi-empirical methods play and will continue to play an important role in the formulation of roll damping and prediction of roll motions, especially when roll motion is asymmetric. It is also for these reasons that the present study was undertaken with special emphasis on experimental aspects.

In current practice, there exist two major categories of experimental methods to determine roll damping. The first one is known as the *Forced Roll Test*. The second one is known by various names: *Roll Decrement Test*, *Free Roll Test* or *Free Decay Test*, etc.. Spouge [5] gave a definition and explanation of these two methods in detail. Here we only present a brief description.

The *Forced Roll Test*, as the name implies, involves applying a pure sinusoidal roll moment to the model. The response of the model can then be recorded for the given exciting moment. Thus, the values of roll damping moment can be determined easily. Methods for the analysis of data from this type of test can be found in reference [5].

The *Free Roll Test* is carried out by giving the model an initial heel angle in still water, and then releasing it. The model will roll freely. In other words, the *Free Roll Test* is analogus to a free vibration induced by an initial displacement. The response is recorded and roll damping can be identified by any one of the methods which will be discussed later in this chapter.

Free and forced roll tests can be carried out with the model free to move in six degrees of freedom. We will refer to these tests as the *Unrestrained Tests*. The tests can also be carried out with the model restrained against motion in some degrees of freedom. We will refer to this class of tests as *Restrained Tests*. Both restrained and unrestrained tests were used in the literature for roll damping measurements. In the present study, both the *Unrestrained* and *Restrained Tests* were carried out for the measurement of roll motion of the model in beam waves. However, for determining roll damping only *Unrestrained Tests* were conducted in still water.

According to Spouge [5], the *Forced Roll Test* would give a more accurate esti-

mate of roll damping because the test can be continued until the model's response is steady. However, because the *Forced Roll Test* involves using a heavy and large instrument, called a *Roll Moment Generator* it is fairly doubtful that this method is suitable for small models, like those used in the present study. It is believed that the *Free Roll Test* gives a better estimate of damping in the case of moderate-amplitude roll of a small ship model. Therefore the *Free Roll Test* technique was chosen for the present study of roll damping.

The study of asymmetric roll motion in beam waves has been carried out both analytically and experimentally. The purpose of the wave test is to determine the ship's roll motion. Because the effect of viscosity on roll motion makes the prediction and simulation difficult, empirical methods are still necessary for the research in this field. For a ship under a biased condition, roll motion may have different characteristics and becomes more difficult to predict or simulate. Therefore, two series of wave tests were carried out in the present study. One is for the study of the effect of bias angle on roll motion of a model without restraint in sway and heave. The other is carried out with the model restrained in heave and sway. It is expected that the results obtained from these two series of tests will reveal some information on the effect of bias and restraints.

Although it is difficult, simulation is still a way to gain further understanding of the mechanism of asymmetric roll motion. A biased condition of a ship does not only affect the hydrodynamic forces in roll mode but it also induces coupling of roll motion with other modes. It is difficult to identify these couplings through experiment. However, simulation sometimes can shed some light on this problem. In addition, a simulation is helpful for the understanding of the effect of the re-

straints. Thus, a simulation was also carried out and will be presented in Chapter 4.

1.3 Methods for Identifying Roll Damping

During the past decade, many methods have been presented for identifying ship's roll damping coefficients. These methods can be divided into two main categories. The first uses the method of slowly varying parameters, known as *Averaging Technique* of Krylov and Bogoliubov [6] [7] [8]. The second uses the Perturbation Technique [9].

Dalzell [6] used the method of slowly varying parameters to find an equation for the rate of decay of the peaks of the roll decay curve as a function of the damping moment parameters. He was then able to identify these parameters through the use of a least squares technique. Haddara [7] used a stochastic version of the same procedure to identify the parameters of different damping models, including angle dependent components. This method is relatively easy to apply and usually yields fairly accurate results for velocity dependent components of damping moment. However, this technique is only suited for the analysis of data of a ship having linear righting arm curves (i.e. GZ curves) which is unrealistic especially when large rolling motion is considered.

Roberts [8], using an energy approach introduced a loss function which is related to the amplitude of roll motion, and the parameters of the roll damping moment. He used experimental values obtained for the loss function to identify the parameters in the roll damping moment by means of a least squares technique. This method is suitable for ships having slightly nonlinear restoring moment. However, because the

averaging technique was used this method also fails to identify the angle dependent components of the same order of magnitude as the velocity dependent components.

Mathiesen and Price [9] used a perturbation series to approximate the free roll motion of a ship. This method is based on the assumption that the nonlinear motion is a small perturbation of the linear motion. Thus, the results obtained using this method are only valid for small nonlinearities. The method is capable of dealing with only simple forms of damping moment.

All of the above mentioned methods share one disadvantage. They all depend on the measurements and fitting of the damping moment form to the peak values of the roll decay curve [26]. Therefore, they require large numbers of these peak values to obtain reasonably accurate results. This means that relatively long roll decay curves must be recorded. For a model with large damping, it is hard to obtain enough decay cycles. In addition, the accuracy is quite doubtful for the latter part of the roll decay curve, i.e. the part with small amplitudes.

Bass and Haddara [10] presented two techniques named *DEFIT* and *Energy Approach*. *DEFIT* is a parameter identification technique. It is based on fitting the experimental data to the solution of an assumed differential equation. *Energy Approach* is predicated on the equivalence of the rate of change of the total energy of the system and the rate of energy dissipation in the damping. These two methods do not depend solely on the peak values of the decay curve but can use the values of the whole curve. Due to its distinct advantages the *Energy Approach* was chosen for the analysis of roll decay curves in the present study. A brief outline of this method is given here.

The differential equation describing the motion of a ship rolling freely in calm

water can be written as:

$$\ddot{\phi} + N(\phi, \dot{\phi}) + R(\phi) = 0 \tag{1.1}$$

where ϕ denotes roll angle, $N(\phi, \dot{\phi})$ represents the damping moment per unit virtual moment of inertia, and $R(\phi)$ is the restoring moment per unit virtual moment of inertia. Dots over the variable denote differentiation with respect to time.

Multiplying equation (1.1) by $\dot{\phi}$ and rearranging, one gets

$$\frac{d}{dt}[\frac{1}{2}\dot{\phi}^2 + G(\phi)] = -N(\phi, \dot{\phi})\dot{\phi} \tag{1.2}$$

where

$$G(\phi) = \int_0^{\phi} R(x)dx$$

Let

$$V(t) = \frac{1}{2}\dot{\phi}^2 + G(\phi)$$

and

$$H(t) = V(t + dt) - V(t)$$

equation (1.2) can be rewritten as

$$H(t) = -\int_t^{t+dt} N(\phi, \dot{\phi})\dot{\phi}dt \tag{1.3}$$

Equation (1.3) implies that the loss in the total energy of the ship during a time dt is equal to the energy dissipated by the damping moment during the same period of time. The different forms for the damping moment discussed in the literature can be summarized as follows [11]:

Linear plus linear angle dependent

$$N_1(\phi,\dot{\phi}) = 2\zeta\omega_n(1+\varepsilon_1|\phi|)\dot{\phi} \tag{1.4}$$

Linear plus quadratic angle dependent

$$N_2(\phi,\dot{\phi}) = 2\zeta\omega_n(1+\varepsilon_2\phi^2)\dot{\phi}$$

Linear plus quadratic velocity dependent

$$N_3(\phi,\dot{\phi}) = 2\zeta\omega_n(1+\varepsilon_3|\dot{\phi}|)\dot{\phi}$$

Linear plus cubic velocity dependent

$$N_4(\phi,\dot{\phi}) = 2\zeta\omega_n(1+\varepsilon_4\dot{\phi}^2)\dot{\phi}$$

where ω_n is the natural frequency, ζ is the nondimensional linear damping coefficient and $\varepsilon_i, i = 1,...,4$ are measures of the nonlinearity. For any one of these forms equation (1.3) can be expressed as

$$H(t) = \zeta[U_1(t) + \varepsilon_k U_{k+1}(t)] \tag{1.5}$$

where k=1,...,4 and

$$U_1(t) = -2\omega_n \int_t^{t+dt} \dot{\phi}^2 dt$$

$$U_2(t) = -2\omega_n \int_t^{t+dt} |\phi|\dot{\phi}^2 dt$$

$$U_3(t) = -2\omega_n \int_t^{t+dt} \phi^2\dot{\phi}^2 dt$$

$$U_4(t) = -2\omega_n \int_t^{t+dt} |\dot{\phi}|\dot{\phi}^2 dt$$

$$U_5(t) = -2\omega_n \int_t^{t+dt} \dot{\phi}^4 dt$$

The method of least squares is then used to determine the coefficients of damping moment in equation (1.5).

1.4 Investigation of the Effect of Bias on Roll Motion and Roll Damping

A ship at sea would suffer a bias condition under each of the following circumstances or their combinations:

1. The center of gravity of the ship is not in the longitudinal plane of symmetry. This condition can be induced by a shift in the cargoes' position or caused by an asymmetric distribution of weight.

2. Steady wind load on one broadside of a ship makes it heel at a bias angle. In this case, the bias moment can be considered a constant external moment.

3. A large quantity of water on deck.
   The shift of center of gravity in this case may be dynamic in the sense that it continuously shifts with the motion of the ship.

4. Operation of a fishing vessel dragging a net in one side.

5. One or more compartments at one side are flooded.

Some attention has been paid to the study of the asymmetric roll motion of a biased ship and its roll damping. The research work done falls into two main categories, experimental studies [12-17] and simulations [18-23]. The first part of this section will present some results of the experimental and analytical studies related to the effect of bias on asymmetric rolling motion. The results concerning influence of bias on roll damping will appear in the second part of this section.

Marshfield [12-16] is a major contributor to the experimental study in this field. He carried out a series of tests for the investigation of the capsize of biased and

unbiased ships. In his experiments, a biased model was subjected to beam waves at zero forward speed. In his typical tests presented in [13], the model was lightly tethered in drift and yaw while allowing it to roll, heave and pitch freely. One of the important and interesting findings of this study is that the frequency response of the model biased towards the wave source (wave maker) differed significantly from that of the model biased away from the wave source. Bias towards the wave source made the model much more likely to capsize as compared with a model with zero bias or biased away from the wave source [13,16]. However, higher amplitudes of roll motion were recorded when the model was biased away from the wave source. This is hard to explain. It has attracted strong interest from several researchers and triggered some analytical studies [19] [20].

Féat and Jones [20] developed a mathematical model to predict the asymmetric motion of a biased ship subjected to beam waves. They took into account the variations in displacement volume and the effect of the position of a ship in waves. This effect is well known as the *Smith Effect*. Their way of taking *Smith Effect* into account is followed by many other researchers [19] [21] and will also be followed in the present study. Their work, to some extent, paved the way for the following related analytical studies. However, in the frequency responses under two different bias conditions, no significant differences were predictable from their mathematical model [19].

Bass [19] investigated analytically the effect of bias on harmonic roll motion. In his mathematical model, he showed that time and angle dependent variation in GZ curves have an influence on the response of a biased ship in beam waves. He derived a function to link the time-dependent GZ curve with the variation in

ship's displacement volume which was caused by relative heave. This important step makes his prediction more realistic and reasonable. His prediction of the roll motion of the biased ship model used by Marshfield ([12] through [14]) showed a good qualitative agreement with experimental results. It is especially worth mentioning that Bass's prediction also gave higher amplitudes of response when the model was biased away from the wave source.

Nayfeh and Khdeir [4] also studied analytically the roll motion of biased ships in beam waves. They used the method of multiple scales to determine an up to second-order approximate solution for the asymmetric motion of biased ships. Their simulation apparently gave higher accuracy. Unfortunately, they failed to consider the effect of the direction of the bias which was shown by Marshfield [13] to affect the roll amplitude significantly.

Compared with the study of the roll response of a biased ship, the damping of a biased ship has attracted less attention. Theoretical work for predicting or simulating roll damping of a ship in a bias condition is rare. Experimental studies on the damping of a biased ship are also scarce. Tamiya's result [3] is one of few experimental data available. The data (in the form of graphs) summarized the results of a series of tests conducted in Japan. The tests were carried out with two models, a small cargo ship model and a refrigerated carrier model. For the small cargo ship the damping was found to decrease with bias angle when the bias angle was small. When the bias angle has increased to a value at which the model's deck begins to immerse the roll damping increased with the bias angle. However, when the bias angle reachs another certain point the damping would decrease if the bias angle is further increased. For the refrigerated carrier, the situation was more

complicated. The roll damping was not only influenced by bias condition but was also affected by the transverse metacentric height (i.e. GM). Damping increased with bias angle for some GM values but it decreased with bias for other GM values. For some GM values the damping was apparently not affected by bias angle. His results indicate that the effect of bias on roll damping also depends on the hull form and many other factors.

Marshfield ([12] through [16]) also measured the roll damping of the biased model used in his tests. Because his main purpose was to study roll response in waves he did not systematically study the effect of bias on roll damping. The damping was measured only for two or three bias angles so it is difficult to draw any conclusion from his results. From the data arranged in [16] it seems that the roll damping increases with bias angle.

Chapter 2

Free Roll Tests for the Study of Roll Damping

Haddara and Bass [11] summarized all the possible forms of roll damping used in the literature. These expressions of roll damping do not include the effect of bias angle. For a biased ship, bias angle may not be a negligible factor in the damping function. Although some experimental results in reference [3] show some aspects of the effect of a bias angle, knowledge of the effect of bias angle on damping is still lacking. Therefore, more attention should be paid to the effect of bias angle on roll damping of ships, especially in the case of fishing vessels because of their special hull form.

From Tamiya's results [3], it is clear that the effect of bias on roll damping for a small cargo ship is quite different from that for a refrigerated carrier. This implies that the hull form of a ship also plays some role in the effect of bias on roll damping. Although Himeno [1] presented methods for evaluating the effect of ship hull form on damping, it is doubtful that these prediction methods are suitable for a biased ship.

The study being presented in this chapter will focus on the effects of bias angle

on roll damping of small fishing vessels. The hull form effect and the effect of bias angle on damped roll natural frequency will also be discussed. Owing to time and facility limitations, only three fishing vessel models with distinctive hull forms are used in the experiments. The number of models may not be sufficient; but it is still expected to reveal some information about the effects of bias angle and hull form on roll damping.

2.1 The Models

Three small fishing vessel models were used in the present experimental study and will be denoted by M363, M365 and M366. These models are chosen from a series of six fishing vessel models built in IMD. There are two main reasons for this choice. One is their typical main hull forms and their distinctive features. The other is that Haddara, Bass and their students [11,33] have used these models in many related experimental studies. If the same models are used for various studies of roll damping, the knowledge of roll damping about these models can be accumulated and more insight into the roll damping can be gained.

The full scale fishing vessels for these three models all lie in the "less than 25 m " class. They are all of similar dimensions, but have varied hull forms, ranging from the hard chine (e.g. Model M363) to the rounded bilge hull form (e.g. Model M366). M363 and M366 have similar position of the center of gravity, but M365 has a much higher center of gravity, also a higher transverse metacenter. In addition, M363 has a higher freeboard, a deep skeg and a comparatively high rise of floor. Of these three models, M366 has the smallest *Midship Section Coefficient* C_M (see Table 2.1). C_M is defined by

$$C_M = \frac{A_M}{BT}$$

where A_M is the area of the midships section. B and T denote waterline beam and draught at midships respectively. C_M describes the degree of the hull's fullness at midship. Moreover, the characteristics of the GZ curves of the three models also vary from model to model. The distinctive features of these models may result in an apparent difference in the characteristics of their roll damping.

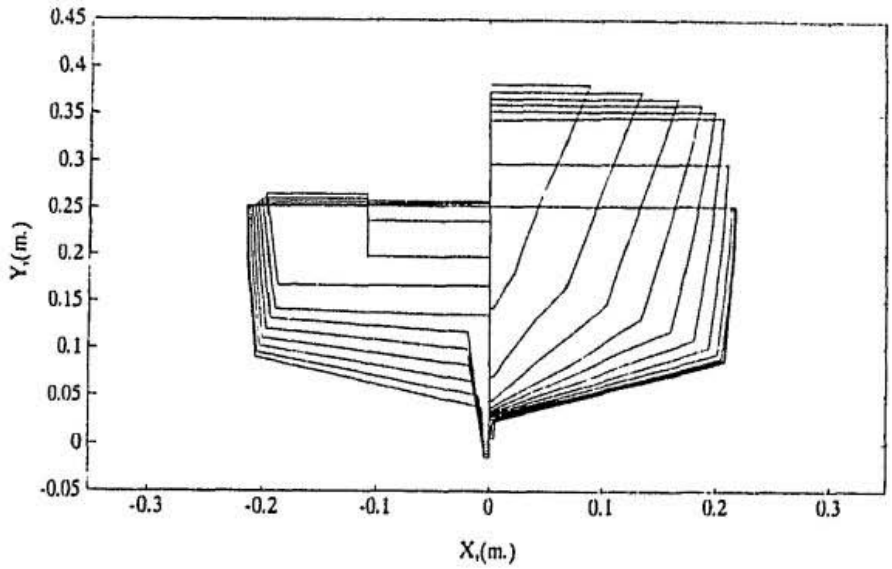

Figure 2.1: Body plan of M363

The general dimensions for the models are shown in Table 2.1, and the lines plans are shown in Figures 2.1 through 2.3. In Table 2.1, μ_1 and μ_2 denote the coefficients of the GZ curve. These coefficients will be explained in the next section.

Model	M363	M365	M366
Scale	1:12	1:9.1	1:6.8
LWL (m)	1.551	1.336	1.568
Beam (m)	0.507	0.542	0.506
Draft (m)	0.221	0.215	0.205
LCB (m)	-0.109	-0.052	-0.1375
C_M	0.746	0.705	0.612
KG (m)	0.269	0.304	0.263
Mass (kg)	79.70	54.36	69.40
GM at bias=0 (m)	0.029	0.0312	0.037
ω at bias=0 (r/s)	2.713	3.168	2.967
μ_1 at bias=0	1.611	-0.717	-0.158
μ_2 at bias=0	-2.013	-1.75	-1.03

Table 2.1: Particulars of Models

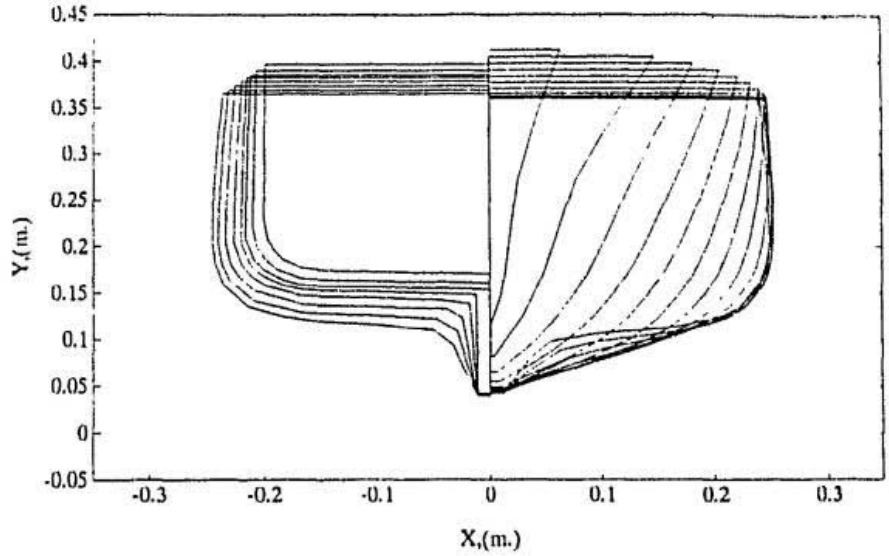

Figure 2.2: Body plan of M365

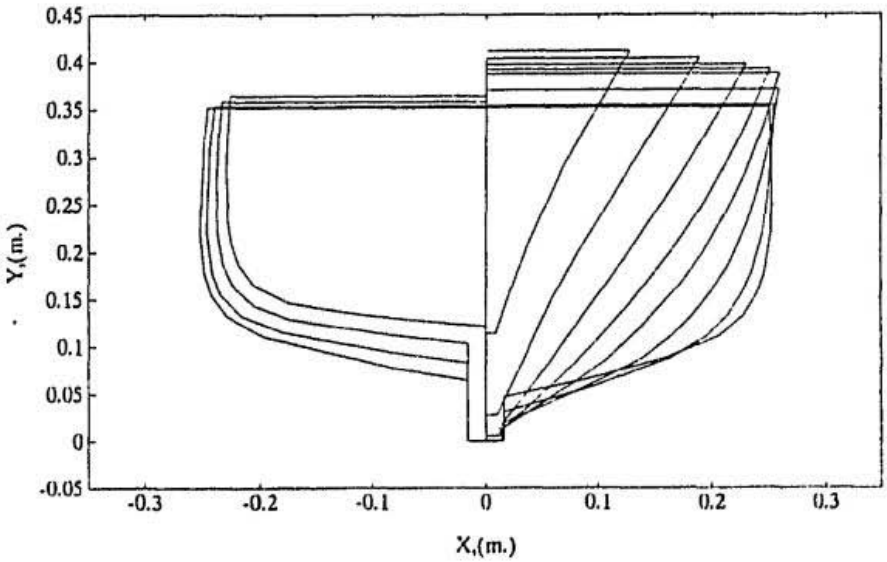

Figure 2.3: Body plan of M366

2.2 Set-up of the Models

Three models, M363, M365 and M366, were ballasted and trimmed to the correct waterlines and displacement. A set of weights were arranged in each model in such a way that the height of the center of gravity (KG) makes the value of GM to be approximately 5 to 10 percent of the model's beam. In addition, natural frequencies of the three models should also have similar values. Once the arrangement was satisfactory, all the weights were fixed to the model. The transverse center of gravity was kept in the longitudinal plane of symmetry for *no bias condition* by means of a symmetric distribution of weights. The upright condition was checked with an inclinometer. A bias condition for each model can be obtained by transversely changing the location of a movable weight W_b.

An inclining experiment was conducted for each model. The weight, W_h, used in these experiments was taken as 200 grams.

The relation of GM to the heel angle and heel moment can be expressed as follows.

$$m_i = GM\Delta tan\phi_i \tag{2.1}$$

where ϕ_i represents a heel angle and m_i is heel moment. Δ denotes the model's displacement. i denotes ith move of the weight W_h.

$$m_i = W_h d_i$$

d_i is the distance for the ith move. A method of least squares was then used with equation (2.1) to obtain the value of GM.

The vertical center of gravity was then given by:

$$KG = KB + BM - GM \tag{2.2}$$

where KG and KB denote the height of the vertical center of gravity and vertical center of buoyancy above datum respectively. BM is the transverse metacentric radius and GM is the transverse metacentric height.

The GZ curve can be approximated by

$$GZ(\phi) = GM(\phi + \mu_1\phi^3 + \mu_2\phi^5) \tag{2.3}$$

The values of GZ calculated by Bass with a computer sorftware package [35] were used in the present study. The values of μ_1 and μ_2 were determined using a polynomial fitting computer program. The GZ curves for the three models are shown in Figures 2.4 through 2.6. The values of GM, μ_1 and μ_2 of the three models are listed in Table 2.1.

2.3 Arrangement for the Tests

The tests were carried out in the Memorial University towing tank. The towing tank measures 58.27 meters long, 4.57 meters wide and 3.0 meters deep. It is equipped with an MTS servohydraulic piston type wave generator at one end. At the other end there is a wave absorbing beach to reduce the effect of the reflected waves. The tank has a towing carriage which runs on parallel rails 4.88 meters apart.

In the present study, it is assumed that both roll amplitude and bias angle have significant effect on roll damping. Therefore, average roll amplitude ϕ_0 (the definition will be given in Section 2.4) and bias angle ψ were chosen as two main

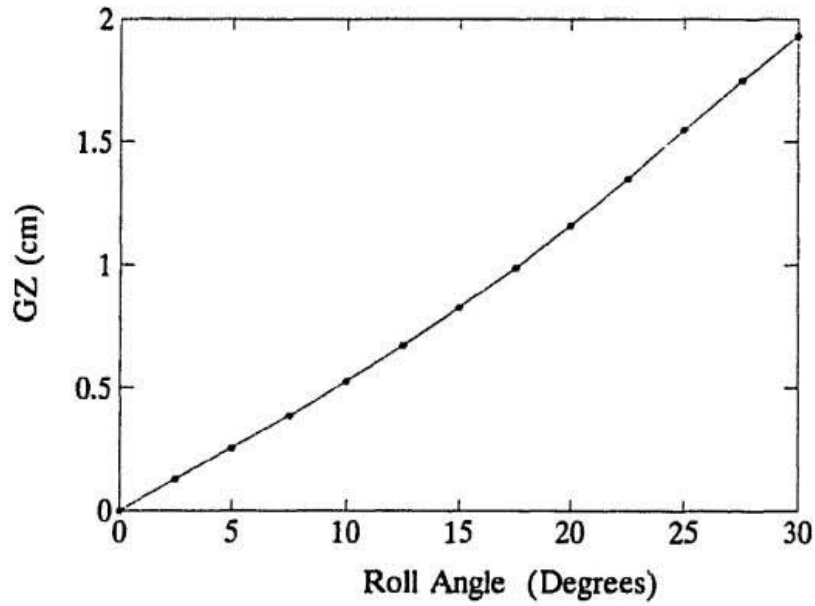

Figure 2.4: GZ curve of M363

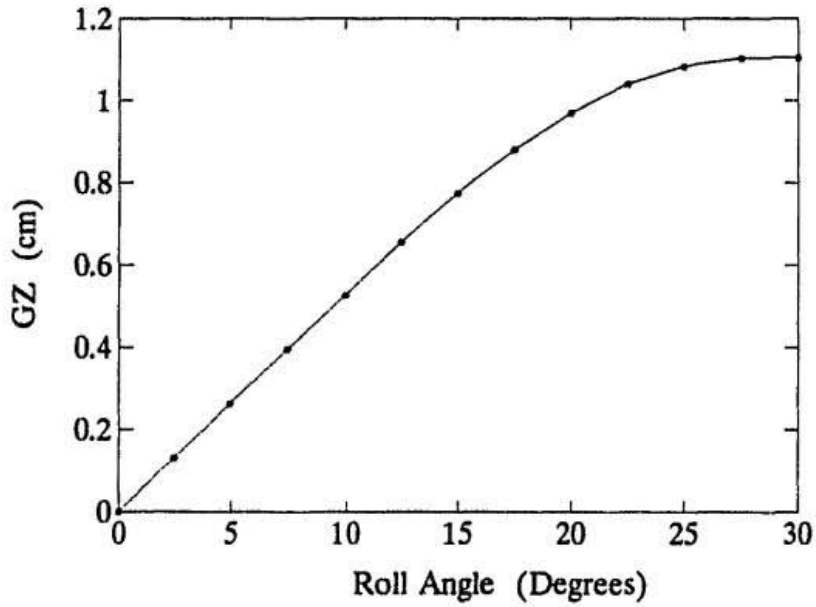

Figure 2.5: GZ curve of M365

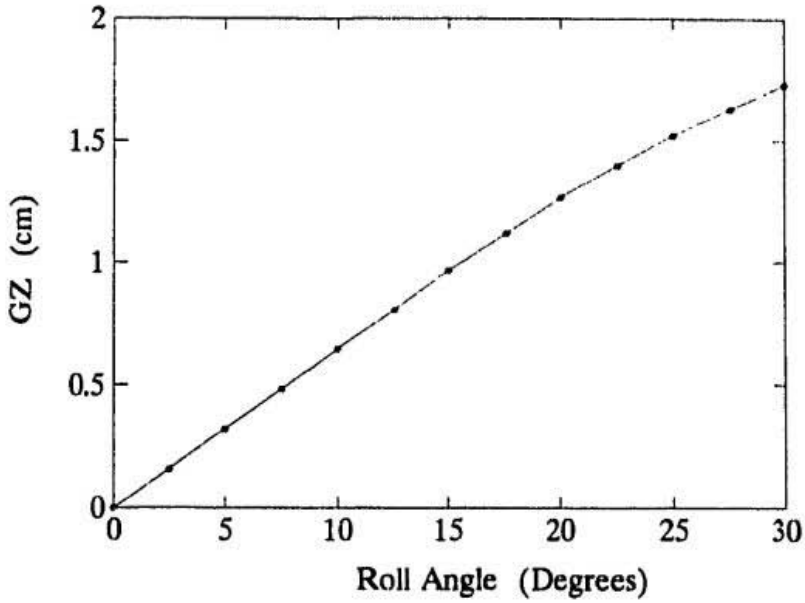

Figure 2.6: GZ curve of M366

variables. Changing these two variables in tests, one may find the effect of these two factors on roll damping. Roll amplitude can be changed by means of changing initial roll angle.

The initial roll angle was obtained by employing as pure a heeling moment as possible. This was achieved in the following way: two hands of the experimenter were used to hold on the bulwarks of the model at the position of the longitudinal center of gravity, one on left side of the model, the other on right side. One side of the model is then pushed down while pulling up the other side with approximately the same force. Once the model is stably heeled at a certain angle it is released. The model then rolls freely.

During this procedure attention was paid to two points: the hands must be put as close to the longitudinal center of gravity as possible; the two hands must

impress approximately the same force. If the hands were put somewhere away from the longitudinal center of gravity, the model would trim. If the force from two hands were much different, heave of the model would occur.

Nine bias angles were used for each model and 9 initial angles were tested for each bias condition. The bias angle was measured with a gyroscope and checked with an inclinometer. The initial roll angle increased with a step of about 2 to 3 degrees. The maximum initial roll angles for M363, M365 and M366 are 30, 25 and 27 degrees respectively. A total of 81 decay curves was recorded for each model. The bias angles are listed in Table 2.2.

Model	*Bias Angle (Degrees)*								
M363	0.443	2.174	3.37	4.67	6.06	7.17	8.772	9.92	12.48
M365	0.09	1.40	3.00	4.09	6.075	7.55	9.182	10.67	12.14
M366	0.05	2.206	3.76	4.69	5.987	7.35	9.02	10.3	12.2

Table 2.2: Bias Angles for Free Roll Tests

Roll angles were measured using a gyroscope. All the data were recorded using an IBM P.C.. A plotting program was used to plot the decay curve after each run. If a noisy or strange curve was found the test would be repeated. A ten minute interval between two runs was given to let the water calm down. This ensures that the decay curves are less noisy.

2.4 Analysis of Data

A damping form for the damping moment must be chosen before an analysis of roll decay curves can be carried out. Some previous studies (see [24] to [26]) suggested an angle dependent form. Watanabe-Inoue (see [1]) developed a form of roll amplitude dependent damping as a consequence of the concept of equivalent linear damping used by them. Bass and Haddara [27] also applied the concept of equivalent linear damping in their study of roll damping of small fishing vessels. They assumed that the equivalent linear roll damping coefficient is roll amplitude dependent. Their work indicates that the amplitude dependent damping form is reasonable, useful, practical and simple. In fact, the concept of amplitude dependent linear damping is particularly used in conducting parametric studies such as this. It is easy to understand the qualitative variation caused by a single parameter. Moreover, it significantly simplifies the analysis. Thus, it was decided that the concept of equivalent linear damping and the amplitude dependent damping form will be applied to the present analysis.

If B_E is used to denote the equivalent linear damping coefficient, the damping can usually be represented as

$$N(\phi, \dot{\phi}) = B_E(\phi_0, \psi)\dot{\phi} \tag{2.4}$$

where ϕ_0 and ψ denote roll amplitude and bias angle respectively. This equivalent damping should dissipate the same amount of energy as that dissipated by the nonlinear damping within a single cycle.

There are two ways to analyse the decay curves from a biased model for obtain-

ing roll damping coefficient. They are described below.

In the first, the upright condition (referred to as *no bias condition*) of the model is taken as the reference condition. The roll equation can be written as:

$$I\ddot{\phi} + B_E(\phi_0, \psi)\dot{\phi} + \rho g \bigtriangledown GZ(\phi) = M_e \tag{2.5}$$

where M_e is a heeling moment and can be expressed as

$$M_e = -W_b d cos\phi \tag{2.6}$$

This moment is considered as an *external moment.*

The symbols in equation (2.5) are explained as follows. A dot over a variable indicates differentiation with respect to time. ϕ denotes roll angle, measured from upright condition. ϕ_0 denotes roll amplitude and ψ represents bias angle. $B_E(\phi_0, \psi)$ is amplitude-dependent roll damping coefficient (N.m.sec). $\rho\bigtriangledown$ is model mass (kg) and $\bigtriangledown$ is displacement volume of the model (m^3). $GZ(\phi)$ is angle dependent restoring lever (m). I is virtual moment of inertia (kgm^2)

$$I = I_G + A_{44}$$

where I_G is the inertia moment of the model about its center of gravity and A_{44} is the added moment of inertia. d is the transverse distance between longitudinal plane and the new location of the movable weight W_b.

The negative sign on the right side of equation (2.6) is due to the coordinate system. In this thesis, roll angle and bias angle are defined to be positive when the model rolls or heels past its upright condition and towards its starboard, whereas, d and GG' (the transverse distance between new and original center of gravity)

have negative values when W_b is moved towards model's starboard side (refer to Figure 4.1, the coordinate system will be explained in detail in Chapter 4). Thus, a negative d will result in a positive bias angle. To keep sign of angle and d (or GG') consistent, a negative sign appears in equation (2.6). This role will also be applied to equation (2.11) and the equations related to the relation of bias angle to d or GG' in Chapters 3 and 4.

The first term on the left side of equation (2.5) is an inertia moment. The second term is a damping moment and the last term is restoring moment. The term on the right side of the equation is considered as an *external moment* resulting from the change of position of the movable weight W_b. This moment is sometimes referred to as the *bias moment*. This moment can also be considered to be a correction term of restoring moment by means of including it in the expression of restoring moment. The corrected restoring moment can be expressed as follows

$$\rho g \bigtriangledown \overline{GZ}(\phi, \psi) = \rho g \bigtriangledown GZ(\phi) + W_b d cos\phi \tag{2.7}$$

Thus, equation (2.5) can be normalized as

$$\ddot{\phi} + 2\zeta_E \omega_n \dot{\phi} + \omega_n^2 D(\phi) + M_0 cos\phi = 0 \tag{2.8}$$

The last two terms in the above equation together constitute the normalized corrected restoring moment.

ζ_E in equation (2.8) denotes nondimensional equivalent linear damping coefficient. Comparing equation (2.8) with equation (2.5), we have:

$$\zeta_E = \frac{B_E(\phi_0, \psi)}{2I\omega_n} = \zeta_E(\phi_0, \psi) \tag{2.9}$$

The natural frequency ω_n in equation (2.8) is given by

$$\omega_n = \sqrt{\frac{\rho g \bigtriangledown GM}{I}} \tag{2.10}$$

$D(\phi)$ is the restoring arm function. According to equation (2.3), $D(\phi)$ can be approximated by:

$$D(\phi) = \frac{1}{GM} GZ(\phi) = \phi + \mu_1 \phi^3 + \mu_2 \phi^5$$

The amplitude of the normalized *external moment* M_0 is determined by

$$M_0 = \frac{W_b d}{I}$$

When the model is balanced at a given bias angle ψ, we have

$$-W_b d cos\psi = \rho g \nabla GZ(\psi) \tag{2.11}$$

Thus, the *external moment* can be expressed as

$$M_0 cos\phi = -\frac{\rho g \nabla GZ(\psi)}{I cos\psi} cos\phi \tag{2.12}$$

Substituting equation (2.12) into equation (2.8), one can note that a positive bias condition (corresponds to a positive bias angle) will reduce the restoring moment.

Employing the Energy Approach to equation (2.8), one can obtain ζ_E. With ϕ measured from the *upright condition* the reference system used for the above equations will be referred to as the *upright reference system.*

A second approach can be used in the analysis by taking the stable biased condition as the reference condition. This will be referred to as the *bias reference system.* In this system, the roll angle will be measured from the bias condition, not

the *upright condition.* If ϕ_1 is used to denote the roll angle in *bias reference system*, the relation of ϕ_1 to roll angle ϕ in the upright reference system is of the form

$$\phi_1 = \phi - \psi$$

The roll equation under this reference system can be written as

$$\ddot{\phi}_1 + 2\zeta_E\omega_n\dot{\phi}_1 + \omega_n^2 D(\phi_1 + \psi) + M_0 cos(\phi_1 + \psi) = 0$$

Theoretically speaking, these two ways of analysis should give the same results.

In the present study, the *upright reference system* was used in the analysis. The analysis was carried out using the *Energy Approach* [27] to obtain ζ_E.

Multiplying equation (2.8) by $\dot{\phi}$ gives

$$\frac{d}{dt}[\frac{1}{2}\dot{\phi}^2 + G(\phi)] = -2\zeta_E\omega_n\dot{\phi}^2 \tag{2.13}$$

where

$$G(\phi) = \omega_n^2 \int_0^{\phi} D(x)dx + M_0 sin\phi \tag{2.14}$$

Let

$$V(t) = \frac{1}{2}\dot{\phi}^2 + G(\phi) \tag{2.15}$$

$$H(t) = V(t + dt) - V(t) \tag{2.16}$$

Then the equation (2.13) can be rewritten as

$$H(t) = \zeta_E U(t) \tag{2.17}$$

where

$$U(t) = -2\omega_n \int_t^{t+dt} \dot{\phi}^2 dt \tag{2.18}$$

ζ_E can be obtained by means of a least squares technique using equation (2.17). From equation (2.17), we can see that the accuracy of the analysis is strongly dependent on the accuracy in the estimates of energy variations. It is also shown in equation (2.15) and (2.18) that roll velocity is one of the most important contributors to the energy. A smooth roll decay curve is needed for accurate estimation of roll velocities.

As is mentioned in Chapter 1, one of the advantages of the *Energy Approach* is that only one cycle of roll decay curve is needed for the prediction of damping coefficient. This ensures higher accuracy in the analysis because the latter part of roll decay curve is more noisy and the accuracy is doubtful. Even in the first cycle, some of the roll decay curves obtained from experiments are not smooth enough, especially, the curves with small initial roll angles. A filter was used during the tests; but, it cannot eliminate all noise. In fact, the noise is rather large in some recorded decay curves.

To improve the accuracy of analysis, we must eliminate or reduce the noise to an acceptable degree. A moving averaging technique and a spline technique were used to smooth the decay curves before the analysis. If the roll angle at time t_i is $\phi(t_i)$, and the angles before and after t_i in turn are $\phi(t_{i-1})$ and $\phi(t_{i+1})$, the moving averaging technique can be described as

$$\bar{\phi}(t_i) = \frac{1}{2}[\phi(t_{i-1}) + \phi(t_{i+1})]$$

Then, the $\phi(t_i)$ was substituted by $\bar{\phi}(t_i)$. Following the same procedure, one can reduce the noise by using this averaging process throughout all the recorded roll angle data except for the first and the last points. A spline technique was then used to fit all the points after the averaging process.

A typical decay curve is shown in Figure 2.7. The dash line stands for the original values of roll angle from tests and solid line represents smoothed values. It is fairly clear that the solid line gives a smoother but still accurate representation of the original roll curves.

To reflect the effect of bias angle ψ and roll amplitude ϕ_0 on roll damping, ζ_E in equation (2.8) is assumed to be a function of roll amplitude and bias angle. The average roll amplitude ϕ_0 which is referred to as *roll amplitude* is the mean of two roll amplitudes with the same sign in the first cycle. In order to make the expression of ζ_E reflect the effect of actual roll amplitude, the amplitude used here is the one measured from the bias condition. The roll amplitude can be obtained simply by subtracting bias angle from the measured roll amplitude measured from the upright. The reason for use of roll amplitude, rather than roll initial angle, is that roll amplitude, not initial angle, is the appropriate parameter for a ship steadily rolling in waves. Thus, ζ_E can be expressed as

$$\zeta_E = \zeta_E(\phi_0, \psi) \tag{2.19}$$

For a given bias angle ψ_i, ζ_E is a function of roll amplitude ϕ_0. i.e.

$$\zeta_{E,\psi_i} = \zeta_E(\phi_0, \psi_i) \tag{2.20}$$

Some typical values of ζ_{E,ψ_i} for M363, M365 and M366 are shown in Figures 2.8, 2.9 and 2.10 respectively.

On the other hand, ζ_E is also a function of bias angle ψ for a given roll amplitude $\phi_{0,i}$. In this case, ζ_E can be expressed in the form

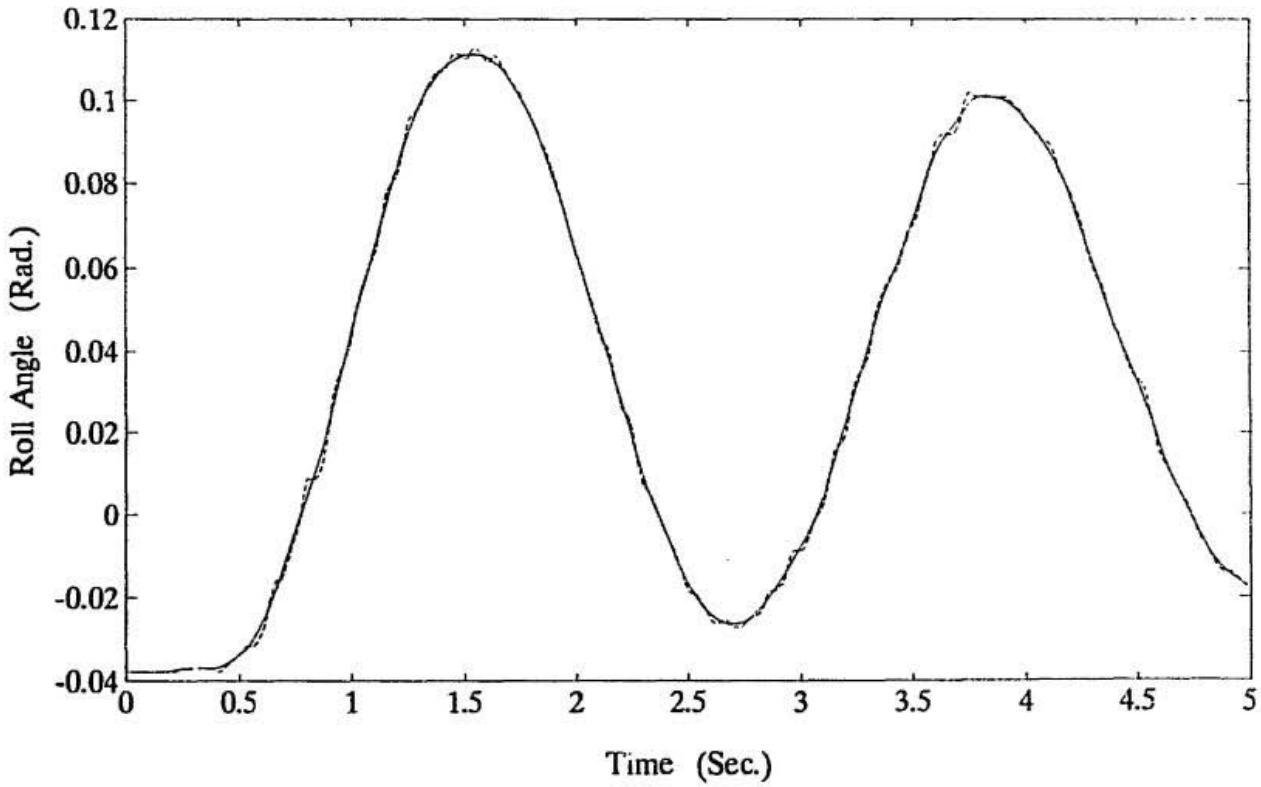

Figure 2.7: Smoothed and Unsmoothed Roll Decay Curve

$$\zeta_{E,\phi_{0,i}} = \zeta_E(\phi_{0,i}, \psi) \tag{2.21}$$

A few typical values of $\zeta_{E,\phi_{0,i}}$ plotted against bias angle ψ are shown in Figures 2.11, through 2.13.

Further discussion about these results will be presented in the next section.

2.5 Results and Discussions

The graphs in Figures 2.8 through 2.10 show the dependence of ζ_E on the roll amplitude ϕ_0. In all these figures and others in this section, lines, including dash, solid and dash dot lines represent the polynomial regression values; the discrete points, including "*", "+" and "o" denote the values obtained from the analysis of experimental data. It is clearly shown in Figures 2.8, 2.9 and 2.10 that the relation of ζ_E to ϕ_0 is linear and can be expressed in the form

$$\zeta_E = m(\psi)\phi_0 + c(\psi) \tag{2.22}$$

Both m and c are dependent on bias angle. Because all values of ζ_E increase with roll amplitude ϕ_0, $m(\psi)$ has positive values in all cases (see Figures 2.8 through 2.10).

The magnitude of c is indicative of the wave damping component of roll damping and the magnitude of m is indicative of the viscous component of roll damping . The values of m and c for the three models are shown in Figures 2.14, 2.15, and 2.16. These graphs indicate clearly that the values of c are much smaller than the values of m. It implies that viscosity plays a significant role in roll damping for these models.

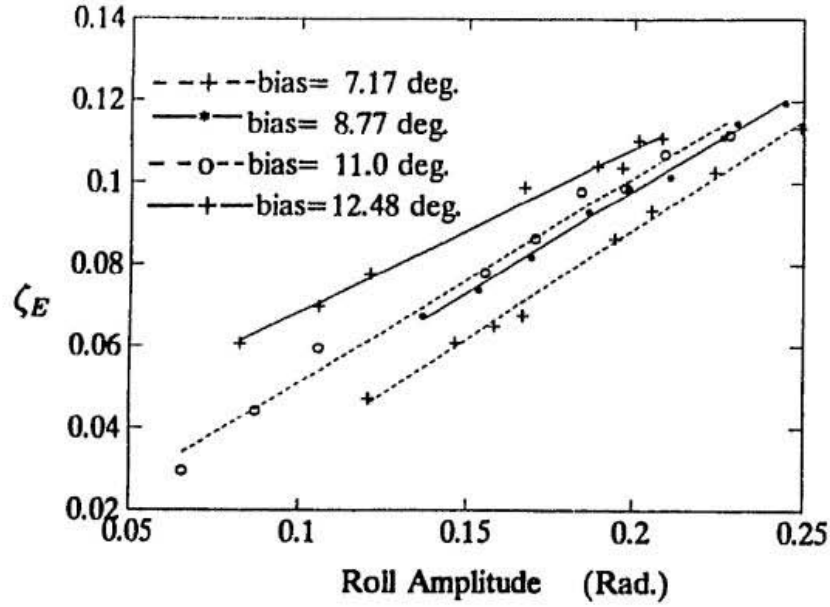

Figure 2.8: ζ_E for Fixed Bias Angles, M363

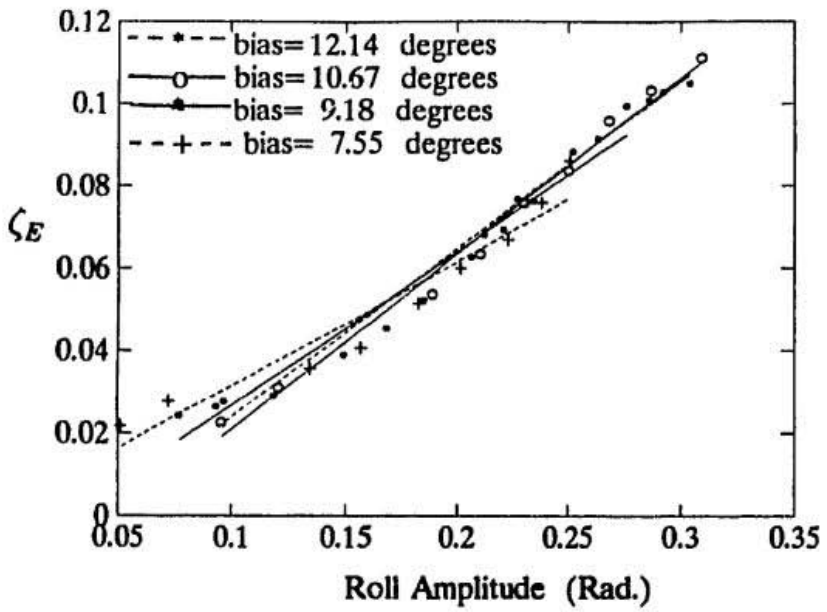

Figure 2.9: ζ_E for Fixed Bias Angles, M365

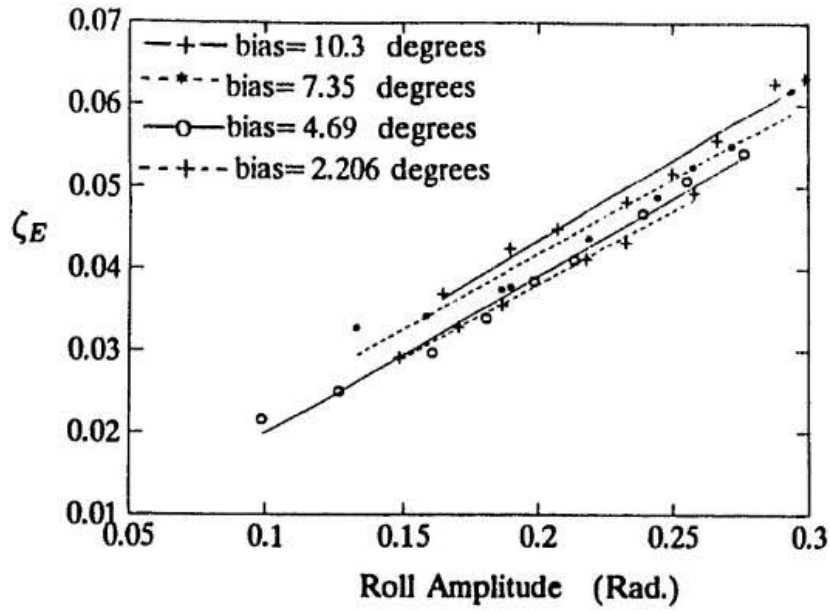

Figure 2.10: ζ_E for Fixed Bias Angles, M366

It is shown that the dependence of ζ_E on the bias angle varies from the linear, in the case of the model M366, Figure 2.10, to the quadratic, in the case of the model M363 , figure 2.11. In other words, the characteristics of dependence of ζ_E on bias angle ψ varies from model to model. We will discuss them one by one.

The graphs in Figure 2.11 show that ζ_E is highly nonlinear when the roll amplitude is small. ζ_E of the model M363 decreases with increase of bias angle until a value about 7 degrees is reached, then it increases as the bias angle increases. Figure 2.14 shows that the dependence of viscous roll damping component on bias angle for the model M363 is quadratic; m increases first, then decreases, as bias angle increases. The turning point is also at the bias angle of 7 degrees. The wave damping component behaves in the opposite way to this, but, its variation is relatively slight.

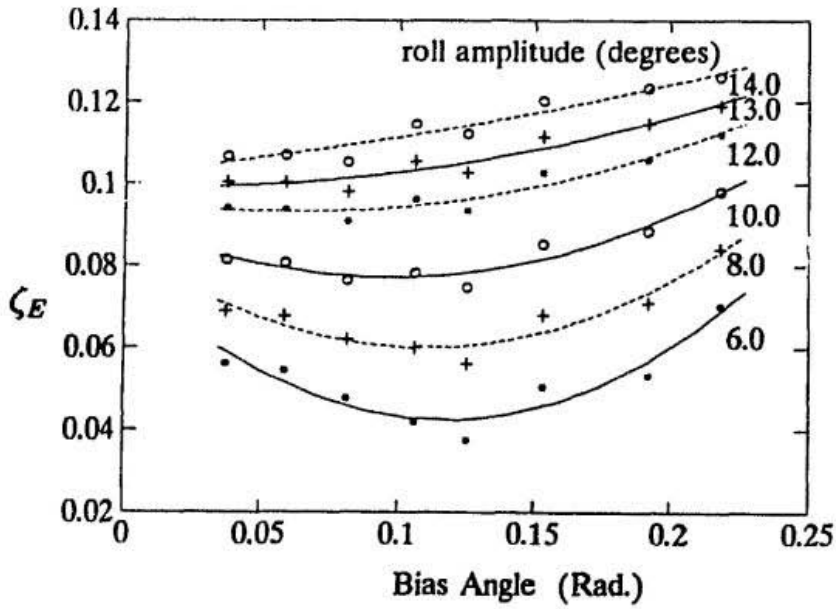

Figure 2.11: ζ_E for Fixed Roll Amplitudes, M363

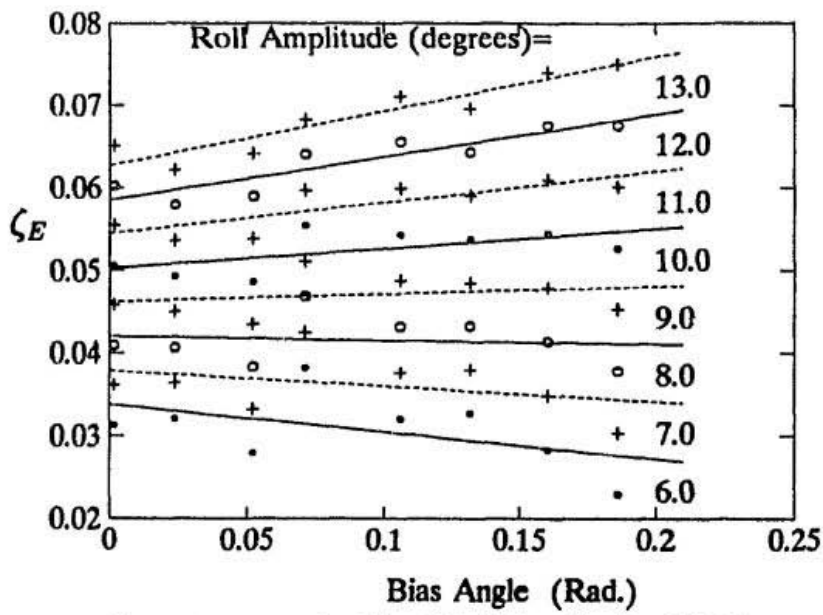

Figure 2.12: ζ_E for Fixed Roll Amplitudes, M365

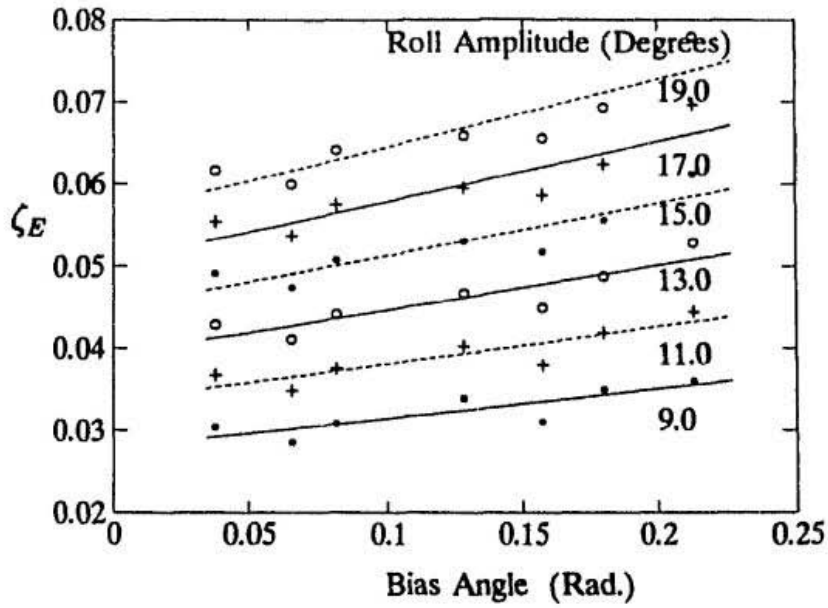

Figure 2.13: ζ_E for Fixed Roll Amplitudes, M366

Comparing the graphs in Figure 2.11 with those in Figure 2.14 , one may have further insight into ζ_E of M363. As is mentioned above, the wave damping component c, shown in Figure 2.14, decreases with increase of bias angle when the bias angle is smaller than 7 degrees. Then it increases when the bias angle is larger than 7 degrees. When the roll amplitude is small ζ_E varies with bias in a similar way (see Figure 2.11). This indicates that the wave damping component plays an important role in ζ_E in the case of small roll amplitude. In the case of large roll amplitude, we can note, in equation (2.22), that the viscous component will dominate ζ_E. It is shown in Figure 2.14 that the graphs of the wave damping component vs. ϕ_0 and that of the viscous component coefficient m are convex. Their combination may be a straight line when the roll amplitude increases to a certain value. This analysis is supported by the graphs with large roll amplitude in Figure 2.11. These

graphs indicate that ζ_E increases almost linearly as the bias angle ψ increases. The mechanism of the nonlinear dependence of ζ_E on bias angle is fairly complicated. It will be discussed later in this section.

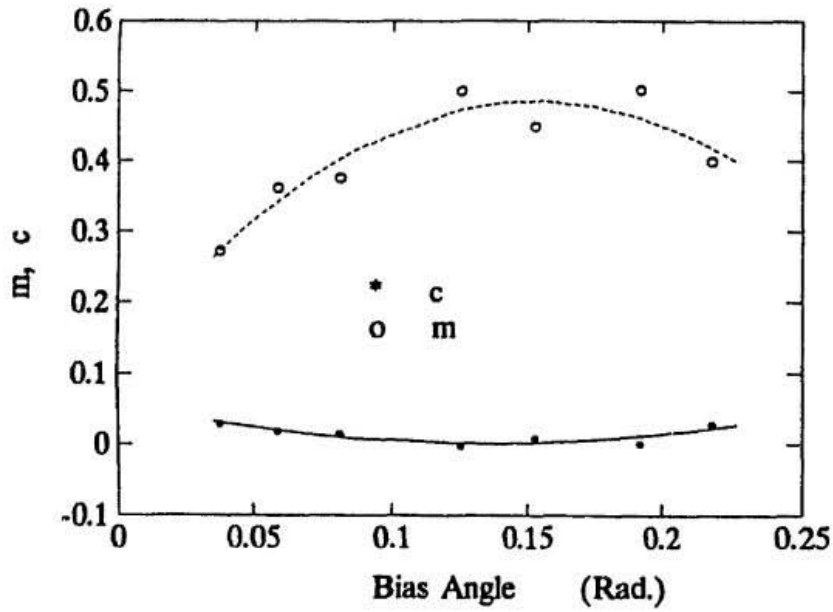

Figure 2.14: m and c of M363

Now, let us turn to the case of M366. From Figure 2.13, one can note that ζ_E of M366 increases linearly with increase of bias angle ψ. The viscous damping component of ζ_E, the m, increases also linearly as bias angle increases, see figure 2.16. On the other hand, its wave damping component c is almost constant. It seems that the bias angle has a significant effect only on the viscous component of roll damping [11]. Because m increases with the increase of bias angle the effect of viscosity increases as both bias angle ψ and roll amplitude ϕ_0 increase. This is the simplest case of the three models.

Lastly, let us examine the case of M365. The dependence of ζ_E on bias angle ψ,

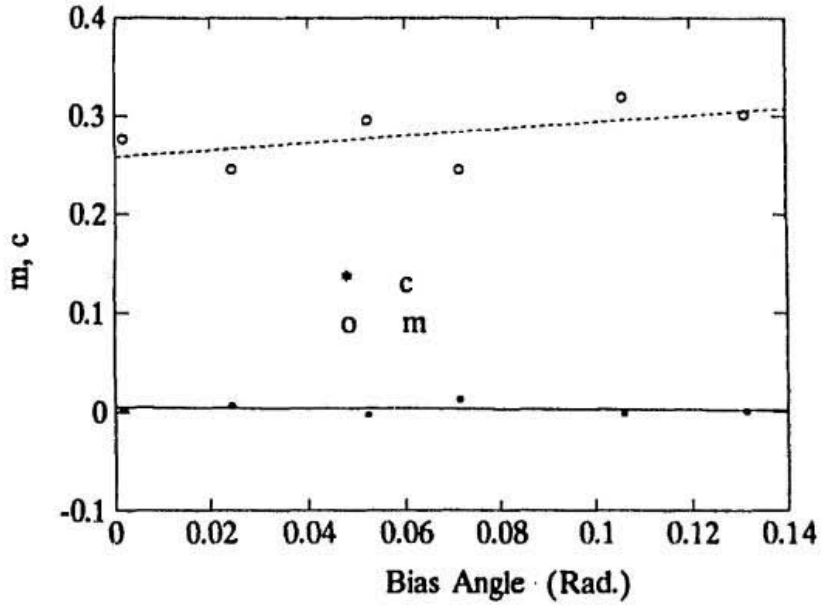

Figure 2.15: m and c of M365

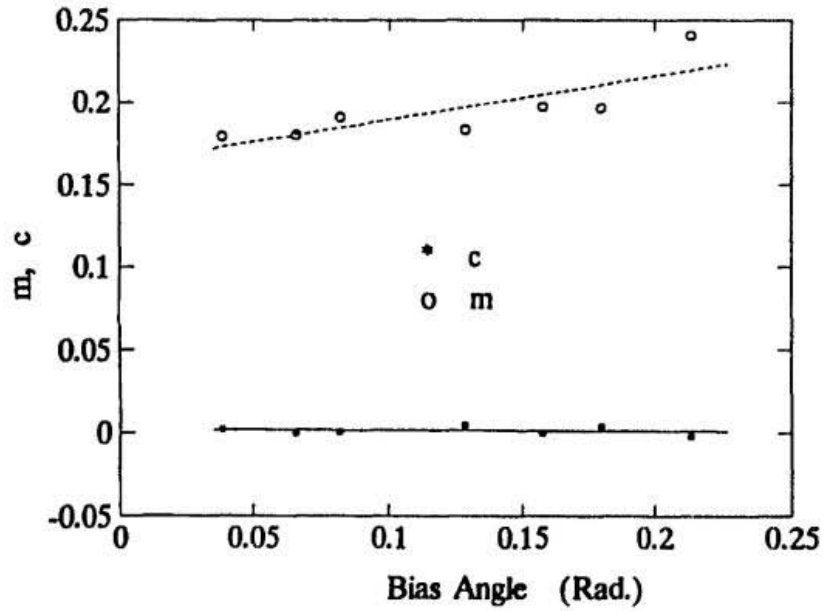

Figure 2.16: m and c of M366

as in the case of M363, is also complicated. Its ζ_E, in Figure 2.12, decreases with the increase of bias angle for a roll amplitude less than 8 degrees. In other cases, ζ_E increases as bias angle increases. Although there is some scatter in the data in Figure 2.15 one can get a picture of the characteristics of m and c. The wave damping component c shown in Figure 2.15, slightly decreases with the increase in the bias angle, but the viscous component m increases. One can also conclude that the viscous component of the damping has a dominant effect at large roll amplitude.

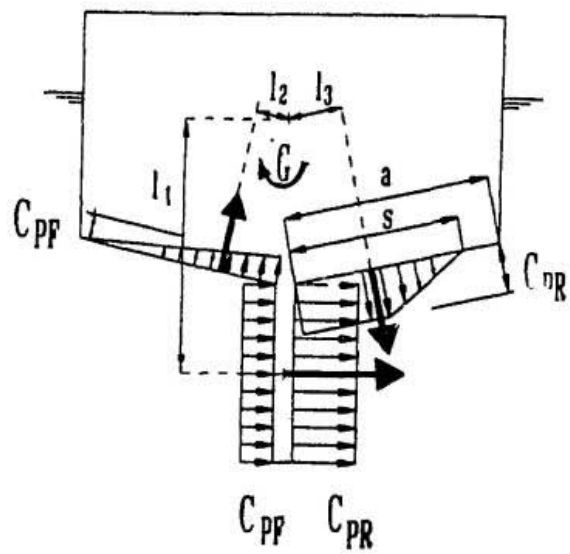

Figure 2.17: Pressure Distribution on Skeg and Bottom of a Fishing Vessel

The nonlinear behaviour of the damping coefficient in the case of M363 may be explained by referring to Figure 2.17 which has been reproduced from reference [28]. The Figure shows the assumed pressure distribution on the bottom and the skeg of a model whose features are similar to that of M363.

Ikeda et al [28] expressed the damping moment as:

$$M_d = \frac{1}{2}\rho U^2[(C_{PF} - C_{PR})l_s l_1 - \frac{1}{2}C_{PF}al_2 + \frac{3}{4}C_{PR}sl_3]$$

where U represents the velocity of the edge of the skeg, and l_1, l_2 and l_3 denote the moment arms shown in Figure 2.17. The pressure coefficients C_{PF} and C_{PR}, and the length of the negative pressure region s was assumed as follows

$$C_{PF} = 1.2$$

$$C_{PR} = -3.8$$

$$s = 1.65 l_s K_c^{\frac{3}{5}}$$

where K_c is the Keulegan-Carpenter number and was defined as

$$K_c = U_{max} T / l_s$$

U_{max} denotes the maximum value of U and T denotes the period of roll motion.

To apply the pressure distribution shown in Figure 2.17 we assume that the biased M363 approximately has a similar pressure distribution when its absolute roll amplitude is not large. When the roll angle is large the model's hard chine and part of its bottom will emerge out of the water; thus, the pressure distribution may be much different from that shown in Figure 2.17. Therefore the following explanation is only suitable for the cases of small and moderate roll amplitudes.

If the center of gravity G is slightly moved a horizontal distance to the left , to simulate the effect of a small bias angle, one can see that the arm l_2 decreases while the arm l_3 increases. This will result in an increase in the magnitude of the negative moment thus causing the magnitude of the damping moment to decrease.

However, if we keep moving G further to the left G will reach the point at which l_2 becomes zero. If G is moved beyond this point the l_2 becomes negative. This causes a part of the moment on the bottom to be of the same sign as the moment on the skeg, thus, damping begins to increase as the bias angle increases. On the second half cycle, the l_3, not l_2, will become negative when G is moved beyond l_3.

It is estimated for M363 that for most sections l_2 varies in the range of 0.17 to 0.24 cm. Bias angle is about 4.6 degrees when GG' is equal to 0.2 cm, the average value of l_2. Thus, the turning point should have approximately appeared at a bias angle of 4.6 degrees which is slightly different from the value shown in Figure 2.11 (the change happened at the bias angle of about 7 degree in Figure 2.11).

However, this reasoning cannot be applied to model M365 and M366. Unlike M363, M365 and M366 do not have hard chines (see Figures 2.2 and 2.3). These features of hull form make M365 and M366 sufficiently different from those defined in reference [28] that we cannot assume that M365 and M366 also have a similar pressure distribution.

The above reasoning is based on the assumption that the pressure distribution on the skeg and bottom of the biased M363 with a moderate roll amplitude and velocity is similar to that of the model shown in [28]. This may be questionable because it is doubtful that bias angle does not affect the pressure distribution. To avoid this disadvantage, we will view it from the point of view of energy as follows.

The Figures 2.18 and 2.20 show the total roll energy of the models M363 and M366, and Figures 2.19 and 2.21 show the dissipated energy due to damping per unit virtual inertia moment of these two models. The total roll energy is $V(t)$ in equation (2.19) and the dissipated energy is the absolute value of $U(t)$ in equation

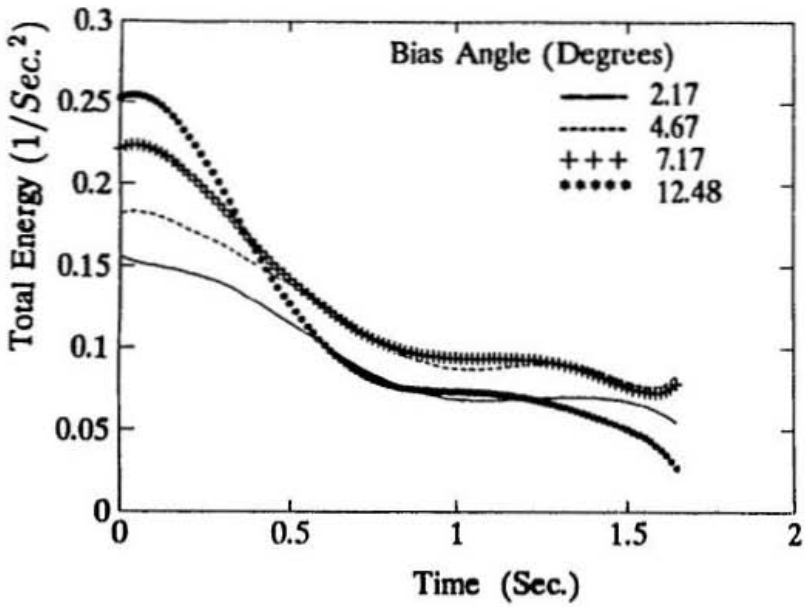

Figure 2.18: Total Energy of M363

(2.22). The corresponding roll amplitude for these graphs is 10 degrees.

Equations (2.17) and (2.21) indicate that the loss of the total energy should be equal to the energy dissipated due to roll damping in the same period of time. This can also be interpreted as saying that the greater the decrease in total energy, the larger the damping coefficient will be if U(t) is constant. In other words, if U(t) increases constantly and uniformly, a large damping coefficient will result in a sharp decrease in total energy . In Figure 2.20, the total energy, in the case of no bias condition (i. e. upright condition), decreases a small amount. It decreases more in the case of bias angle of 4.67 degrees. A very sharp decrease for the bias angle of 10.3 degrees is shown. Meanwhile, the U(t) increases approximately uniformly, as shown in Figure 2.21. This demonstrates that the dependence of damping coefficient on bias angle is linear. This tendency is in coincidence with that shown in Figure 2.13.

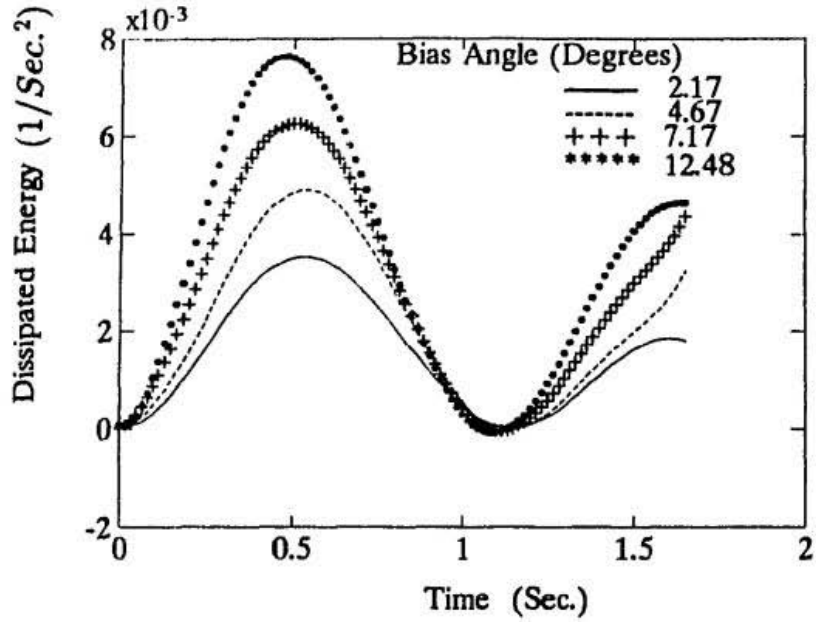

Figure 2.19: Dissipated Energy of M363

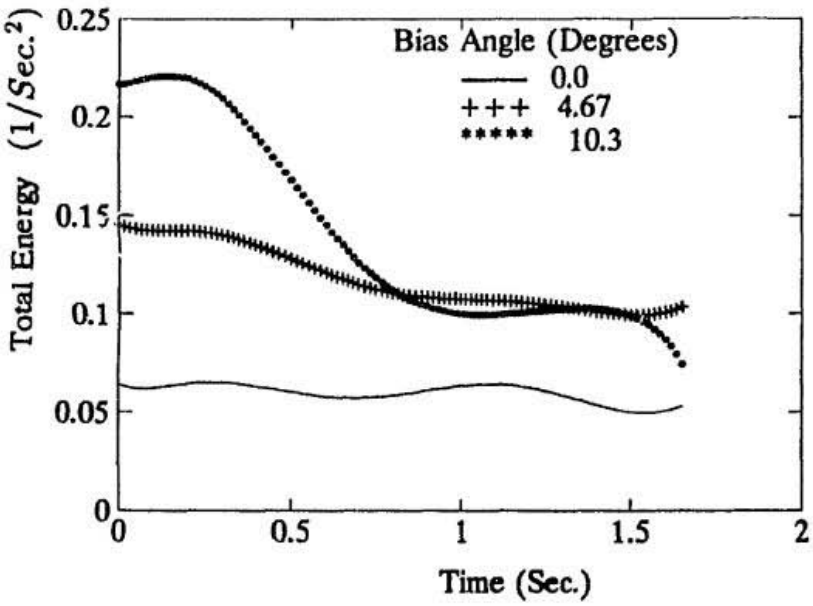

Figure 2.20: Total Energy of M366

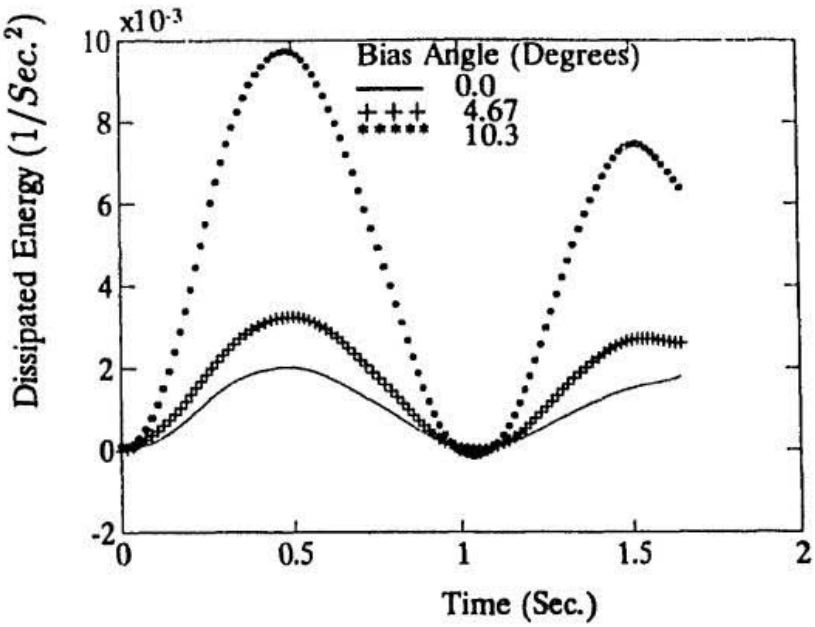

Figure 2.21: Dissipated Energy of M366

On the other hand, the U(t) in Figure 2.19 seems to increase almost uniformly. The decrease in total energy shown in Figure 2.18, however, is in quite a varying amount. For the bias angles of 2.17 degrees and 4.67 degrees, the total energy decreases by approximately the same amount. This means that the damping coefficient is smaller in the case of bias angle of 4.67 degrees because the U(t) increased. For these two bias conditions, the damping coefficient decreases with increase of the bias angle . For the other pair, bias angles of 7.17 degrees and 12.48 degrees, U(t) increases by a similar amount, but the total energy for the bias angle of 12.48 degrees decreases twice as much. This shows that ζ_E increases as bias angle increases. These four cases demonstrate the behaviour of the nonlinear dependence of damping coefficient on bias angle.

As implied above, hull form and other distinctive features of these three models

may be responsible for their different characteristics of ζ_E. Ikeda et al [28] pointed out : " the characteristics of roll damping of small fishing vessels are quite sensitive to the changes of hull form ...". It will be shown in the following paragraph that their conclusion is also supported by the results of the present experiments.

One of the conclusions from the study presented in reference [28] says " the hard chine increases roll damping significantly". The study also shows that skeg and high rise floor will result in a large roll damping. As mentioned above, a hard chine, a deep skeg and a comparatively high rise of floor of M363 make it distinct from M365 and M366. Thus we can safely say that the higher ζ_E of M363 is partly due to its angular hull form, deep skeg and comparatively high rise of floor. In the cases of M365 and M366, M365 has a larger value of C_M and a higher center of gravity compared with those of M366 (see table 2.1). It is indicated in reference [3] that a higher center of gravity will increase roll damping too. The larger C_M is also one of the factors increasing roll damping. In short, both the position of the center of gravity and the degree of fullness in hull form contribute positively to M365's roll damping which, as a result, becomes larger than that of M366.

It was noticed during the tests that the bias angle also affects the model's damped natural frequency ω_d which is obtained from the analysis of decay curves. The damped natural frequencies of M363, M365 and M366 are shown in Figures 2.22 through 2.24.

The graphs in Figure 2.22 and Figure 2.24 show that the DNF ω_d of M363 and M366 increases as bias angle increases. The DNF ω_d of M365, on the other hand, decreases as bias angle increases. Within the range of the bias angle with maximum value of 12.48 degrees in the present experiments, the ω_d increased by 10 percent

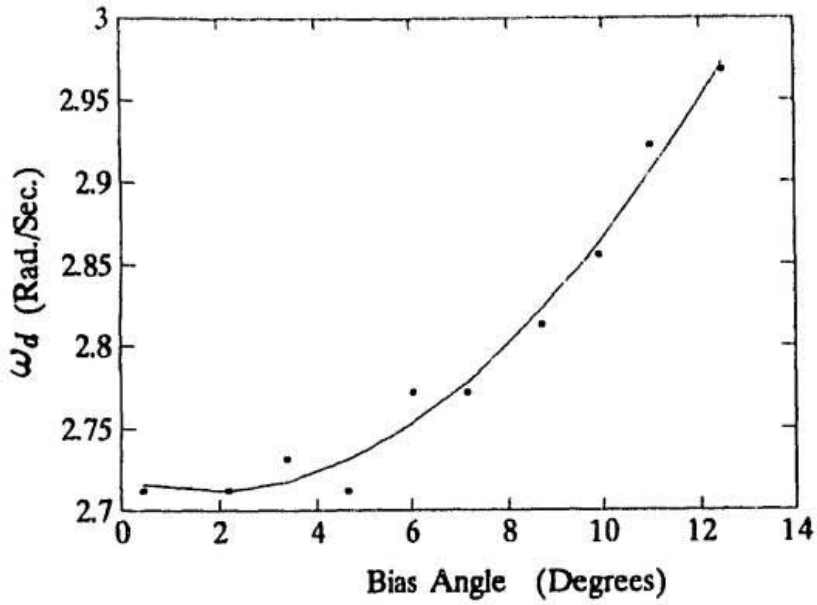

Figure 2.22: ω_d of M363

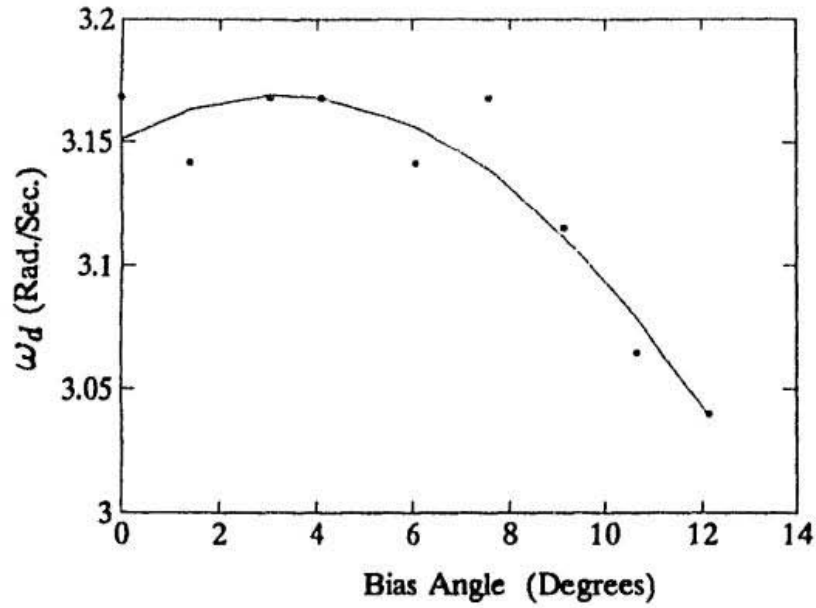

Figure 2.23: ω_d of M365

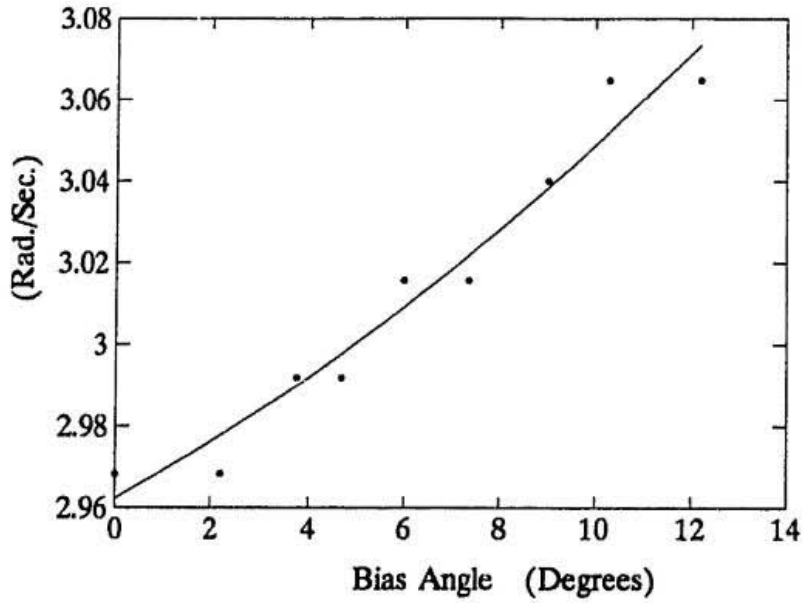

Figure 2.24: ω_d of M366

for M363, four percent for M366 and decreased also by four percent for M365 (see Figures 2.22 through 2.24). The dependence of ω_d on bias angle is nonlinear for all three models.

The ω_d can be expressed in terms of natural frequency ω_n and ζ_E

$$\omega_d = \omega_n \sqrt{1 - \zeta^2} \tag{2.23}$$

It can be seen from equation (2.10) and (2.23) that the ω_d of a model is affected by many factors: virtual moment of inertia, ζ_E, GM and displacement. Equation (2.23) also tells us that ω_d decreases with the increase of ζ_E. For a given ship model, the displacement and the inertia moment can be assumed constant. From Figures 2.8 and 2.10 it seems that ω_d should decrease, not increase, with increase of the bias angle for the models M363 and M366 because their ζ_E increases with the increase of bias angle for large roll amplitude (please refer to Figure 2.11). This makes the

phenomenon difficult to understand. However, besides the ζ_E, GM also depends on the bias condition. In other words, the bias angle also affects the value of GM. For a given bias angle ψ, substituting equation (2.11) into equation (2.7) gives

$$\overline{GZ}(\phi,\psi) = GZ(\phi) - \frac{GZ(\psi)}{cos\psi}cos\phi \tag{2.24}$$

where $\overline{GZ}(\phi,\psi)$ is the corrected GZ curve, $GZ(\psi)$ is the value of GZ at $\phi = \psi$. The GM, in this case, can be obtained from the following equation :

$$GM(\psi) = \frac{d}{d\phi}\overline{GZ}(\phi,\psi)|_{\phi=\psi} \tag{2.25}$$

Equations (2.24) and (2.25) indicate that $GM(\psi)$ is bias angle dependent. Whether the $GM(\psi)$ increases or decreases with increase of ψ depends on the slope of $\overline{GZ}(\phi,\psi)$. To demonstrate this quantitatively, two groups of data for M363 and M365 are shown in Table 2.3.

The corresponding value of roll amplitude for ζ_E in Table 2.3 is 12 degrees which is the same as the value of roll amplitude for the graphs of ω_d shown in Figures 2.22 through 2.24. The two bias angles for each model listed in Table 2.3 are the minimum and maximum values used in experiments.

Equations (2.10) and (2.23) can be combined and rearranged as follows

$$\begin{aligned}\omega_d &= \omega_n\sqrt{1-\zeta_E^2} \\ &= \sqrt{GM(1-\zeta_E^2)\frac{\rho g\nabla}{I}} \\ &= J\sqrt{\frac{\rho g\nabla}{I}}\end{aligned} \tag{2.26}$$

where

$$J = \sqrt{GM(1-\zeta_E^2)} \tag{2.27}$$

Model	*Bias Angle* (Degrees)	GM (cm)	ζ_E	J	Q
M363	0.443	2.87	0.084	1.688	9.7
	12.48	3.46	0.097	1.851	
M365	0.09	3.12	0.059	1.763	-6.0
	12.14	2.76	0.069	1.657	

Table 2.3: Comparison of Natural Frequencies

The values of J for the minimum and maximum bias angles of M363 and M365 are listed in the column five in Table 2.3. Q in Table 2.3 denotes the rate of increase of J, and is given by

$$Q = \frac{J_2 - J_1}{J_1} \times 100 \tag{2.28}$$

where J_1 is the value of J at minimum bias angle and J_2 is the value of J at maximum bias angle.

It is clearly shown in Table 2.3 that J, or ω_d increases by 9.7 percent for M363 and decreases by 6.0 percent for M365. These values are very close to the rate of change of damped natural frequencies shown in Figures 2.22 and 2.23. Now, it is clear that the combined effect of GM and ζ_E makes the damped natural frequency

have the tendency shown in Figures 2.22 and 2.23.

Chapter 3

Asymmetric Roll Tests in Beam Waves

As mentioned in Chapter 1, a bias can be a result of various environmental and/or loading conditions. The bias caused by each condition may have different characteristics. The bias condition considered in the present study, sometimes referred to as *static bias*, is induced by a shift of the center of gravity. The shift of the center of gravity was achieved by a transverse displacement of a movable small weight in the model. In this case, the bias is considered to be *static*, only in the sense that the magnitude of bias is constant. In fact, even in this case the bias moment, as shown in equation (2.12), is still roll angle and bias angle dependent. Because the roll angle varies with time, we can say that the bias moment is also time dependent. This bias condition is the most common and the simplest one. The study of the effect of this bias condition on asymmetric rolling motion is considered to be the first step towards a further understanding of the asymmetric motions under other bias conditions.

Marshfield carried out a series of wave tests with models under *static bias* conditions. In one group of his tests [13] with a low freeboard model (denoted by

Form 1 in [13]), Marshfield found that bias away from the wave source resulted in a higher roll amplitude but the model was less likely to capsize as compared with the condition of bias towards the wave source. He conjectured that the phenomenon was a result of tethering in drift and yaw [13]. In his report [13] , he wrote " the model drift restraint provides a possible explanation for these results ". To clarify this matter, Marshfield conducted another two sets of tests [14] [15] and he rejected his conjecture in a later report [14]. The conclusion is that " the effect due to tethering were within the scatter range of the experiment " and "On the evidence presented it would appear that tethering the model in beam waves has little effect on the roll behaviour of the model"[14]. This probably can be explained by the low degree of the restraint used in Marshfield's tests. Actually, the restraint he used was pretty loose. Marshfield described it by using the word *tethering*, not *restraining*. The mechanism of the effect of bias and restraint on roll behaviour is interesting. Unfortunately, it has been rather hard to find a parallel study to obtain insight into this problem.

Sellar's [29] investigation offered some related information about the restraint in drift and sway for a model in the upright condition. The investigation was based on the tests reported by Dalzell in [30] and Rogalski [31] (the information on [30] and [31] is obtained from [29]). The results can be summarized as follows.

1. Broadside drift was found to increase the roll of a ship by 20 percent compared with zero drift condition [31] (see [29]).

2. When sway is restrained the roll exciting moment is increased and larger roll motion results compared with coupled roll and sway.

These results are helpful for considering the effect of restraint on roll behaviour.

Unfortunately, the model used in these tests was in the upright condition. The results cannot be used to compare with those presented by Marshfield [12-16].

To fill this gap and obtain some first-hand data about bias and restraint effects, two sets of experiments were conducted in Memorial University's wave tank.

The first set of tests, referred to as *Unrestrained Wave Test*, were conducted by loosely tethering the model only in drift and yaw with all other modes free.

The second set of tests, *Restrained Wave Tests*, were performed using the same model, M363, with same loading condition, but it was restrained in all degrees of freedom except for roll.

In both cases, the model was subjected to regular beam waves and with several bias conditions. The restraint condition of the model in these two sets of tests are quite different. So it was expected to give information not only on the effect of bias but also on the effect of restraint in some degrees of freedom of roll motion.

3.1 Unrestrained Roll Tests in Beam Waves

In this group of tests, the model was loosely tethered to restrain its motion in drift and yaw. The tethering was achieved by using a light nylon cord attached to the bow and the stern of the model at the level of its center of gravity. The other end of the cord was loosely tied to a bolt on the side wall of the tank. The tethering was such that the model was allowed to roll, heave, sway and pitch freely. This tethering is not only to produce some restraint but also to protect the instruments in the model and ensure the reliability of data measured. In these experiments the rolling angles were measured using a gyroscope.

The model M363 possesses the highest freeboard of all the three models used in

the free roll tests. It was roughly estimated from trial tests that the models M365 and M366 would be swamped if they were used in these tests. Even for M363 it was doubtful that the model could stay dry for the waves with a nominal wave height of 6 cm. In addition, the model M363 has a typical fishing vessel hull form (hard chine, skeg, etc.). For these reasons, the model M363 was chosen for this group of tests.

Four bias conditions plus the upright condition were tested. In these conditions, the bias angles used were 4.1 degrees and 7.99 degrees, towards and away from the wave source (wave maker). The bias angle was checked and confirmed in two ways. One is by employing a digital inclinometer to read the heel angle directly. The other is through the gyroscope.

A wave probe was set up at a location 2.25 meters away from the model in the direction towards the wave maker to measure the waves. The roll motion was measured with a gyroscope. Both the gyroscope and the wave probe were carefully calibrated before starting the tests every day. The signal obtained from the gyroscope and the probe was sent through a filter and then recorded on an IBM P.C.. The P.C is equipped with special plotting software which gives the experimenter a simultaneous observation of the waves at the probe and response of the model from the recordings.

The wave maker, a closed loop device, is capable of producing both regular and irregular waves. For making regular waves, the wave maker receives a sinusoidal function from a simple function generator. Once the wave height and frequency are given to the function generator, the wave maker, theoretically speaking, should produce a regular wave with the given wave height and frequency. Unfortunately it

does not. The frequency has a nonlinear effect on the wave height. Whenever the frequency is changed to another value the wave height will shift as well even though it was fixed at the same nominal value. The proper wave height can be obtained by means of trial and error.

The nominal wave heights were 4, 5 and 6 cm. In all 10 wave frequencies were used. They were 0.33, 0.37, 0.41, 0.43, 0.45, 0.47, 0.49, 0.55 and 0.59 (in Hz). The frequencies were chosen so that they could cover the resonant, subresonant and superresonant ranges, and more frequencies were arranged in the resonant region. In this way, sufficient data can be collected for the resonant region to determine the peak value of roll amplitudes. The waves which were used in the tests of five bias conditions are shown in Figures 3.1 through 3.5. In the caption of these figures, the positive and negative bias angles represent the bias towards and away from the wave source respectively.

The recording time must be carefully determined. If it is set too long the reflecting waves would change the characteristics of the waves. The data may not be sufficient for analysis if too short a recording time is given. The wave tank is only 58 meters long. From the relation between propagation speed of waves ,V_W , and wave frequency, ω,

$$V_W = g/\omega$$

one is able to determine that V_W will be as much as $4.7m/s$ in the case of these tests. The model was set 10 meters away from wave maker. That means only 96 meters for the wave to propagate and reflect before it gets back to pass the model. A recording time of 20 seconds was chosen. This is longest time we can take before the waves reflect to the position of the model although it is, in the cases of large

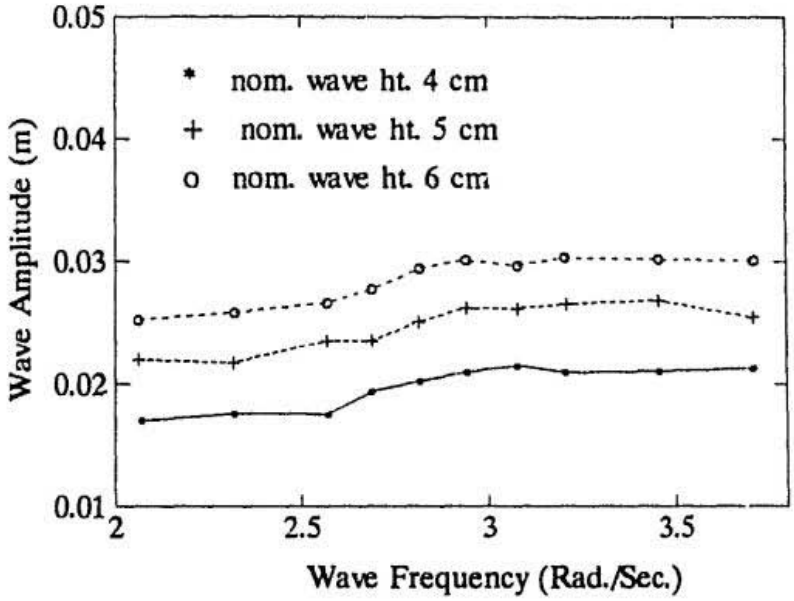

Figure 3.1: Wave Amplitudes and Frequencies, *No Bias Condition*

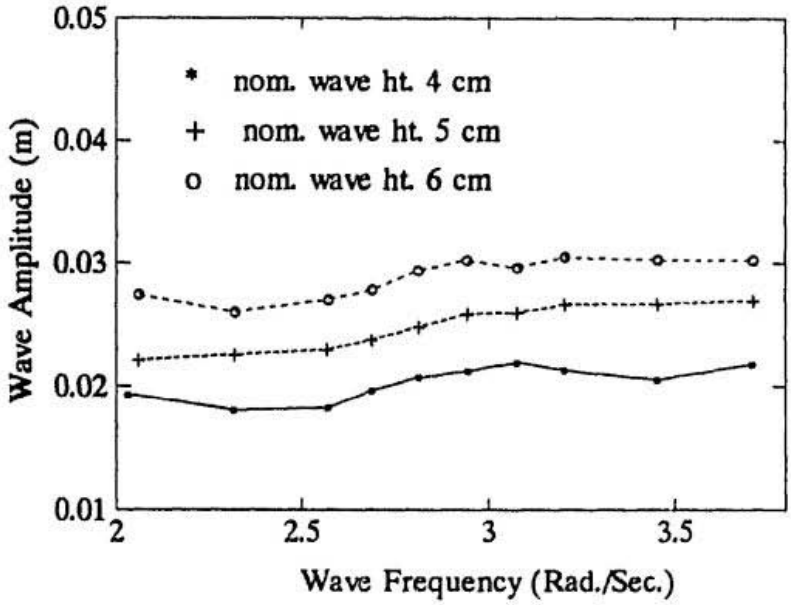

Figure 3.2: Wave Amplitudes and Frequencies, Bias Angle: 4.1°

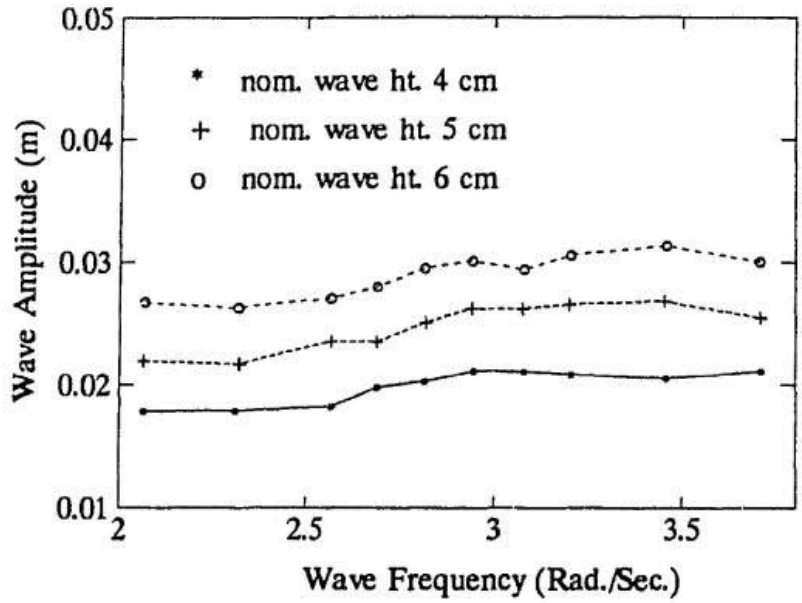

Figure 3.3: Wave Amplitudes and Frequencies, Bias Angle: −4.1°

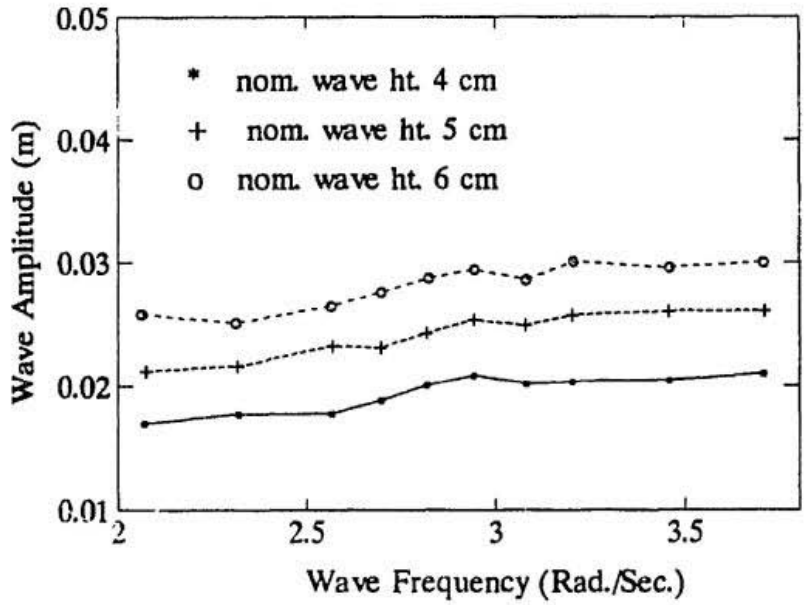

Figure 3.4: Wave Amplitudes and Frequencies, Bias Angle: 7.99°

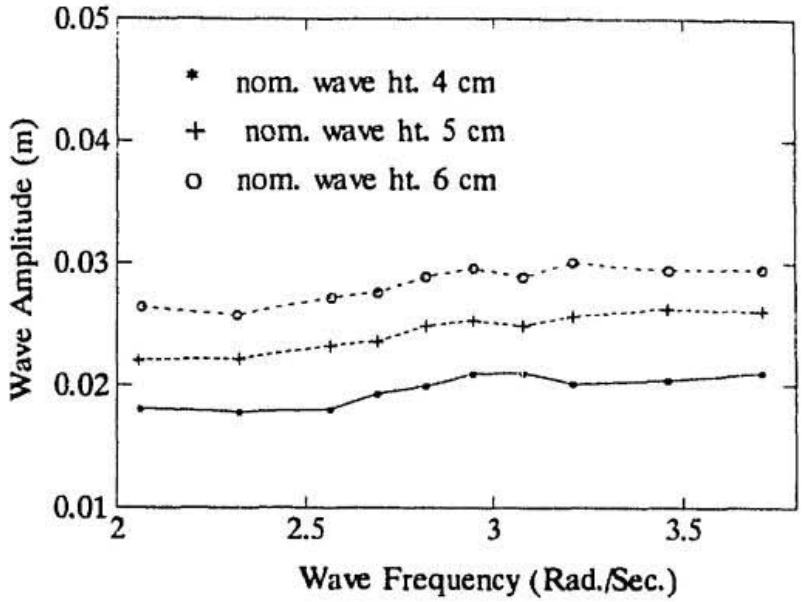

Figure 3.5: Wave Amplitudes and Frequencies, Bias Angle: $-7.99°$

waves, somewhat insufficient for the model to stabilize.

The test procedure is described as follows.

1. For each bias condition, including the upright condition, check and adjust bias angle to the desired value.

2. For each bias condition, choose a nominal wave height then give a wave frequency for each run.

3. Leave 10 minutes or more between two runs to let the water and the model calm down. Check the bias angle again when the model is still.

4. When the 10 runs are finished set the next wave height and repeat steps 2 to 4 until all three wave heights are tested.

A set of free roll decay tests and inclining tests were also performed just before the wave tests to measure the natural frequency and roll damping.

3.2 Restrained Roll Tests in Beam Waves

The model M363 was also used in these restrained tests. All degrees of freedom except for roll were restrained by using a pivot-shaft system. This system consists of a pivot, a rod, a linear bearing and a frame. The model is connected to the pivot with a platform which is fixed to the model with four bolts. Then the pivot is attached to the rod which goes is fixed to the frame. The rod is also fixed to the bearing with two clamps, one over the bearing, the other under it. The frame is fastened to the carriage. Thus the model is allowed to roll about the pivot but all other modes are restrained. The pivot position can be changed vertically and horizontally. The vertical position can be adjusted by moving the platform up or down. There is a row of holes in a transverse direction on the platform. These holes fit with the holes on the floor of pivot. Thus the horizontal position of the pivot can be shifted by choosing different pairs of holes on the platform.

The pivot position is one of the key points in the present tests. Roberts and Dacunha [32] suggested a way to decouple roll and sway. The separation can be approximately obtained by setting the coordinate center at point O . The vertical distance between O and the center of gravity G was given as

$$\overline{OG} = \frac{-A_{42}}{A_{22} + \rho\nabla}$$

where A_{42} denotes hydrodynamic added mass in roll due to sway (kg.m), A_{22} denotes hydrodynamic added mass in sway (kg), and $\rho\nabla$ represents model mass (kg).

For the restrained test, the vertical coordinate of the pivot was at the roll center O. Therefore, sway and roll are expected approximately to be decoupled.

Zou [33] performed a set of tests using M363 to study the couplings between roll and sway. The loading condition of M363 for Zou's tests is very close to that for the present experiments. The position of the *roll center* which Zou found, is about 0.3 cm below the center of gravity, is used in the present experiments.

To see the effect of the transverse positions of the pivot, two positions of the pivot were chosen in the present tests. One is denoted by O whose transverse coordinate is the same as that of the original center of gravity G; this position will be referred to as *Position 1*. The other denoted by O' has the same transverse coordinate as that of the new center of gravity G'; this position will be referred to as *Position 2*. The vertical coordinate of the pivot for both cases is the vertical coordinate of the *roll center* O which is 0.3 cm below the center of gravity. The horizontal position of the original center of gravity is in the center plane. The new center of gravity , G', can be calculated from the following equation.

$$GG' = \frac{W_b d}{\rho g \nabla}$$

where GG' is the horizontal distance between the original center of gravity G and new center of gravity G' (m), $\rho\nabla$ is the mass of the model (kg), and W_b is the movable weight (N.). d is the distance from original position of the movable weight W_b to its final position for the bias angle ψ (m) and can be expressed as

$$d = -\frac{\rho g \nabla GZ(\psi)}{W_b cos(\psi)}$$

When the weight W_b or the center of gravity is moved towards the wave source (the model's staboard side), d and GG' have negative values, but bias angle is defined to

be positive in this condition. Thus a negative sign appears in the above equation.

The difference between the results from these two pivot positions is expected to show the effect of horizontal position of the pivot. Also, the difference between the results obtained from the restrained and the unrestrained tests is expected to partly explain the effect of restraint.

To study the effect of bias direction, the model was first biased towards the wave maker then away from the wave maker, both at 7.5 degrees for the two pivot positions. To identify the different bias conditions and pivot positions, we use A1 and T1 to denote the conditions that the model is pivoted at *Position 1* and is biased away from and towards the wave source respectively, A2 and T2 denote the conditions that the model is pivoted at the *Position 2* and is biased away from and towards the wave source respectively. The wave tests for the model pivoted at roll center O and with the center of gravity at G were also performed. This condition is referred to as *No bias Condition* or *Upright Condition*.

The beam waves were generated at three different wave heights, at the nominal values of 3, 4 and 5 centimeters. There was a reduction of 1 centimeter compared with those used in the unrestrained wave tests. This was based on the consideration that the model would have a higher response than in the unrestrained tests. The freeboard was estimated to be not enough to keep the model from being immersed if 6 centimeters were chosen for the maximum nominal wave height. Ten frequencies were used for each wave height. They were chosen in a range of frequencies straddling the natural frequency of roll. The wave amplitudes and frequencies are shown in Figure 3.6 through Figure 3.10.

As explained in the last section, it is hard to keep the wave amplitude constant.

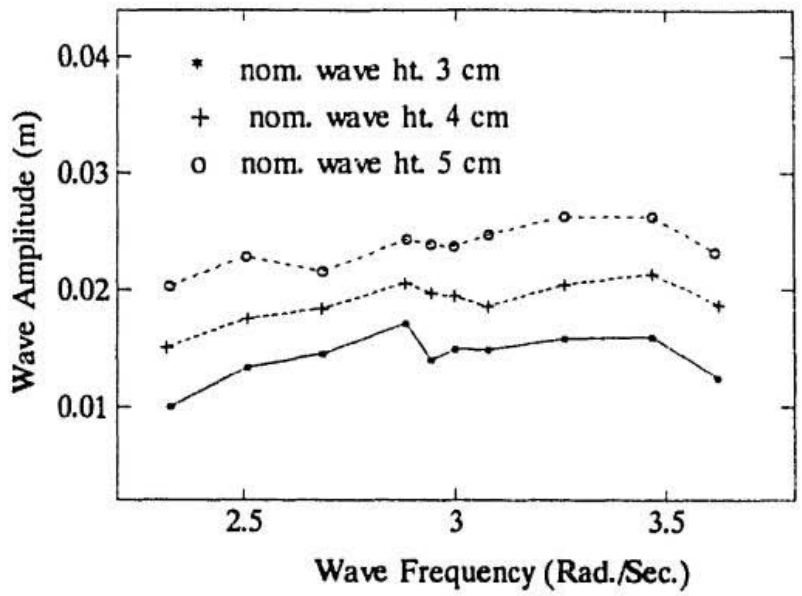

Figure 3.6: Wave Amplitudes and Frequencies, *No Bias Condition*, Restrained

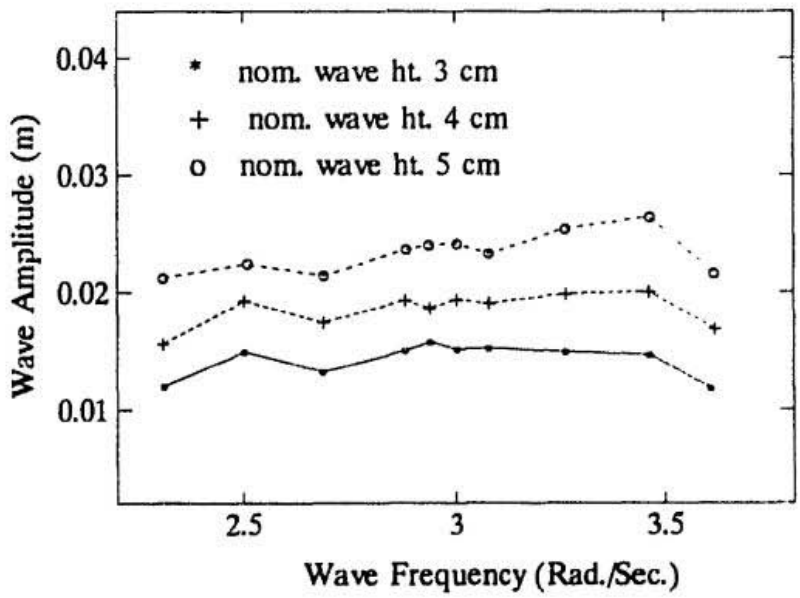

Figure 3.7: Wave Amplitudes and Frequencies, T1

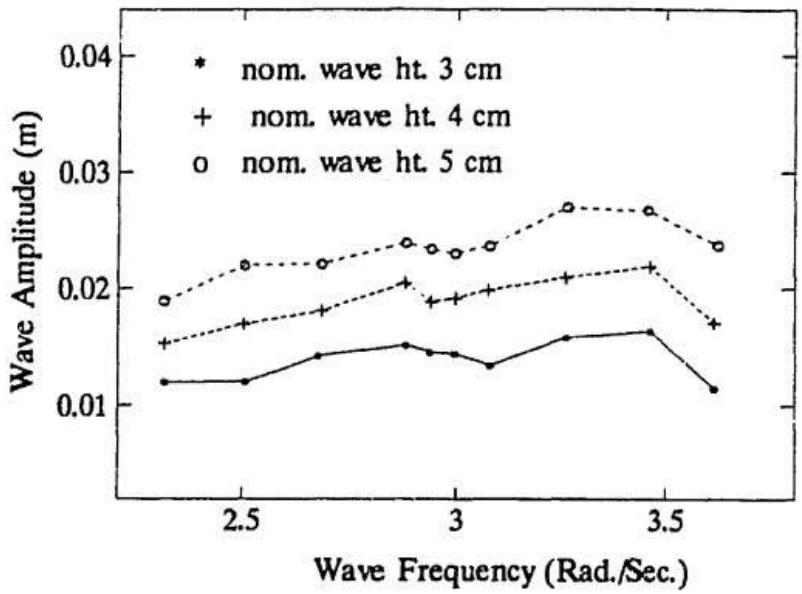

Figure 3.8: Wave Amplitudes and Frequencies, A1

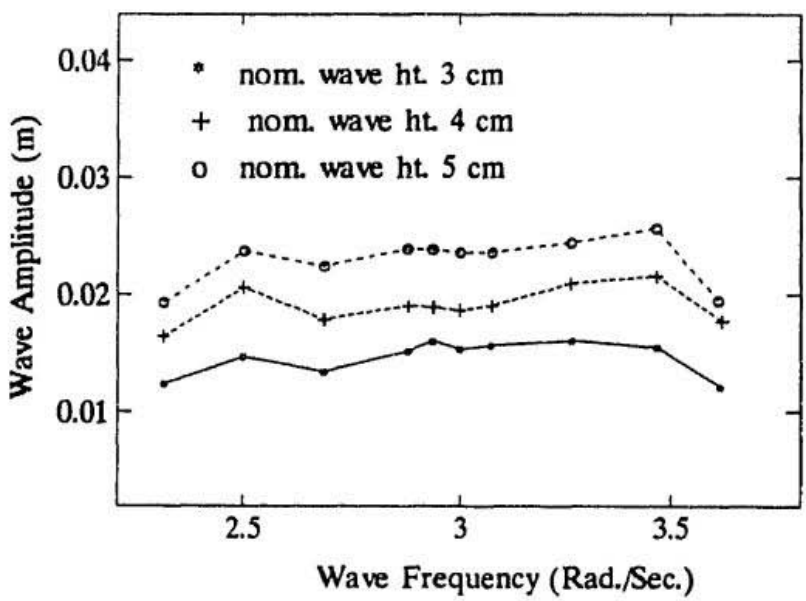

Figure 3.9: Wave Amplitudes and Frequencies, T2

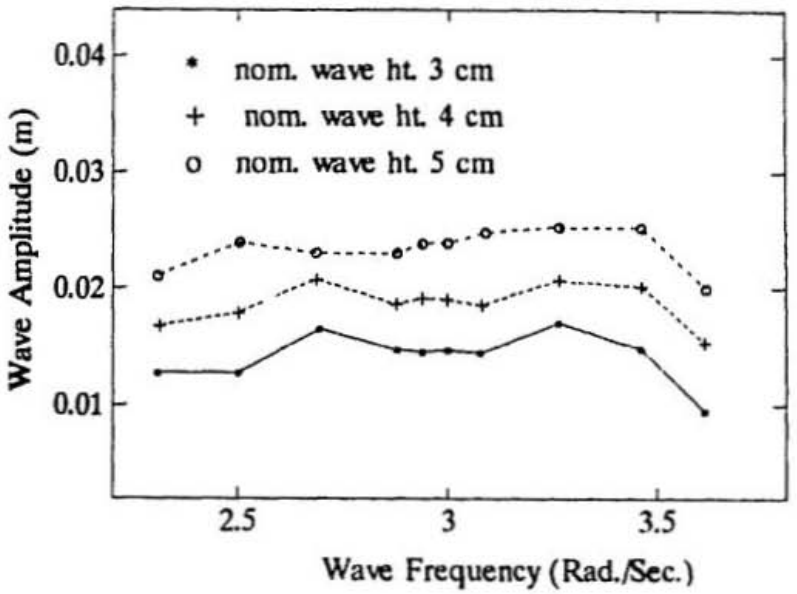

Figure 3.10: Wave Amplitudes and Frequencies, A2

In most cases shown in Figures 3.6 through 3.10, the variation of amplitude was up to twenty five percent. The analysis being presented in the section 3.4 is based on the real wave amplitudes shown in these figures.

A much longer time was required for the interval between two runs. If the water and model were not completely calmed down the bias angle would have been changed due to the relative heave and restraint. The response of the model to the waves was measured with a gyroscope. The waves were recorded through the wave probe as well. The tests followed the same procedure as described in the last section.

3.3 The Analysis Technique

Fourier analysis was used to obtain the frequency response of the model. The method described in reference [34] was applied in the present analysis. It is briefly described as follows.

It is assumed that the response of the model and the waves in general, contain up to two frequency components. The response, in the time domain, can be expressed as:

$$x_t = \psi + R_1 cos(\omega_1 t + p_1) + R_2 cos(\omega_2 t + p_2) + \epsilon_t \qquad (3.1)$$

where ψ is the mean. In the case of roll, it represents the mean angle; $R_1 cos(\omega_1 t + p_1)$ is the first component with amplitude R_1, frequency ω_1 and phase p_1; $R_2 cos(\omega_2 t + p_2)$ is the second component; R_2, ω_2 and p_2 are its amplitude, frequency and phase respectively. ϵ_t is the residual.

The recorded curves showed that the response data did have a second component although quite small. The phenomenon of two components mainly occurred at a frequency far away from the resonant frequency. In most cases, the amplitude of the second component is negligible.

Expanding equation (3.1) gives

$$x_t = \psi + A_1 cos\omega_1 t + B_1 sin\omega_1 t + A_2 cos\omega_2 t + B_2 sin\omega_2 t + \epsilon_t \qquad (3.2)$$

where t denotes the moments at which the data are collected; $t = 0, 1, \ldots, n-1$, and

$$A_1 = R_1 cos(p_1)$$

$$A_2 = R_2 cos(p_2)$$

$$B_1 = -R_1 sin(p_1) = R_1 sin(-p_1)$$

$$B_2 = -R_2 sin(p_2) = R_2 sin(-p_2)$$

The method of least squares can be used to identify the parameters ψ, A_1, A_2, B_1, B_2, ω_1 and ω_2.

The general idea of the method is to optimize the values of parameters by minimizing the sum of squares of the residual ϵ_t. The parameters can be divided into three subsets. The first subset only contains the constant ψ. The second consists of the amplitudes A_1, A_2, B_1 and B_2. The two frequencies, ω_1 and ω_2 comprise the last subset. The optimization with respect to the parameters in any one subset should be done under the condition of the remaining parameters being held fixed. When the optimization in one subset is finished the values of the parameters should be substituted into the next subset. Repeat the same procedure for the rest of the subsets until a complete cycle results in an effectively zero change in the function to be optimized. The function for optimization, $T(\psi, A_1, A_2, B_1, B_2, \omega_1, \omega_2)$ can be written as:

$$T = \sum_{t=0}^{n-1} [x_t - \psi - \sum_{j=1}^{2} (A_j cos\omega_j t + B_j sin\omega_j t)]^2 \qquad (3.3)$$

The first step is to optimize the constant ψ, bias angle, by holding all remaining parameters fixed.

$$\frac{\partial T}{\partial \psi} = -2 \sum_{t=0}^{n-1} [x_t - \psi - \sum_{j=1}^{2} (A_j cos\omega_j t + B_j sin\omega_j t)] \qquad (3.4)$$

Let

$$\frac{\partial T}{\partial \psi} = 0$$

One can obtain the ψ in terms of the remaining parameters. Substitute ψ back to equation (3.3) then optimize the amplitudes by fixing the frequencies ω_1 and ω_2.

$$\frac{\partial T}{\partial A_j} = -2\sum_{t=0}^{n-1} cos\omega_j t[x_t - \psi - \sum_{i=1}^{2}(A_i cos\omega_i t + B_i sin\omega_i t)] \tag{3.5}$$

$$\frac{\partial T}{\partial B_j} = -2\sum_{t=0}^{n-1} sin\omega_j t[x_t - \psi - \sum_{i=1}^{2}(A_i cos\omega_i t + B_i sin\omega_i t)] \tag{3.6}$$

where $j = 1, 2$. Again, let

$$\frac{\partial T}{\partial A_j} = 0$$

$$\frac{\partial T}{\partial B_j} = 0$$

One can obtain four linear equations for amplitudes A_1, B_1, A_2 and $B_2$and determine these parameters by solving these four equations. Then, following the same procedure, one can determine ω_1 and ω_2. In practice, the constant ψ can be approximated by

$$\frac{1}{n}\sum_{t=0}^{n-1} x_t$$

After finishing all the optimizations one can obtain the amplitudes and phases in (3.1) by:

$$R_1 = \sqrt{A_1^2 + B_1^2}$$

$$R_2 = \sqrt{A_2^2 + B_2^2}$$

$$p_j = \begin{cases} arctan(-\frac{B_j}{A_j}) & A_j > 0 \\ arctan(-\frac{B_j}{A_j}) - \pi & A_j < 0, B_j > 0 \\ arctan(-\frac{B_j}{A_j}) + \pi & A_j < 0, B_j \leq 0 \\ -\frac{\pi}{2} & A_j = 0, B_j > 0 \\ \frac{\pi}{2} & A_j = 0, B_j < 0 \\ arbitrary & A_j = 0, Bj = 0 \end{cases}$$

where $j = 1, 2$. A Fortran program by Dr. Bass, was written on the basis of the method described above. All the data for the unrestrained and restrained wave tests were analyzed using this program. After many trials for various frequencies, amplitudes and bias conditions it was evident that the second component is insignificant compared with the main component, the one with the wave frequency. Therefore, the results presented in the next section will show the main component only.

The results can be presented either in dimensional or nondimensional form. In the nondimensional representation, we have

$$\xi = \frac{\phi}{\eta_a K} \tag{3.7}$$

where ξ is nondimensional roll amplitude, ϕ is roll amplitude, K is wave number and η_a is wave amplitude,

$$K = \frac{\omega^2}{g} \tag{3.8}$$

where ω is wave frequency in radian.

Substituting (3.8) into (3.7) shows that the nondimensional roll amplitude is inversely proportional to ω^2 and η_a. Due to the reasons mentioned earlier in this

chapter, the wave amplitude is hard to be kept as a constant for different frequencies. Due to the nonlinearity in damping the relationship of roll response to waves is nonlinear. In other words, the roll angle is nonlinearly dependent on $\eta_a K$. In this case, using equation (3.7) to present response may not show the real characteristics of roll response. For this reason, the dimensional form will be used to present roll amplitude in the next section.

3.4 Results and Discussions

In this section, first of all, we shall present and discuss the results of roll damping and the natural frequencies which were obtained from the unrestrained and restrained roll decay tests. Then, the results of the unrestrained wave tests will be shown and briefly discussed. In the last subsection, we shall present the results of the restrained wave tests first; then discuss them by comparing them with those from the unrestrained wave tests.

3.4.1 Roll Damping and Natural Frequency

Before the wave tests, roll decay tests with the model M363 were performed for both unrestrained and restrained conditions. In the restrained condition, the roll decay tests were carried out with the pivot both at the *Position 1* and *Position 2*. The conditions of restraint and weight distribution for the roll decay tests were exactly the same as those for the wave tests. However, these conditions are slightly different from those for the tests described in Chapter 2. Because the analysis of the wave tests was based on the model's parameters measured from these roll decay tests the difference of loading condition between these tests and those in Chapter

2 will not influence the results and the discussion hereafter.

ζ_E and ω_d for the unrestrained condition are shown in Figure 3.11 and Figure 3.12 respectively. The average roll amplitude, ϕ_0, in these figures is the same as that defined in the Section 2.4. GM, in these tests was measured 2.90 cm.

The graphs in Figure 3.11 show that the dependence of ζ_E on ϕ_0 is linear. The graphs in Figure 3.12 indicate that ω_d, ω_ϕ, is almost constant. Comparing the graphs in Figure 3.11 with those in Figure 2.8 in the last chapter, one may note that a slight change in the center of gravity does not affect the roll damping very much. ω_d, on the other hand, is more sensitive to the weight distribution. It can be seen from the Figure 3.12 that ω_d increases. This is similar to the trend shown in Figure 2.22.

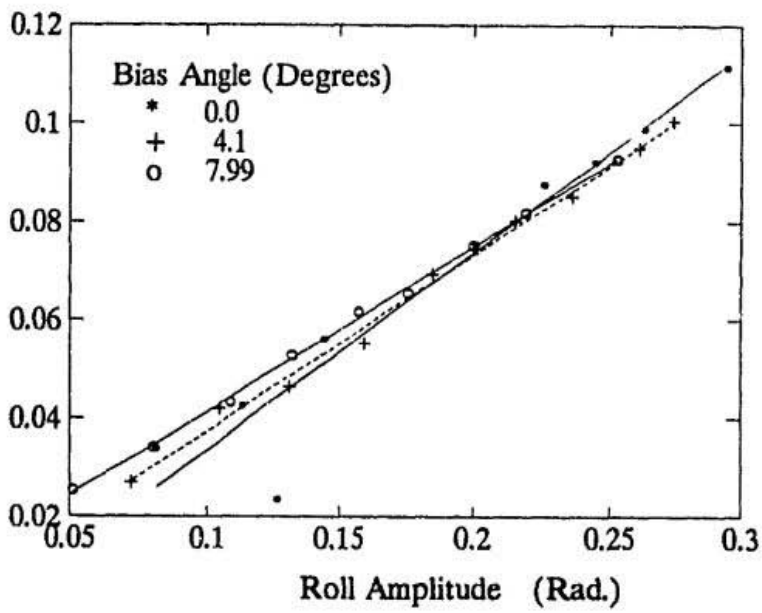

Figure 3.11: ζ_E for Unrestrained Wave Tests

ζ_E and ω_d from roll decay tests for the restrained wave tests are shown in Figure

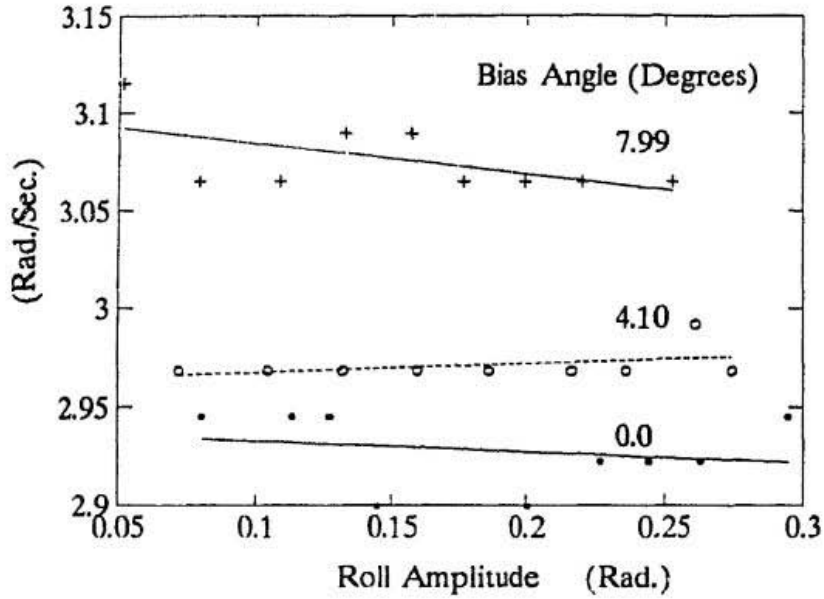

Figure 3.12: ω_d for Unrestrained Wave Tests

3.13 through 3.16.

ω_d for *Position 1*, Figure 3.15, is lower than that for *Position 2*, Figure 3.16. This can be explained by referring to the definition of ω_d in equations (2.26) which can be rewritten as

$$\omega_d = \sqrt{\frac{GM}{I}}\sqrt{\rho g \nabla (1 - \zeta_E^2)} \tag{3.9}$$

where

$$I = I_G + \rho \nabla r_G^2 + \rho \nabla p_G^2 + A_{44} \tag{3.10}$$

r_G and p_G in turn denote the transverse and vertical distance between the pivot and the center of gravity. For both *position 1* and *position 2*, we have

$$p_G = \overline{OG} \tag{3.11}$$

For conditions A1 and T1, because the pivot is placed at the *roll center* O and the model's center of gravity is moved to G', r_G is given by

$$|r_G| = GG' \tag{3.12}$$

For the *No Bias Condition*, because both the pivot position O and the center of gravity G are on the center plane; for the *Position 2* (A2 and T2) the pivot position O' and the center of gravity G' have the same transverse coordinate; thus, for the *No Bias Condition* and *Position 2*, we have

$$r_G = 0 \tag{3.13}$$

It is clear that I is larger for position 1 compared with that for position 2. At the end of the Section 2.5, it was indicated that GM for M363 increases with the increase in the bias angle. Because the bias angles are equal for both *Position 1* and *Position 2*, ω_d for *Position 2* is higher than that for *Position 1*. Compared with the ω_d for No Bias Condition, ω_d for *position 2* is also higher because their I are the same but *Position 2* has a larger GM due to its bias angle.

Figures 3.13 and 3.14 indicate that the slope of ζ_E, m (see equation (2.25) for the definition of m), with respect to ϕ_0 is larger for the conditions with bias compared with that for upright condition. This means that the viscous component of ζ_E for biased condition is stronger. The nonlinearity of the roll response in waves due to damping may be stronger for the biased condition (this will be evident later).

3.4.2 Frequency Responses of the Unrestrained Wave Tests

The results from unrestrained wave tests are shown in Figures 3.17 through 3.21. The negative sign for the bias angle in these figures means bias away from

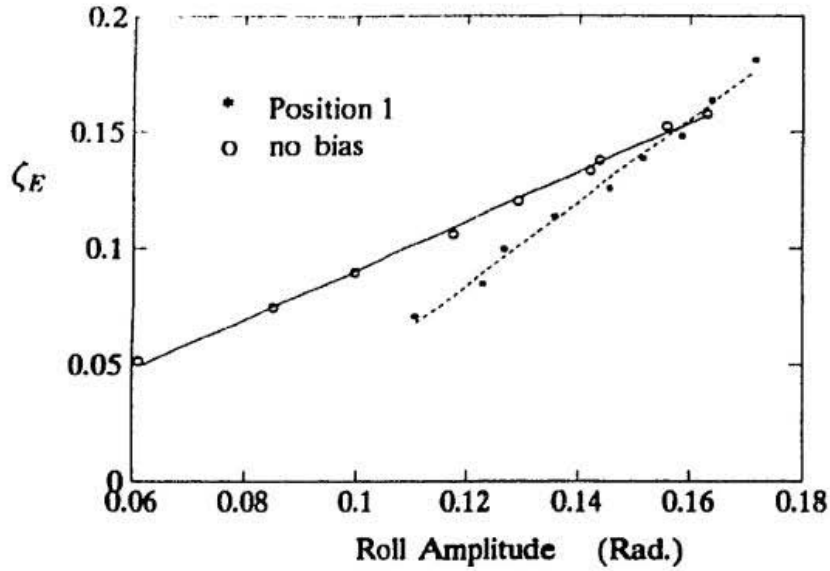

Figure 3.13: ζ_E for Restrained Wave Tests, Position 1

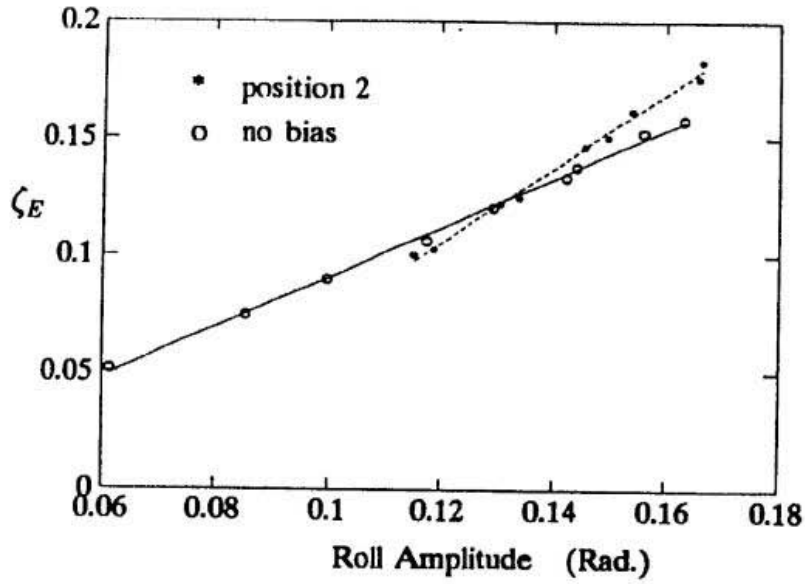

Figure 3.14: ζ_E for Restrained Wave Tests, Position 2

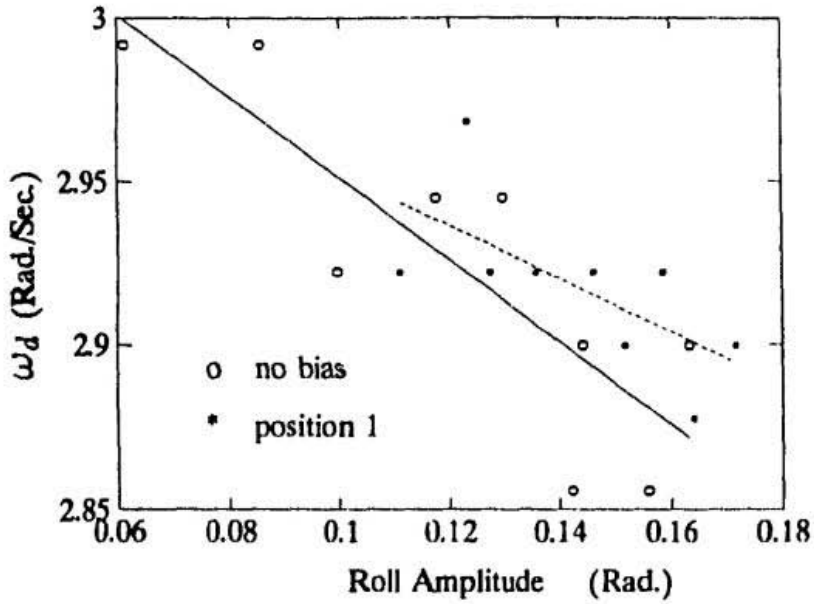

Figure 3.15: ω_d for Restrained Wave Tests, Position 1

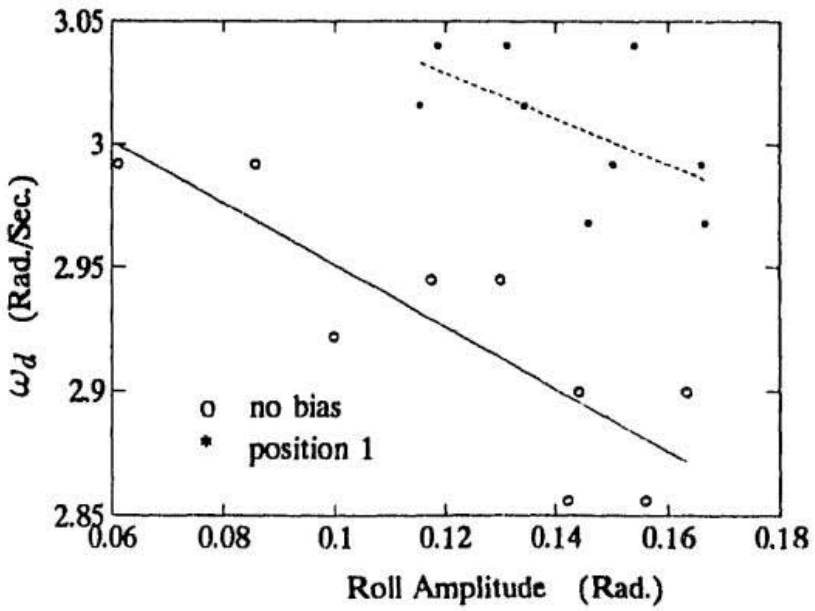

Figure 3.16: ω_d for Restrained Wave Tests, Position 2

wave source (wave maker). The bias towards the wave source is indicated by a positive sign.

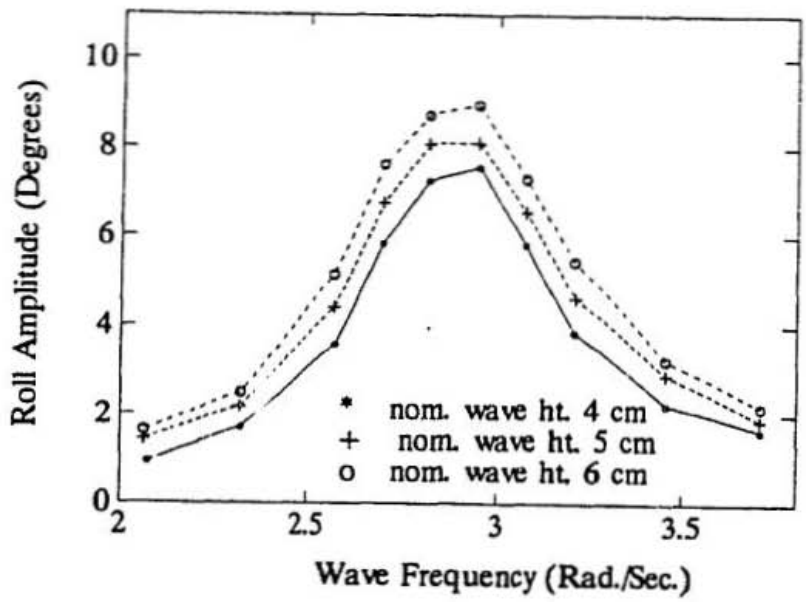

Figure 3.17: Unrestrained Roll Response in *No Bias Condition*

Comparing the graphs in Figure 3.17 with those in Figure 3.18 and 3.19, one may note that in the case of bias towards the wave source the peak values of response for the bias of -4.1 degrees is slightly larger than the rest. On the other hand, a slight, but steady increase in peak response with bias angle can be observed from the graphs for the condition of bias away from the wave source, shown in Figures 3.17, 3.20 and 3.21.

As mentioned at the beginning of this chapter, Marshfield [13] found that the peak of roll amplitude for the bias away from the wave source is higher compared with those for the rest conditions. In the case of bias angle of ± 7.99 (Figures 3.19 and 3.21), the results from the present tests support Marshfield's results. However,

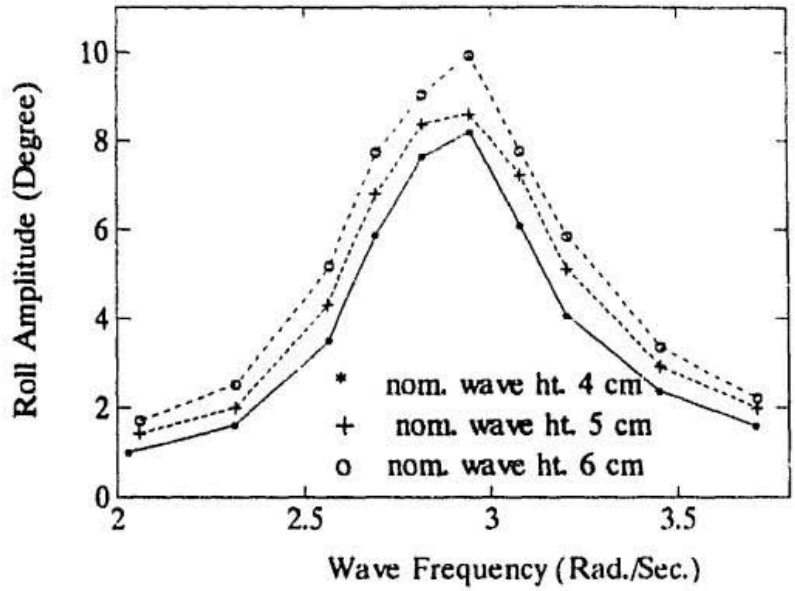

Figure 3.18: Unrestrained Roll Response, Bias Angle: 4.1°

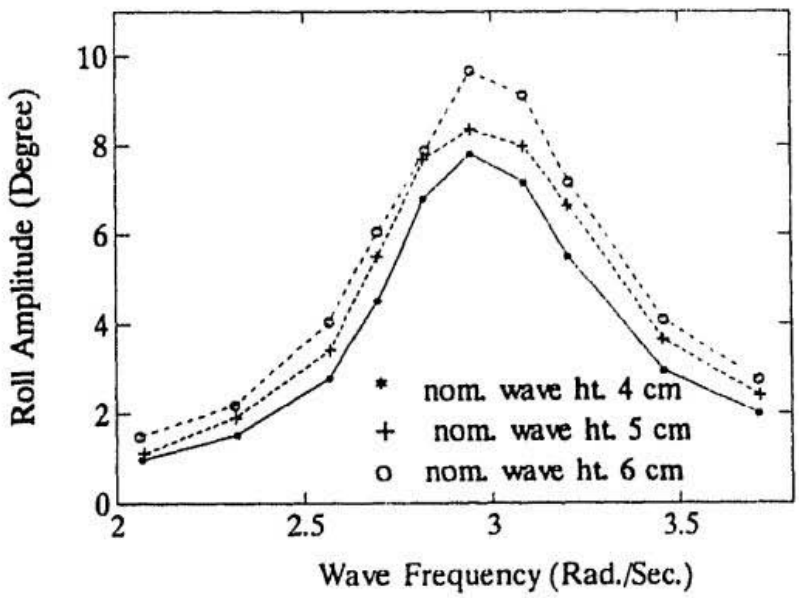

Figure 3.19: Unrestrained Roll Response, Bias Angle: 7.99°

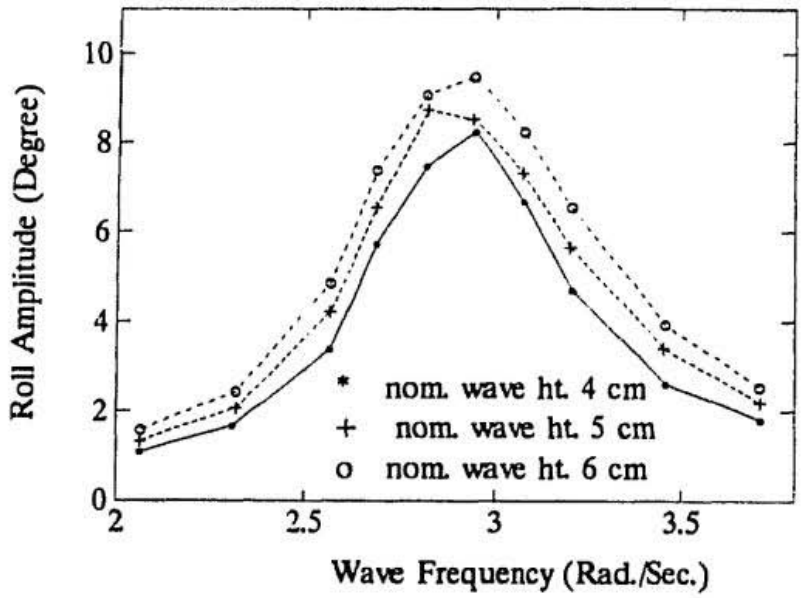

Figure 3.20: Unrestrained Roll Response, Bias Angle: $-4.1°$

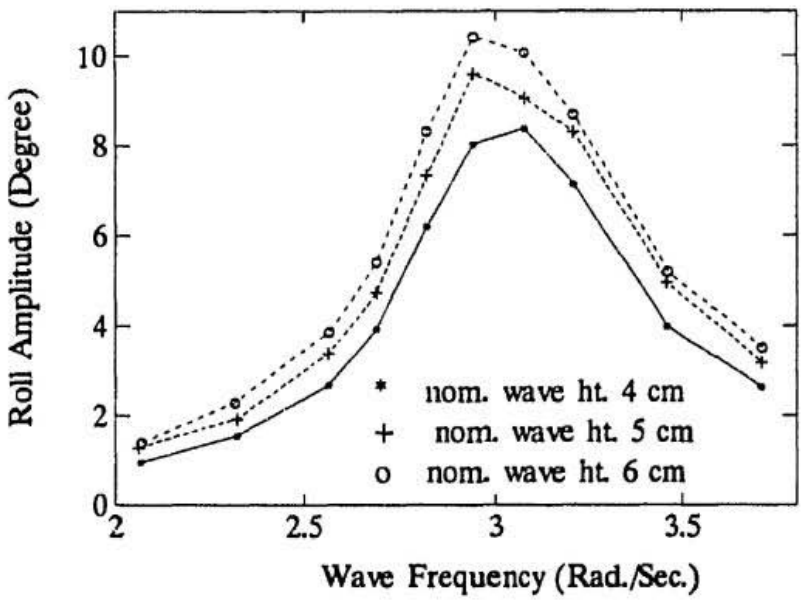

Figure 3.21: Unrestrained Roll Response, Bias Angle: $-7.99°$

the results from the case of bias angle of ±4.1 degrees with nominal wave height of 6 cm (Figures 3.18 and 3.20) in the present tests indicate that the roll amplitude is slightly higher when the bias is towards the wave source. The reason is not very clear, but the following factor may contribute to this difference. In the reference [13], the wave slope for the condition of bias towards the wave source is about 8 percent lower compared with the no bias condition and 10 percent lower compared with the bias away from the wave source. In the present tests, on the other hand, wave slopes for the three conditions (bias towards and away from the wave source and no bias condition) at given wave frequency and nominal wave amplitude are almost constant. (please refer to Figures 3.1 through 3.5 and 3.17 through 3.21). In addition, the experimental environment and the ship hull form may also play some role in the difference. Moreover, the wave amplitudes used in [13] are higher than those used in the present tests. The high wave amplitude usually brings a stronger nonlinearity to the response.

The frequency shift in the present tests is significant. Comparison of resonant frequencies in Figure 3.17 through 3.21 with the natural frequencies in Figures 3.12 indicates that the resonant frequency is shifted up to 5 percent towards the lower direction. This agrees with one of Marshfield's results [16]. Marshfield found that " the peak of the response (*Form 2*) occur at frequencies below the natural frequencies noted in the roll decay tests". Moreover, the wave frequency for the peak roll amplitude for the *no bias condition*, bias angles 4.1 degrees and 7.99 degrees in turn slightly increased (they are 2.90, 2.92 and 2.95 rad./sec. respectively). The effect of bias direction on the value of the resonant wave frequency seems to be very insignificant.

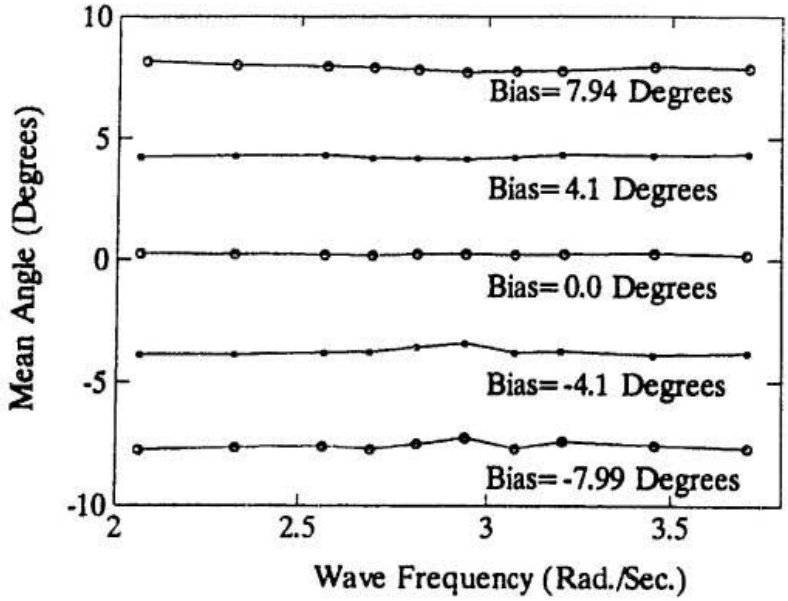

Figure 3.22: Mean Roll Angle from Unrestrained Wave Tests

The mean angles from experimental analysis are shown in Figure 3.22. These graphs correspond to the tests with waves of a nominal height of 5 centimeters. For other wave heights, the mean angles approximately have the same values. From the graphs in Figure 3.22, an interesting phenomenon can be observed. All the mean angles towards the wave source are increased and the bias angles away from the wave source are decreased. This could be due to the effect of the second order lateral wave force and the tethering in drift.

3.4.3 Frequency Responses of the Restrained Wave Tests

The roll amplitudes for the restrained condition, plotted against wave frequencies, are shown in Figure 3.23 through Figure 3.27.

The mean angles with wave frequencies are shown in Figure 3.28 and Figure 3.29. These mean angles, like those for unrestrained tests, are from the analysis

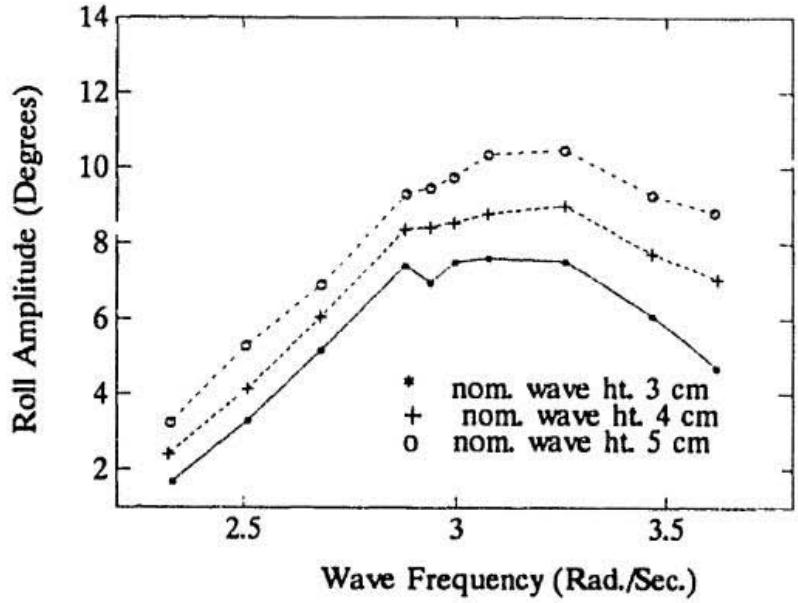

Figure 3.23: Roll Amplitude from Restrained Wave Tests, No Bias

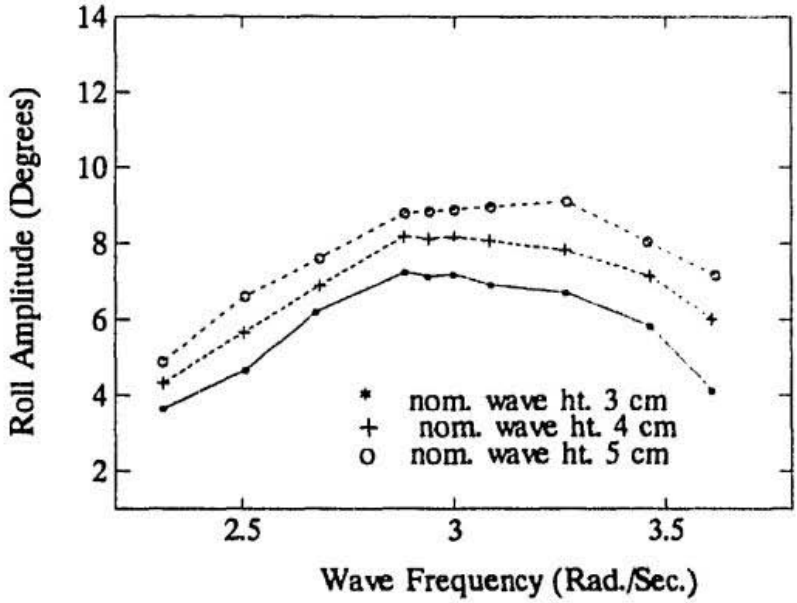

Figure 3.24: Roll Amplitude from Restrained Wave Tests, A1

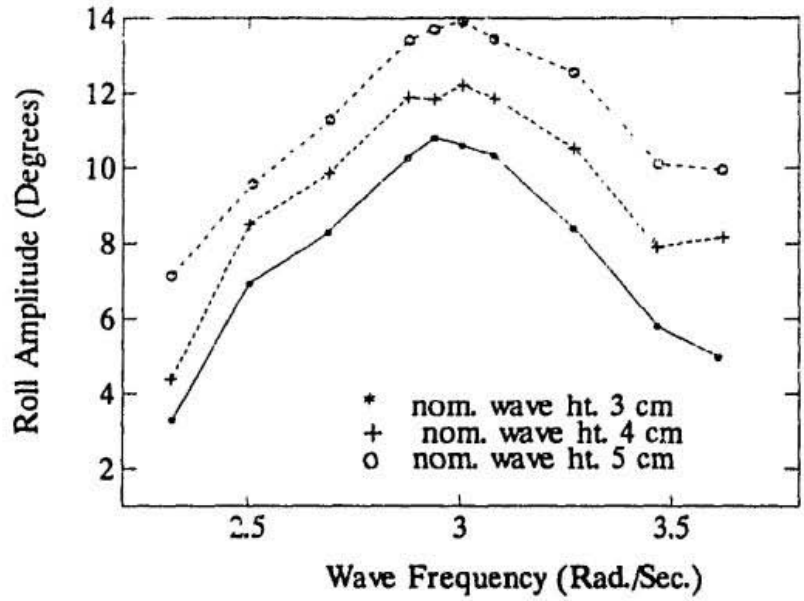

Figure 3.25: Roll Amplitude from Restrained Wave Tests, T1

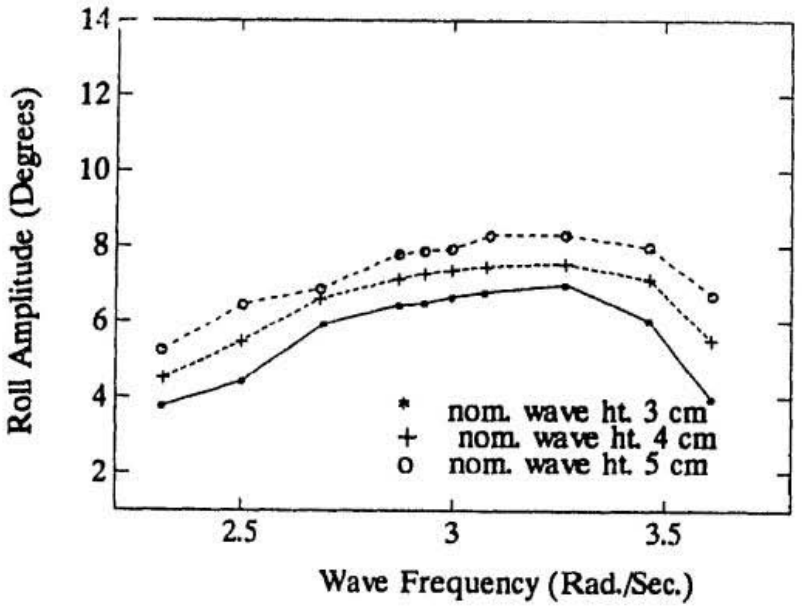

Figure 3.26: Roll Amplitude from Restrained Wave Tests, A2

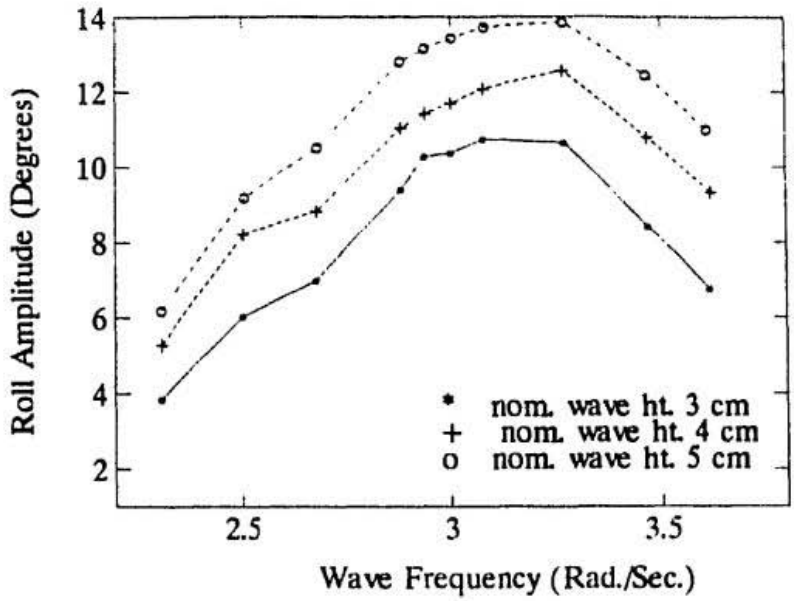

Figure 3.27: Roll Amplitude from Restrained Wave Tests, T2

of the recorded data. "Position 1" and "Position 2" in the figures means that the pivot was placed at *position 1* and *position 2* respectively.

The effect of wave direction on mean angles is not uniform as that in unrestrained wave tests. For *position 1*, the mean angles towards waves decrease with the increase in the wave frequency. The mean angles away from the wave source, decrease first, then increase a little. For the *position 2*, a similar tendency is shown.

Comparing the graphs in Figure 3.23 through Figure 3.27 with those in Figure 3.17 through Figure 3.21, one may see that the roll responses from the loosely tethered and the firmly restrained conditions are significantly different. Several features of the graphs in Figures 3.23 through 3.29 could be noticed.

1. Although the responses become larger in the resonant region the resonant phenomena are not so strong as those that occurred in the unrestrained wave

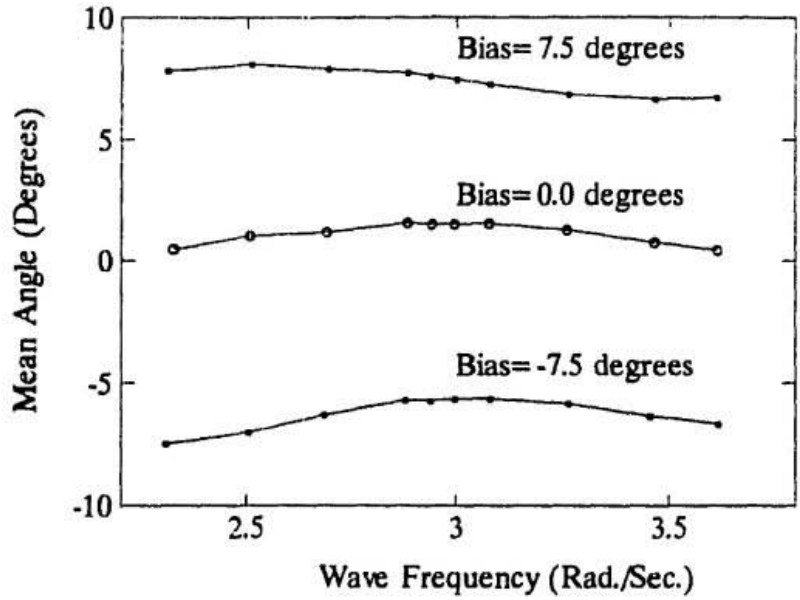

Figure 3.28: Mean Angle from Restrained Wave Tests, Position 1

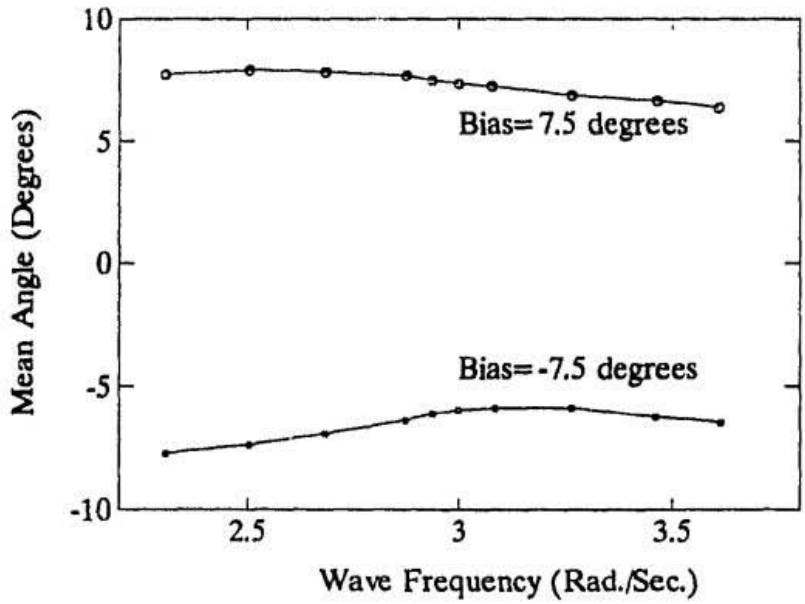

Figure 3.29: Mean Angle from Restrained Wave Tests, Position 2

tests; especially for the condition of bias away from wave source with the pivot at the position 2 (A2), the response shows a pretty flat variation with wave frequency.

2. The responses are clearly not symmetric about resonance. In addition, the responses at the frequencies higher than the resonant frequency are significantly larger than those on the other side of resonance.

3. Compared with the conditions of no bias and the bias away from the wave source, the bias towards the wave source gives higher response amplitudes, especially the peak values of roll amplitudes.

4. The difference between the results from the tests with the pivot at different positions, relatively speaking, is not very significant.

In the following, we shall discuss these features by comparing them with those for the unrestrained wave tests. When comparing the results from these two sets of wave tests, one should notice the difference of wave amplitudes for these tests. The nominal wave amplitudes used in the unrestrained wave tests are 4, 5 and 6 centimeters. Those for the restrained wave tests are 3, 4 and 5 centimeters. Thus, the roll amplitudes represented by *dot dash line* with "o" from unrestrained tests are comparable with those in *dash line* with "+" from restrained tests. In this pair of lines the corresponding nominal wave height is 5 cm. In the same way, the *solid line* for the unrestrained tests are paired up with the *dash line* for unrestrained tests; this group corresponds to the nominal wave height of 4 cm. This rule will be applied throughout the discussion related to these two sets of wave tests.

The following discussion will focus on the restrained and unrestrained tests both in the upright condition. Then the bias conditions will be considered. The comparison will be carried out mainly between the results from the unrestrained tests and those from the restrained wave tests with the pivot at *position 1*. If it is not specially mentioned the " restrained test" in the following comparison and discussion will refer to the restrained test with the pivot at *position 1*. The effect of pivot position will be discussed at the end of this section.

In the upright condition, roll responses from unrestrained tests, in Figure 3.17, are approximately symmetrical about the resonant frequency. On the other hand, the responses of the restrained model, in Figure 3.23, do not possess any symmetry. For the restrained tests, the roll amplitudes within super-resonant region are almost double those within the sub-resonant region. The frequency shift is also different. The peak value of roll amplitude of the restrained model occurred at a frequency between 3.07 rad./sec. and 3.28 rad./sec.. The natural frequency in this case, shown in Figure 3.15, is about 2.9 rad./sec.. This indicates that resonant frequency shifts from natural frequency to a higher frequency by a value of at least 0.17 rad./sec., about 5.8 percent. It was previously shown that the resonant frequency in the unrestrained tests in the upright condition was shifted, in the opposite direction, about 5 percent. The graphs in Figure 3.23 combined with those in Figure 3.6 show a nonlinear relationship between wave amplitude and response amplitude. The step between three wave amplitudes at the frequencies of 2.34 and 3.64 rad./sec. is approximately constant . However, the distance between three roll amplitudes at the frequency of 3.64 rad./sec. is much larger than that at frequency of 2.34 rad./sec..

Sellars [29] discussed the effect of sway restraint on roll motion. His results indicate that sway restraint could significantly increase roll amplitude. The results from Zou's tests [33] show that the restraint reduced the peak values of roll amplitude about ten percent. The resonant frequency was also 5 percent lower than the natural frequency. The features shown in Zou's results are rather different from those presented by Sellars.

In the present experiments, the vertical position of the pivot is at the supposed vertical " roll center ". The position of this roll center was estimated from Zou's calculation [33]. According to Zou [33], the damping cannot be decoupled even though the pivot is put at the roll center. This can be interpreted as that the effect of restraint in other modes on roll motion cannot be completely ignored. The restrained condition of the present tests is different from both Zou's and Sellar's. In their tests, the model was allowed to heave freely. In the present restrained wave tests, on the other hand, the heave, sway, yaw, pitch, drift and surge were all restrained. This special restrained condition may make some contribution to the roll amplitudes. However, the results from the present restrained tests seem to support Sellar's finding. The graphs in Figure 3.17 and Figure 3.23 show that the restraint results in a about twenty eight percent increase in the peak values of roll amplitude. Unfortunately, both Zou's and Sellar's results are based on the tests with an unbiased model. Thus no further comparison can be made.

The graphs in Figure 3.21 with those in Figures 3.24, and the graphs in Figure 3.19 with those in Figure 3.25 are approximately comparable because the difference in bias angle is only 0.49 degrees. The first group of graphs corresponds to the condition of bias away from wave source. The peak of roll amplitude from the

restrained wave tests is close to that from the unrestrained wave tests. The second group corresponds to the condition of the bias towards the wave source; the peak of roll amplitude from the restrained wave tests is about 5.2 degrees higher than that obtained from the unrestrained wave tests.

The comparison between the graphs in Figure 3.24 and that in Figure 3.25 indicates the effect of bias direction in the restrained condition. It is shown that the peak of the roll amplitude for bias towards the wave source is on average about 5.7 degrees higher than that for bias away from the wave source. This result is in contrast to that presented by Marshfield [13] who found that the model biased away from wave source experienced a higher roll amplitude.

Moreover, the roll amplitude for bias towards the wave source does not show explicit resonant phenomena. If considering the slight variation in wave amplitude, shown in Figure 3.7 and 3.8, one may note that the roll amplitudes vary with respect to the varying wave frequency.

For both biases away from and towards the wave source, a stable roll motion was observed during the tests (no capsize occurred). Marshfield [13], on the other hand, discovered that the roll motion for bias away from wave source was more stable.

Another two pairs of graphs can be compared to show the effect of the pivot position; one is from Figures 3.24 and 3.26, the other is from Figures 3.25 and 3.26. These graphs show that the difference is comparatively slight. The insignificant difference in roll amplitude between *position 1* and *position 2* may be explained by the very small shift of pivot position. The center of gravity was shifted, i. e. the distance between two pivot positions, only 0.5 centimeters for the bias of 7.5

degrees which is only 0.9 percent of the model's beam.

The reason for the different roll behaviour under different bias and restrained conditions is still not clear. One possible explanation may be that these asymmetric features are mainly due to the combination of effects of bias direction and restraints. The bias changes the relative position of ship hull in waves and makes it asymmetric. This results in an asymmetric distribution of water pressure. All the terms in the roll equation may be changed. The change in damping moment due to bias was indicated in Chapter 2. Restraint could also change the exciting moment, which was mentioned in reference [29]. In the present experiments, the restraint in heave changes the model's displacement as well as the values of GZ, consequently changes restoring moment. However, further conclusions cannot be made because of the lack of knowledge about the effects of bias and restraint on hydrodynamic forces.

Chapter 4

Numerical Simulation of the Asymmetric Motions

The experimental results presented in the last chapter show that the roll amplitudes are much larger when the model is biased towards the wave source than those when it is biased away from the wave source. This phenomenon is difficult to understand because a lot of factors, such as restraints, wave direction and coupling between roll and other modes may play some role. To further understand the phenomenon, a simulation will be presented in this chapter.

Bass [19], Féat and Jones [20] also did a study of asymmetric rolling motion using simulation. However, Féat and Jones, as was pointed out in Chapter 1, failed to predict the effect of bias direction which was considered to be an important feature of rolling motion of a biased ship in beam waves [19]. Bass, in his mathematical model [19], took into account the variation in GZ curve as well as the variation in displacement due to relative heave. However, it is difficult to estimate the relative heave if one does not solve the coupled heave-roll equation. On the other hand, the relative heave can be estimated to a reasonable degree of accuracy in the present study. Under the restrained conditions described in the last chapter, the ship

model M363 was firmly restrained in heave and sway. Hence, the relative heave is determined by the vertical motion of the waves. In addition, Bass, Féat and Jones did not take into account the hydrodynamic coupling effects of sway and heave into roll. Zou [33] found that even if a pivot is placed at the *roll center*, sway and roll cannot be completely decoupled. Unfortunately, he only studied roll-sway coupling. In the present study, we assume that roll and sway as well as roll and heave cannot be completely decoupled. The effects of the couplings are considered in this simulation even though the effects may not be very significant.

In this chapter, it is also assumed that the model is subjected to beam waves and is completely free in roll but restrained in all other modes. The mathematical model is developed to simulate the motions of a ship model biased towards and away from a wave source at 7.5 degrees heel and pivoted at two different positions. points O and O' (see Figure 4.1), which will be referred to as *Position 1* and *Position 2* respectively. *Position 2* has two positions; one is on the left of O, for the bias towards the wave source; the other is on the right of O, for the bias away from the wave source. When the pivot is at O (*position 1*) the motion of the model without bias is also simulated.

In the Figure 4.1, G denotes the model's center of gravity when it has no bias. G will be referred to as the *original center of gravity.* For the bias angle of 7.5 degrees, the model's center of gravity is moved from G to G'. G' will be referred to as *new center of gravity.* The *new center of gravity* G' also has two positions; one is on the left of G, for the bias towards the wave source; the other is on the right of G, for the bias away from the wave source. The distance between G and G' (i.e. $\overline{GG'}$ or $\overline{OO'}$) is about 0.5 cm. O is 0.3 cm below the original center of gravity G.

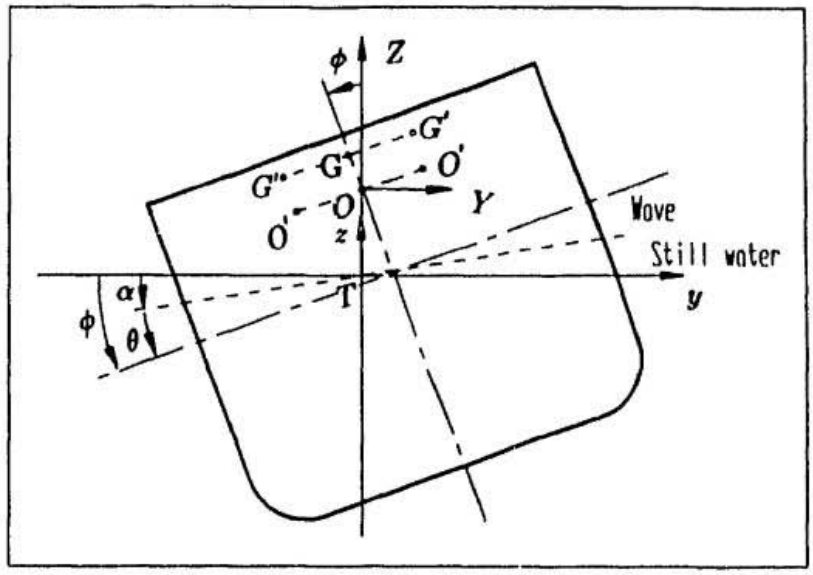

Figure 4.1: The Coordinate System

$\overline{OO'}$ is parallel to $\overline{GG'}$. The transverse coordinate of O is the same as that of the original center of gravity G for *Position 1* and the transverse coordinate of O' is the same as the new center of gravity G' for *Position 2*.

Following the definition in Chapter 3, for the *Position 1*, the condition will be referred to as "T1" when the ship model is biased towards the wave source; when it is biased away from the wave source the condition will be denoted by "A1". Similarly, for *Position 2*, "T2" and "A2" will in turn denote the conditions that the model is biased towards and away from the wave source. The motion of the model in no bias condition with the pivot at *Position 1* will be denoted by *No Bias Condition*.

4.1 Mathematical Model

Figure 4.1 shows the coordinate systems and the positive sense of the model's motion. The coordinate system yTz is used to describe waves. The coordinate system YOZ, for *position 1*, and $YO'Z$ (not shown in Figure 4.1), for *position 2*, are used to describe the model's sway and heave. The roll angle and bias angle have positive values when the model rolls or heels towards the wave source.

The relationship of coordinates yTz and YOZ (or $YO'Z$) is

$$y = Y$$

$$z = Z + \overline{OT}$$

where $\overline{OT}$ denotes the vertical distance between the pivot position O (or O') and water surface when the model is in upright condition.

If the model's upright condition is taken as the reference roll condition, following the equation presented in [19], the governing differential equation is of the form:

$$\begin{aligned} & I_G\ddot{\phi} - \rho\nabla p_G(\ddot{Y} - p_G\ddot{\phi}) + \rho\nabla r_G(\ddot{Z} + r_G\ddot{\phi}) \\ & + B_E(\dot{\phi} - \dot{\alpha}) + \rho g\nabla GZ(\phi - \alpha, \psi) + A_{44}(\ddot{\phi} - \ddot{\alpha}) \\ & + A_{42}(\ddot{Y} - p_G\ddot{\phi} - \dot{u}) + B_{42}(\dot{Y} - p_G\dot{\phi} - u) \\ & + A_{43}(\ddot{Z} + r_G\ddot{\phi} - \dot{v}) + B_{43}(\dot{Z} + r_G\dot{\phi} - v) \;=\; M \end{aligned} \tag{4.1}$$

The first term on the left side of equation (4.1) is the model's roll inertia moment about center of gravity, the second and the third terms are additional inertia moments due to heave and sway motions as well as the separation between the pivot position and center of gravity, the fourth and the fifth terms in turn are roll

damping moment and restoring moment about pivot position (O or O'), the sixth term is hydrodynamic added roll inertia moment, the last four terms represent the hydrodynamic effect of sway and heave on roll. In the above equation, B_E denotes the equivalent linear damping coefficient, ρ denotes effective water density; ∇ is the displacement volume of the model; A_{44} represents the hydrodynamic added roll moment of inertia, A_{42} and A_{43} are hydrodynamic added mass in roll due to sway and heave respectively, B_{42} and B_{43} are damping coefficients in roll due to sway and heave respectively; ψ denotes bias angle and ϕ is absolute roll angle of the model. α is the wave slope, M is an exciting moment due to the variation of displacement which is partly caused by restraint in heave. p_G and r_G in turn are the vertical and horizontal distances between the center of gravity and the pivot. In the coordinate system YOZ, for *No Bias Condition* we have

$$r_G = 0 \qquad p_G = \overline{OG} = 0.003 \quad (m)$$

For the conditions A1 and T1, they are

$$|r_G| = \overline{GG'} = 0.005 \quad (m) \qquad p_G = \overline{OG} = 0.003 \quad (m)$$

In the coordinate system $YO'Z$, for the conditions A2 and T2, we have

$$r_G = 0 \qquad p_G = 0.003 \quad (m)$$

u and v in equation (4.1) denote horizontal and vertical velocities of a particle in the wave; their derivatives with respect to time, $\dot{u}$ and $\dot{v}$, denote the acceleration of a particle in the wave; $\ddot{Y}$, $\dot{Y}$, $\ddot{Z}$ and $\dot{Z}$ in turn represent sway and heave acceleration and velocity of the roll center O (or O').

Let θ denote the relative roll angle. Thus, the relation of absolute roll angle ϕ, wave slope α and the relative roll angle θ is given by

$$\theta = \phi - \alpha \tag{4.2}$$

Substitute equation (4.2) into (4.1), $(\phi - \alpha)$ and its derivatives with respect to time in all the terms are replaced by θ and corresponding derivatives. The first three terms (in the first row) in equation (4.1) become

$$I_G\ddot{\theta} + I_G\ddot{\alpha} - \rho\nabla p_G\ddot{Y} + \rho\nabla r_G\ddot{Z} + \rho\nabla(\ddot{\theta} + \ddot{\alpha})(r_G^2 + p_G^2)$$

This can be rearranged as

$$I_0\ddot{\theta} + I_G\ddot{\alpha} + \rho\nabla(r_G\ddot{Z} - p_G\ddot{Y}) + \rho\nabla\ddot{\alpha}(r_G^2 + p_G^2)$$

where

$$I_0 = I_G + \rho\nabla r_G^2 + \rho\nabla p_G^2$$

Because the model is restrained in heave and sway Z, Y and their derivatives are zero. Thus, equation (4.1) can be rearranged as

$$\begin{aligned} I_0\ddot{\theta} + I_G\ddot{\alpha} + B_E\dot{\theta} + \rho g\nabla GZ(\theta,\psi) + A_{44}\ddot{\theta} \\ -A_{42}\dot{u} - B_{42}u - A_{43}\dot{v} - B_{43}v + \rho\nabla\ddot{\alpha}(r_G^2 + p_G^2) \\ +(\ddot{\theta} + \ddot{\alpha})(r_GA_{43} - p_GA_{42}) + (\dot{\theta} + \dot{\alpha})(r_GB_{43} - p_GB_{42}) \;=\; M \end{aligned} \tag{4.3}$$

Combine the first and the fifth terms of equation (4.3) and then divide the equation by $(I_0 + A_{44})$, equation is normalised as

$$\begin{aligned} \ddot{\theta} + 2\zeta_E\omega_n\dot{\theta} + \frac{\rho g\nabla}{I}GZ(\theta,\psi) - a_{42}\dot{u} - b_{42}u \\ -a_{43}\dot{v} - b_{43}v + \frac{\rho\nabla}{I}\ddot{\alpha}(r_G^2 + p_G^2) \\ +(\ddot{\theta} + \ddot{\alpha})(r_Ga_{43} - p_Ga_{42}) + (\dot{\theta} + \dot{\alpha})(r_Gb_{43} - p_Gb_{42}) \;=\; M_1 + M_2 \end{aligned} \tag{4.4}$$

where

$$a_{12} = \frac{A_{42}}{I} \qquad b_{42} = \frac{B_{42}}{I}$$

$$a_{43} = \frac{A_{43}}{I} \qquad b_{43} = \frac{A_{43}}{I}$$

$$I = I_0 + A_{44} \qquad \zeta_E = \frac{B_E}{2I\omega_n}$$

$$M_1 = -\frac{I_G}{I}\ddot{\alpha} \qquad M_2 = \frac{M}{I} \tag{4.5}$$

The last three terms on the left side of equation (4.4) can be omitted in approximate calculation because r_G and p_G are very small.

Equation (4.4) approximately describes the rolling motion of the model restrained in every degree of freedom except for roll. The roll motion of the model M363 under each different pivot and bias condition can be simulated by substituting the parameters in the equation with those determined in the next section. Solving this equation will give the relative roll angle θ. The absolute roll angle ϕ can be derived from equation (4.2) as

$$\phi = \theta + \alpha \tag{4.6}$$

4.2 Determination of the Parameters

In this section, all the parameters that appear in equation (4.4) will be derived or determined.

Firstly, consider the moments M_1 and M_2. Consider a two dimensional wave travelling in y direction, the direction away from the wave maker and at right angles to the model's longitudinal direction. Assume the wave profile has the form:

$$\eta_z(y,t) = \eta_a sin(ky - \omega t) \tag{4.7}$$

where η_a is wave amplitude, k is wave number, ω represents wave frequency.

The wave slope is given by

$$\begin{aligned} \alpha &= \frac{\partial \eta}{\partial y} \\ &= k\eta_a cos(ky - \omega t) \\ &= \alpha_m cos(ky - \omega t) \end{aligned} \tag{4.8}$$

where

$$\alpha_m = k\eta_a \tag{4.9}$$

In this study it is assumed that the wave is very long compared with the beam and draught of the ship model. In other words, the beam and draught of the ship model is negligible compared with the length of wave. Hence, we can assume $y = 0$ and $kz = 0$ when considering the wave forces acting on the ship model. This results in a simplification of the wave expression and its parameters:

$$\eta(t) = \eta_a sin(-\omega t) \tag{4.10}$$

$$\alpha = \alpha_m cos\omega t \tag{4.11}$$

$$\ddot{\alpha} = -\alpha_m \omega^2 cos\omega t \tag{4.12}$$

Substituting equation (4.12) into equation (4.5) gives

$$\begin{aligned} M_1 &= -\frac{I_G}{I}\alpha_m \omega^2 cos\omega t \\ &= -\alpha_e \omega^2 cos\omega t \end{aligned} \tag{4.13}$$

where

$$\alpha_e = \alpha_m \frac{I_G}{I} \tag{4.14}$$

M_2 is a moment due to the relative heave. Because the heave is restrained the motion of relative heave is just the vertical motion of the wave. A result of this wave motion is an increase in displacement given approximately by:

$$P_w = \rho g A_{wp} \eta(t) \tag{4.15}$$

where A_{wp} is the area of waterplane of the ship model for upright condition.

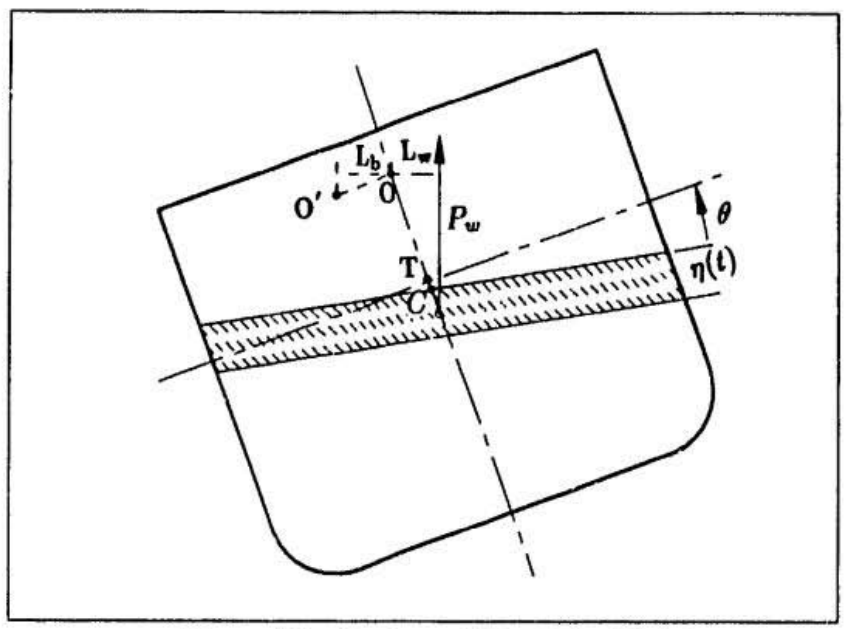

Figure 4.2: P_w, L_w and L_b of the Model

If we assume the center of gravity of the layer added due to relative heave is approximately on the center plane, the arm of the moment M_2, by referring to Figure 4.2, can be generally approximated by

$$L_w = (\frac{1}{2}\eta(t) + \overline{OC})sin\theta - L_b \tag{4.16}$$

where L_b is additional moment arm due to the transverse separation of the pivot position from the original roll center O. L_b for *position 1* (including *no bias condition*) and *position 2* are 0 and $\overline{OO'}cos\theta$ cm respectively. When the pivot is moved in Y direction L_b has a positive value.

$\overline{OC}$ can be approximated by (refer to Figure 4.1):

$$\overline{OC} = \frac{\overline{OT}}{sin(\frac{\pi}{2} - \theta)} sin(\frac{\pi}{2} - \alpha) = \overline{OT}\frac{cos\alpha}{cos\theta}$$

Thus, M_2 is written as

$$\begin{aligned} M_2 &= \frac{M}{I} = \frac{P_w L_w}{I} \\ &= \frac{\rho g A_{wp}}{I}\eta(t)[(\frac{1}{2}\eta(t) + \overline{OC})sin\theta - L_b] \end{aligned} \tag{4.17}$$

The vertical and horizontal components of wave velocities and accelerations can be derived from the wave velocity potential. The wave velocity potential which satisfies Laplace's equation and wave profile in equation (4.7) is given by

$$\Phi = -\frac{\eta_a g}{\omega} e^{kz} cos(ky - \omega t) \tag{4.18}$$

Thus the horizontal velocity and acceleration are

$$\begin{aligned} u &= \frac{\partial \Phi}{\partial y}|_{z=0} \\ &= \frac{\eta_a g k}{\omega} sin(ky - \omega t) \\ &= \eta_a \omega sin(ky - \omega t) \end{aligned} \tag{4.19}$$

At $y = 0$, we have

$$u = -\eta_a \omega sin\omega t \tag{4.20}$$

$$\dot{u} = -\eta_a \omega^2 cos\omega t \tag{4.21}$$

Similarly, we can obtain the expression of wave vertical velocity and acceleration as following

$$v = \frac{\partial \Phi}{\partial z}|_{z=0} = -\eta_a \omega cos(ky - \omega t)$$

At $y = 0$, we have

$$v = -\eta_a \omega cos\omega t \tag{4.22}$$

$$\dot{v} = \eta_a \omega^2 sin\omega t \tag{4.23}$$

Restoring moment is given by

$$GZ(\theta, \psi) = GZ(\theta) + \overline{GG'} cos\theta \tag{4.24}$$

where

$$\overline{GG'} = -\frac{\rho g \nabla GZ(\psi)}{W_b cos\psi}$$

W_b, as defined in Chapter 2, is a movable weight; a heel angle can be obtained by moving W_b. and $GZ(\theta)$ is the restoring moment for *No Bias Condition*. According to equation (2.3) it is of the form:

$$GZ(\theta) = GM(\theta + \mu_1 \theta^3 + \mu_2 \theta^5) \tag{4.25}$$

The parameters GM, μ_1 and μ_2 are obtained from the GZ curve and inclining tests. As was previously indicated, the last term of equation (4.24) is due to the bias condition. It represents the effect of bias on restoring moment.

Finally, let us consider the effective water density ρ. Féat and Jones [20] investigated the *Smith Effect* due to the position of the ship on the wave. A brief outline is given.

Bernoulli's equation for the pressure can be expressed as

$$\frac{p}{\rho_0} + \frac{\partial \Phi}{\partial t} + gz = 0 \tag{4.26}$$

where ρ_0 is is water density.

According to equation (4.18) the middle term of equation (4.26) should be

$$\begin{aligned} \frac{\partial \Phi}{\partial t} &= -\eta_a g e^{kz} sin(-\omega t) \\ &= g e^{kz} \eta_a sin\omega t \end{aligned} \tag{4.27}$$

The variation in pressure can be derived from equation (4.26)

$$\begin{aligned} \frac{\partial p}{\partial z} &= -\rho_0 g[1 + k e^{kz} \eta_a sin\omega t] \\ &= -\rho_0 g(1 + e^{kz} \alpha_m sin\omega t) \end{aligned} \tag{4.28}$$

At $z = 0$ we have

$$\frac{\partial p}{\partial z}|_{z=0} = -\rho_0 g(1 + \alpha_m sin\omega t) \tag{4.29}$$

For the assumption of linear distribution of pressure, the variation of pressure should be

$$\frac{\partial p}{\partial z} = -\rho g \tag{4.30}$$

Comparing equation (4.29) with (4.30), we have

$$\rho = \rho_0(1 + \alpha_m sin\omega t) \tag{4.31}$$

The value of damping coefficient ζ_E shown in the last chapter can be used here. ζ_E is expressed in the form

$$\zeta_E = m\theta_0 + c$$

where θ_0 denotes the amplitude of the relative roll angle θ. m and c are determined by linear regression of the data shown in the last chapter.

Pivot Position	G		G'	T'	
Bias Conditions	No Bias	$\pm 7.5^o$	$\pm 7.5^o$	No Bias	$\pm 7.5^o$
a_{42}	0.83	0.774	0.774	-0.329	-0.397
b_{42}	0.183	0.153	0.153	-0.345	-0.385
a_{43}	0	∓ 0.0573	∓ 0.208	0	∓ 0.0573
b_{43}	0	∓ 0.31	∓ 0.861	0	∓ 0.31

Table 4.1: Coupling Coefficients

Bass estimated the coefficients of coupling terms, sway and heave into roll (i.e. A_{42} etc), by using software prepared by IMD of NRC [35]. The values of parameters a_{42}, b_{42} etc, the normalized values of A_{42} and B_{42} etc by $I = 2.52\ kgm^2$, are listed in Table 4.1. Table 4.1 has 6 columns, the second and the third columns are for

the condition with the pivot at original center of gravity G. The fourth column corresponds to the condition of pivot at new center of gravity G'. The last two columns are for the pivot at the point T, the intercrossing point of water line and the vertical plane parallel to the center plane which goes through the center of gravity G (or G'). Because the vertical pivot position in the simulation and the experiment (Chapter 3) is at a point between the water line and center of gravity, columns 2 and 5 give the range of the parameters (a_{42} etc.) for the no bias condition. Columns 3 and 6 give the range of the parameters for conditions A1 and T1, and columns 4 and 6 show the range for *Position 2* (A2 and T2).

Now, equation (4.4) can be solved numerically. A computer program based on the method of Runge-Kutta was written to solve this equation. A *Fourier Analysis Method* [34] then was applied to the time history of simulated roll motion to transfer the roll amplitude into frequency domain. The frequency response will be shown in the next section.

4.3 Results and Discussions

To simulate roll motions, particular values of the coupling coefficients (a_{42} etc.) are chosen for *No Bias Condition*, conditions A1, T1, A2 and T2. The values are chosen within the range shown in Table 4.1. The choice may not be precise, the effect will be discussed later in this section.

The results of simulation for *No Bias Condition* is shown in Figure 4.3. The lines denote the response values from simulation, and the discrete symbols," * ","+" and "o", present the experimental values of response. The solid line and " * " are for the response to the waves with nominal wave height 3.0 cm. Dash line and "+" are

for the wave with nominal heights 4.0 cm. Dash-dot line and "o" are corresponding to the wave with nominal height of 5.0 cm. This rule will also be applied to the graphs in Figure 4.5 through Figure 4.8.

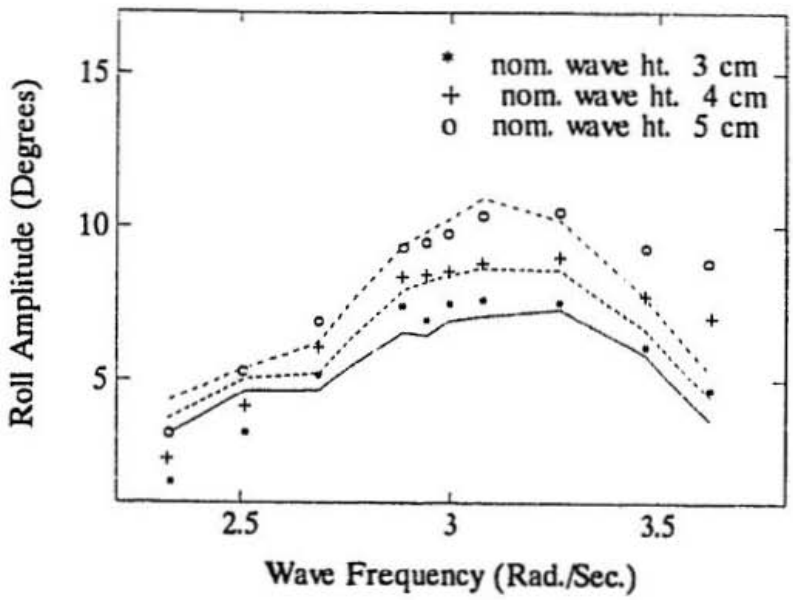

Figure 4.3: Roll Simulation for No Bias Condition

For the simulation of roll response of the model in the *No Bias Condition*, the values of coefficients of sway and heave into roll were chosen as following: a_{42} and b_{42} are 0.55 and 0.15 respectively. a_{43} and b_{43} are set to be zero because the model has no bias angle in *No Bias Condition*.

It indicates in Figure 4.3 that the simulation well reflects the tendency of roll amplitudes varying with wave frequency. However, the error is significant in the nonresonant regions, the largest error occurs at the wave frequency of 3.62 rad./sec. The reasons are complicated. One of them may be that the roll damping coefficient used in the simulation is the one measured from free roll tests with the same model

and shown in Figure 3.13. This damping coefficient corresponds to the model's damped natural frequency. As discussed previously, the damping varies with frequency. In the nonresonant regions, the model rolls at wave frequencies which are different from the model's damped natural frequency. Therefore, the use of the same damping for all frequencies is not proper. Unfortunately, only the damping coefficient for a given natural frequency can be obtained under a defined load distribution.

Another reason for the error may be the inaccuracy in the estimation of the coefficients b_{42}, etc.. Moreover, equation (4.1) itself only is an approximate description of coupled roll motion.

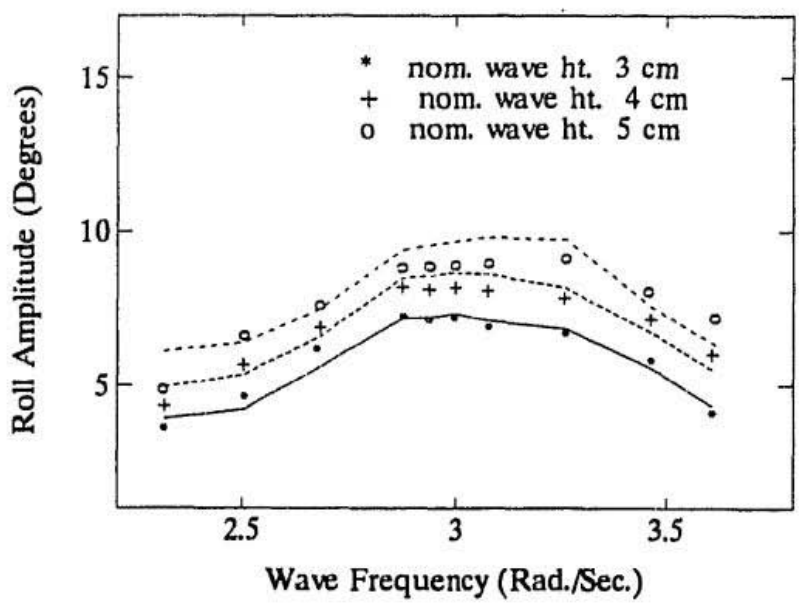

Figure 4.4: Roll Simulation for Condition A1

For *Position 1* (conditions A1 and T1), a_{42} and b_{42} are set the same values as those used in the simulation for *No Bias Condition*, but a_{43} and b_{43} are in turn

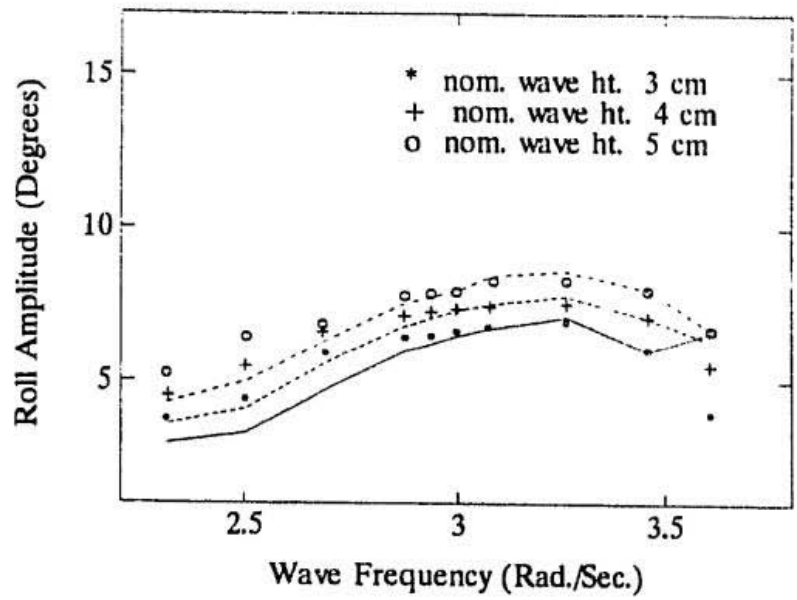

Figure 4.5: Roll Simulation for Condition A2

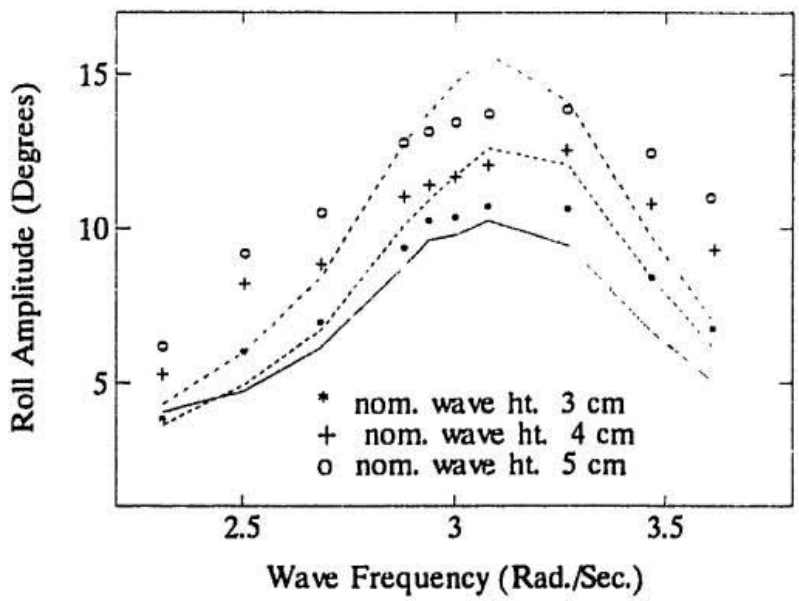

Figure 4.6: Roll Simulation for Condition T1

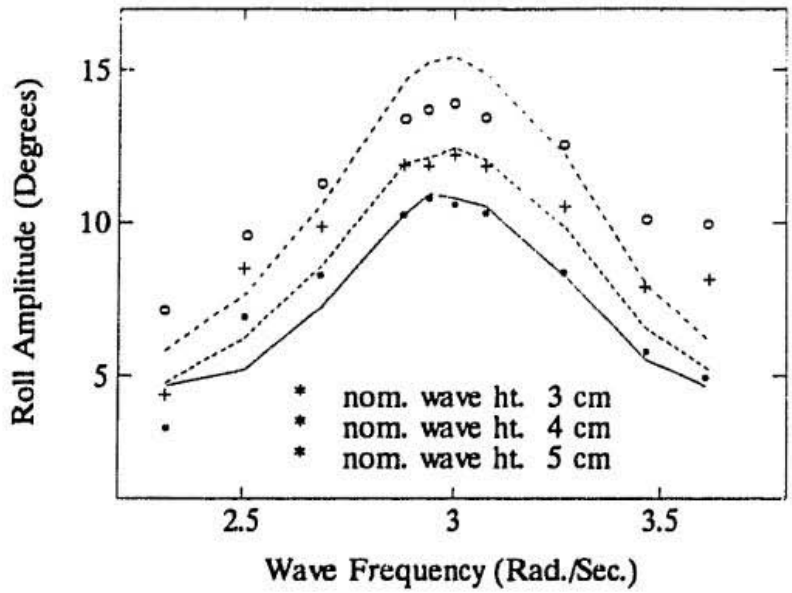

Figure 4.7: Roll Simulation for Condition T2

changed to 0.05 and 0.25 for A1 and -0.05 and -0.25 for T1 because the model is biased at 7.5 degrees in this case. For *Position 2* (conditions A2 and T2), the same values of a_{42} and b_{42} as those in the simulation for *Position 1* are kept. a_{43} and b_{43}, according to Table 4.1, are slightly changed to 0.15 and 0.55 for A2 and -0.15 and -0.55 for T2 respectively. The simulated roll amplitudes plotted against wave frequencies are shown in Figures 4.4 through 4.7.

These simulations preserved the characteristics of roll amplitude for different bias conditions. Under the condition of the ship model biased towards the wave source the simulation also produces larger roll amplitudes compared with those when the ship model is biased away from the wave source. As with the simulation of the response of the ship model in *No Bias Condition*, the simulated roll amplitudes for conditions T1 and T2 are also lower than the experimental values in the regions

of large wave frequencies. However, the simulated values for conditions A1 and A2 show a good agreement with the experimental values.

It is indicated by both experimental results, Figures 3.21 through 3.25, and simulated results, Figures 4.3 through 4.7, that the roll amplitudes for the conditions T1 and T2 are much higher than those for the other conditions. To study the reasons for this phenomenon a group of calculations was done with particular values of the coupling coefficients a_{42}, etc.

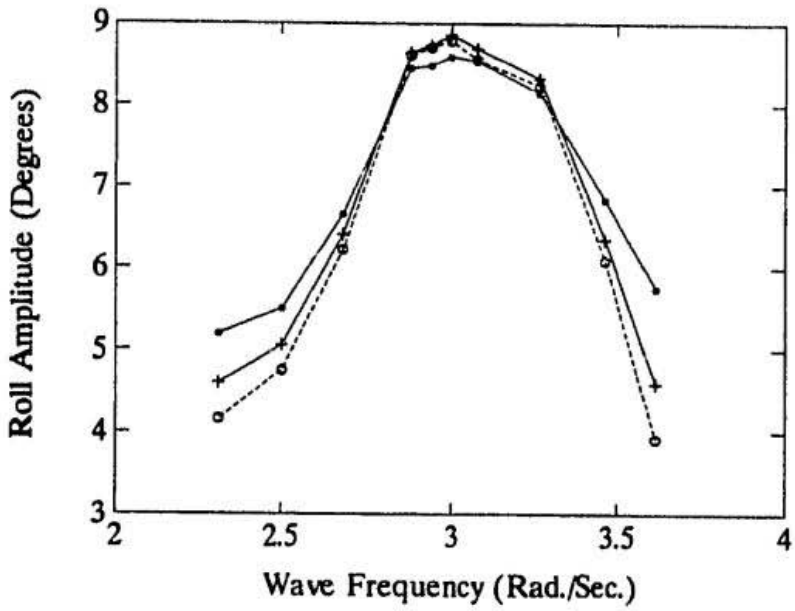

Figure 4.8: Effects of a_{42} and b_{42}, A1

Figures 4.8 through 4.11 show the effect of a_{42} etc. on simulated roll amplitudes for the nominal wave height of 4 cm. All the lines in these figures are obtained with a_{43} and b_{43} fixed to be zero, but with changing values of a_{42} and b_{42}. The solid line with " * " denotes the roll amplitude with $a_{42} = 0.774$ and $b_{42} = 0.153$, the maximum values of these two coefficients in Table 4.1. The dash line with "o" is

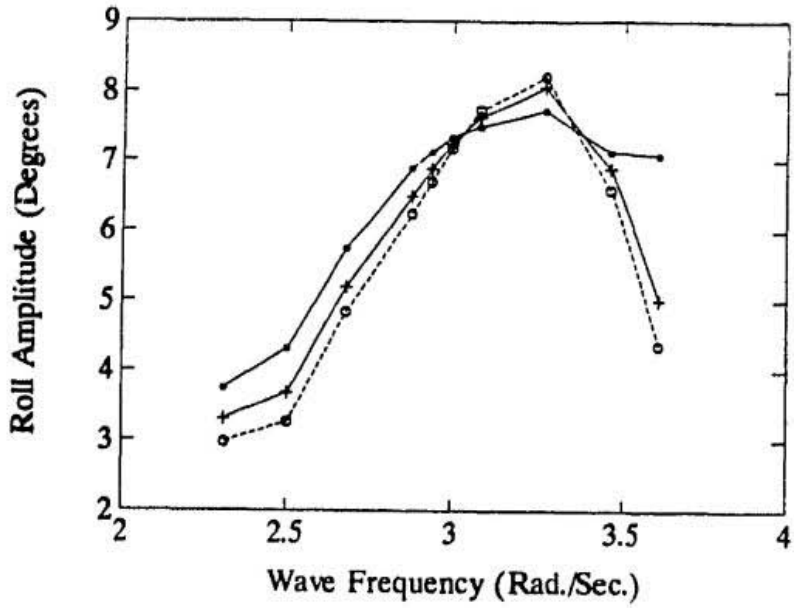

Figure 4.9: Effects of a_{42} and b_{42}, A2

obtained with $a_{42} = -0.397$ and $b_{42} = -0.385$, the minimum values of a_{42} and b_{42}. The solid line with "+" is the results with $a_{42} = b_{42} = 0$.

For conditions A1 and A2, the graphs in Figures 4.8 and 4.9 indicate that the effect of a_{42} and b_{42} is significant in the nonresonant regions; the largest difference in the simulated roll amplitudes for maximum and minimum values of a_{42} and b_{42} reach 2.7 degrees (at wave frequency of 3.61 rad./sec., Figure 4.9). In the resonant region, on the other hand, the simulated roll amplitudes are quite close to each other, the largest difference is only 0.5 degrees, and occurs at wave frequency of 3.26 rad./sec. (Figure 4.8). This means that change in the values of a_{42} and b_{42} does not affect roll amplitude very much in the resonant region for the conditions A1 and A2. These graphs also show that the effect of a_{42} and b_{42} is strongly nonlinear; i.e., the larger values of a_{42} and b_{42} result in higher roll amplitudes in the

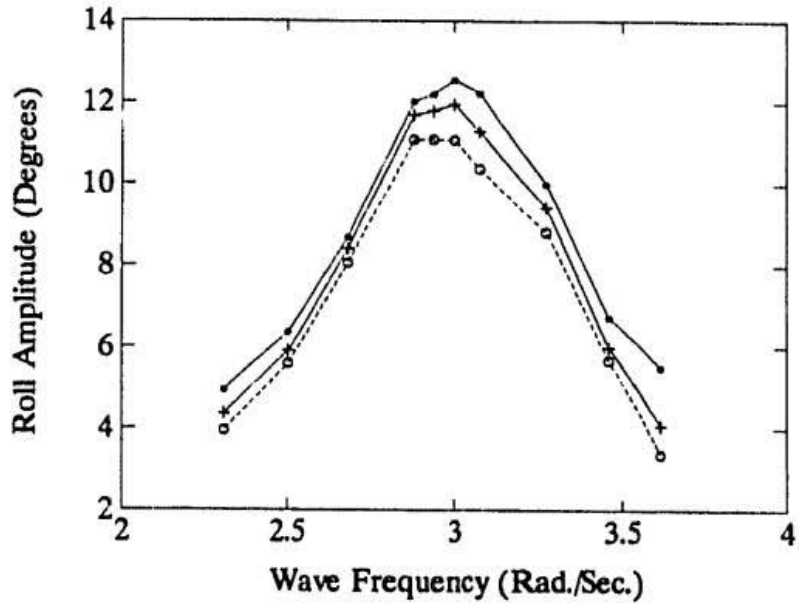

Figure 4.10: Effects of a_{42} and b_{42}, T1

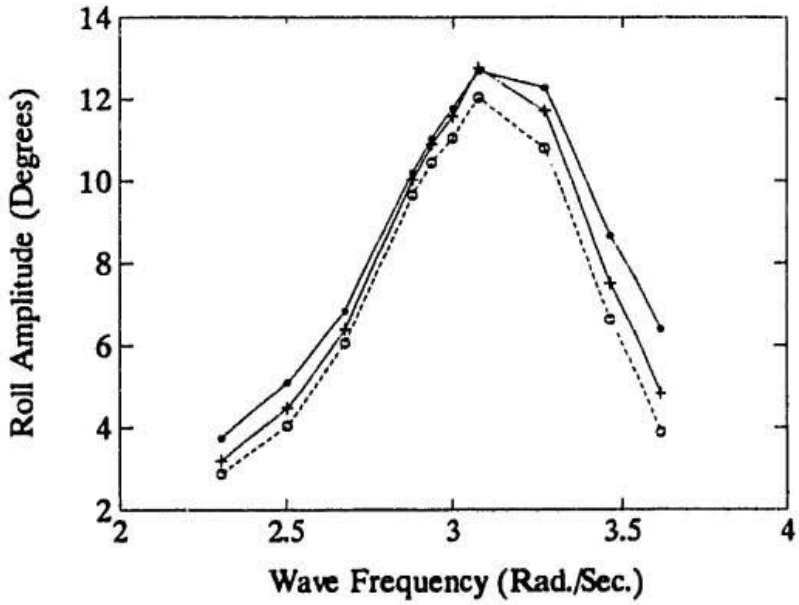

Figure 4.11: Effects of a_{42} and b_{42}, T2

nonresonant regions, but relatively low roll amplitudes in the resonant regions. The roll amplitudes for $a_{42} = b_{42} = 0$ fall between those for maximum and minimum values of a_{42} and b_{42}.

For conditions T1 and T2 (Figures 4.10 and 4.11), the roll amplitudes increase with the increase of the values of a_{42} and b_{42}. In the resonant region the largest difference in roll amplitudes for the maximum and minimum values of a_{42} and b_{42} is 1.7 degrees (at wave frequency of 3.08 rad./sec., Figure 4.10). This value is slightly smaller than that for the conditions A1 and A2. In the nonresonant regions, the largest difference is 2.1 degrees which is slightly larger than that for conditions A1 and A2. This implies that the effect of of a_{42} and b_{42} is slightly stronger in the resonant region and slightly weaker in the nonresonant region when the model is biased towards the wave source compared with that when the model is biased away from the wave source.

Figures 4.12 through 4.15 show the roll amplitudes for $a_{42} = b_{42} = 0$ but with distinctive values of a_{43} and b_{43}. The corresponding nominal wave height is also 4 cm. The solid lines with " * " in Figures 4.12 and 4.14 denote the roll amplitudes for $a_{43} = 0.0573$ and $b_{43} = 0.31$, the maximum values of a_{43} and b_{43} for conditions A1 and T1, shown in Table 4.1. In Figures 4.13 and 4.15, the solid line with " * " represents the roll amplitudes for $a_{43} = 0.208$ and $b_{43} = 0.861$, the maximum values of a_{43} and b_{43} for *position 2.* The dash line with "o" shows the simulated roll amplitudes for $a_{43} = b_{43} = 0$, the minimum values of a_{43} and b_{43} in Table 4.1.

The graphs for two sets of the values of a_{43} and b_{43} in Figures 4.12 through 4.15, especially those in Figures 4.12 and 4.14, are so close to each other that it is hard to find the difference between them. This means that the effect of a_{43} and b_{43} is

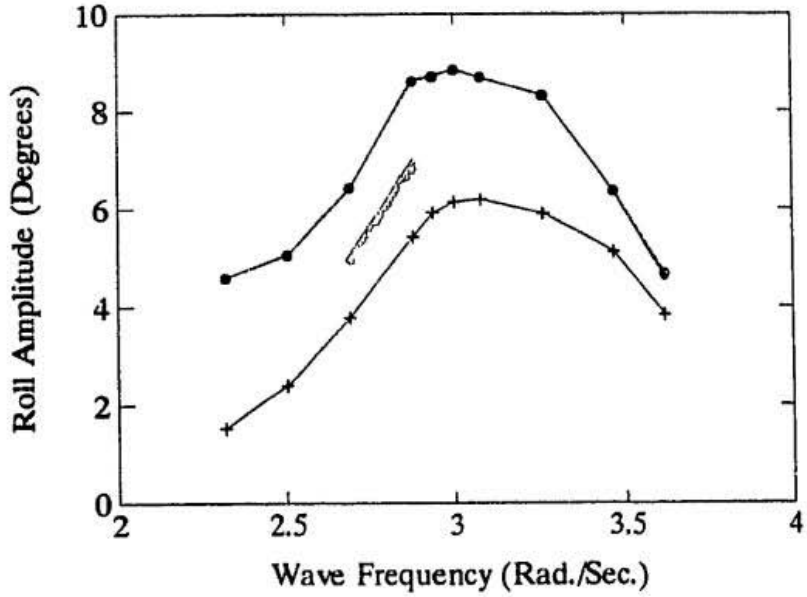

Figure 4.12: Effects of a_{43}, b_{43} and M_2, A1

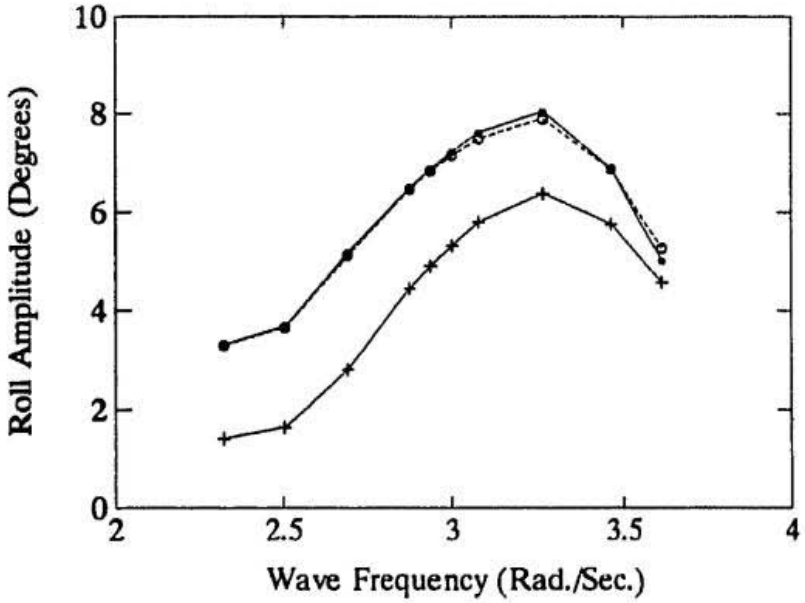

Figure 4.13: Effects of a_{43}, b_{43} and M_2, A2

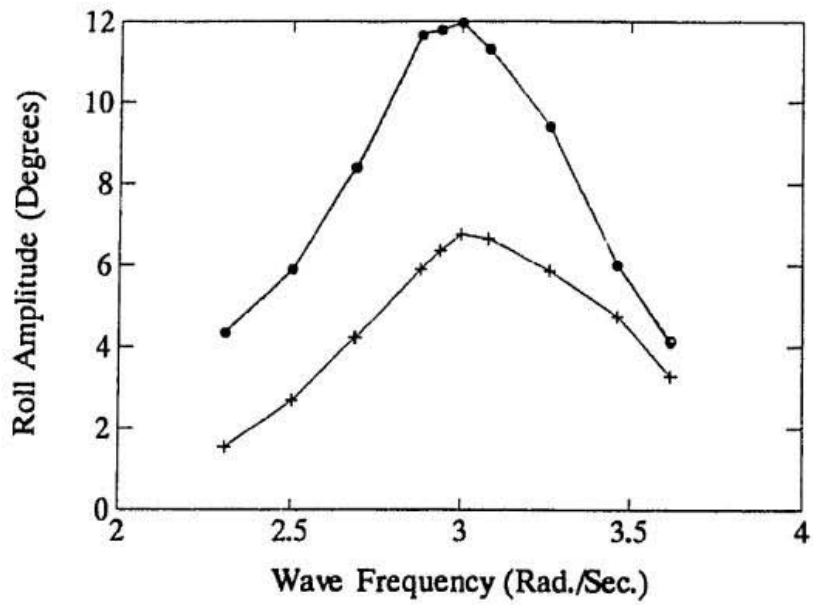

Figure 4.14: Effects of a_{43}, b_{43} and M_2, T1

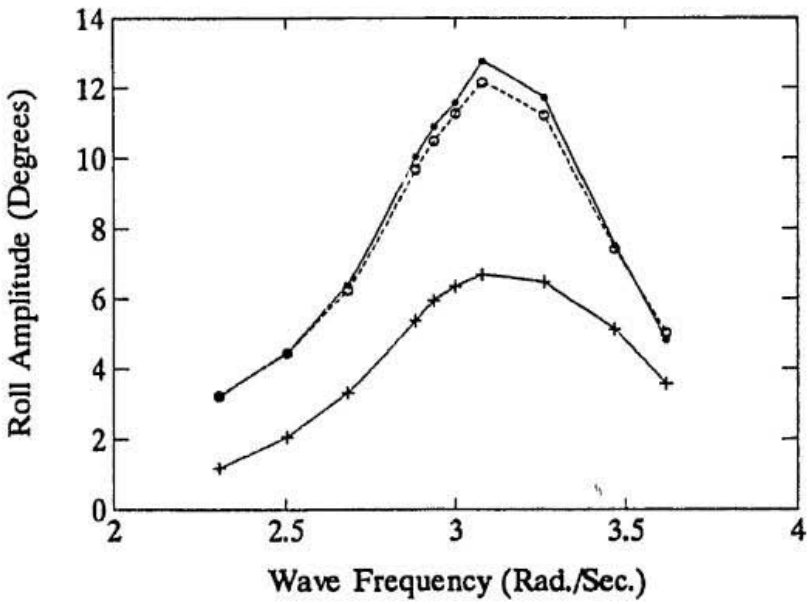

Figure 4.15: Effects of a_{43}, b_{43} and M_2, T2

approximately negligible.

So far, we can only conclude that the effect of the coupling terms, especially those related to sway, in equation (4.4) have an effect on the roll motion, but the effect is not significant enough to make the roll amplitudes for the conditions T1 and T2 almost twice those for conditions A1 and A2. The remarkable difference in roll amplitudes for different bias conditions (i.e. towards the wave source or away from the wave source) shown from both the experiments and the simulation must be mainly caused by other factors, such as restraint etc..

As was pointed out in the section 4.2, M_2 is a moment due to the relative heave and its restraint. If we assume that the roll and heave are uncoupled we can remove the heave restraint by setting $M_2 = 0$. This assumption is made only for the study of the effect of the heave restraint. It should not be used in the simulation of roll motion because heave has an effect on roll, at least on both GZ and displacement [19]. The comparison between the roll amplitudes with and without heave restraint should show the effect of the heave restraint.

Thus, a calculation based on the above consideration is done with $a_{42} = b_{42} = a_{43} = b_{43} = 0$ and $M_2 = 0$. The results denoted by solid line with " + " are shown in Figures 4.12 through 4.15. These curves indicate that the roll amplitudes without heave restraint are up to ninty six percent lower than those in the restrained condition. In other words, the heave restraint could double response amplitude. Comparing these curves, one may notice an interesting result, i.e., the magnitude of roll amplitudes for the conditions of bias towards and away from the wave source are very close, for instance, the peak amplitudes for the conditions A1, A2, T1 and T2 are 6.20, 6.39, 6.75 and 6.69 degrees respectively. The closeness of the values

of roll amplitudes for the four conditions imply that the roll amplitudes for the conditions of bias towards and away from the wave source will not be significantly different if the heave is not restrained. In the sense of the effect of bias direction (i.e., bias towards or away from the wave source), the results from the simulation are in agreement with the results from the unrestrained wave tests presented in the section 3.4. The results from the unrestrained tests indicate that the roll amplitudes for the two bias conditions have no significant difference. Thus, it may be concluded that the restraint in heave is mainly responsible for the phenomenon that the roll amplitude are much higher when the model is biased towards the wave source compared with those when the model is biased away from the wave source.

Chapter 5

Conclusions and Recommendations

This study consists of three parts : the effect of bias angle on roll damping, the influence of bias angle and restraint on rolling motion, and a simulation of the asymmetric rolling motion of a biased ship model. Details of these studies were presented in Chapter 2, 3 and 4 respectively.

From the results and the discussion shown in the last three chapters, the following conclusions can be drawn.

Roll Damping in Calm Water

1. The dependence of the nondimensional equivalent linear damping coefficient ζ_E on the bias angle varies from linear, in the cases of M365 and M366, to the quadratic, in the case of M363. This implies that the effect of bias angle on roll damping also depends on the hull form and its bias condition. Generally speaking, ζ_E for large roll amplitude increases as bias angle increases.

2. The viscous component of roll damping plays an important part, especially for large roll angles.

3. The nondimensional equivalent linear damping coefficient ζ_E increases linearly with the amplitude of roll angle.

Effect of Bias Angle on Rolling Motion in Beam Waves

(including the results from simulation)

1. When the ship model is unrestrained and free to move in all modes except for drift and yaw (which were loosely tethered) the effect of bias on the rolling motion is fairly slight.

2. When the ship model is restrained in every mode but roll, the peak value of roll amplitudes for the ship model biased towards the wave source is much larger than that for the model biased away from the wave source or in the *no bias condition.*

3. When the pivot is placed at *Position 1* the peak value of roll amplitudes are only slightly different from that for the pivot at *Position 2.* The reason for this is probably that the distance between the two centers of gravity is too small. (The definition of *Position 1* and *Position 2* was presented in the section 3.2).

4. The simulation using the roll equation only can approximately describe the asymmetric rolling motion. The general trend of the response obtained from simulation agrees well with that from experiments. However, the error is significant, especially in the nonresonant regions.

5. Heave restraint has a significant effect on magnitude of roll amplitudes.

As was stated at the beginning of this thesis, this study is far from complete and only meant to pave a way for further research on the effect of bias angle. In fact, there is a lot to do in this field. Here are some recommendations on the subsequent work which can employ some of results of the present study.

First, the effect of bias angle on roll damping needs further study. The study should include two aspects. One is the effect of bias for a ship with different hull forms under different loading conditions, i.e., different natural frequencies and GMs because the effect of bias angle is also dependent on these factors. The other is the study of coupled inertia moment and coupled roll damping of roll-sway and roll-heave for a ship in different bias conditions. These studies are expected to provide knowledge for the accurate prediction of the rolling motion of a biased ship.

Second, to develop a more sophisticated mathematical model to predict roll motion of a biased ship, researchers should pay more attention to the effect of heave on roll. The study should be done not only on the effect of sway-roll coupling on the inertia and damping moments but the restoring moment. It is noticed in this study and that in [19] that the effect of heave on restoring moment plays an important role.

In the case of study with a restrained ship model, special attention should be paid to the effect of restraint, especially the heave restraint, which is found in this study strongly to affect the values of roll amplitudes.

References

[1] Himeno, Y., *Prediction of Ship Roll Damping - State of the Art*, College of Engineering, The University of Michigan, No 239, 1981.

[2] Haddara, M. R., *Parametric Identification of Rolling Motion*, Workshop on the Stability of Low L/B Hull Forms, Institute for Marine Dynamics, St. John's, Newfoundland, Canada, Nov. 1988, pp. E1-E19.

[3] Tamiya, S., *On the Characteristics of Unsymmetrical Rolling of Ships*, Journal of the Society of Naval Architects of Japan, Vol. 118, Dec. 1965 and Vol. 120, Dec, 1966, pp. 76-95.

[4] Nayfeh, A. H. and Khdeir, A. A. *Nonlinear Rolling of Biased Ships in Regular Beam Waves*, International Shipbuilding Progress, Vol. 33, No. 381, May 1986, pp. 84-93.

[5] Spouge, J. R., *Nonlinear Analysis of Large Amplitude Rolling Experiments*, International Shipbuilding Progress, Vol. 35, No. 403, 1988, pp. 271-320.

[6] Dalzell, J. F., *A Note on the Form of Ship Roll Damping*, Journal of Ship Research, Vol. 22, No. 3, 1978, pp. 178-185.

[7] Haddara, M. R., *A Note on the Effect of Damping Moment Form on Rolling*, International Shipbuilding Progress, Vol. 31, No. 363, 1984, pp. 416-434.

[8] Roberts, J. B., *Estimation of Nonlinear Ship Roll Damping from Free Decay Data*, Journal of Ship Research, Vol. 29, No. 2, 1985, pp. 127-138.

[9] Mathiesen, J. B. and Price, W. G., *Estimation of Ship Roll Damping coefficients*, Trans. of the Royal Inst. of Naval Architecture, 1984.

[10] Bass, D. W. and Haddara, M. R., *Nonlinear Models of Ship Roll Damping*, International Shipbuilding Progress, Vol. 35 No. 401, 1988, pp. 5-24.

[11] Haddara, M. R. and Bass, D. W. *On the Form of Roll Damping Moment for Small Fishing Vessels*, Ocean Engineering, Vol. 17, No. 6, 1990, pp. 525-539.

[12] Marshfield, W. G., *A. M. T. E. (H)-N. M. I., Capsize Experiments, Series 1*, Admiralty Marine Technology Establishment (Haslar) (A. M. T. E. (H)), TM78011, 1978.

[13] Marshfield, W. G., *A. M. T. E. (H)-N. M. I., Capsize Experiments, Series 2*, A. M. T. E. (H), TR78052, 1978.

[14] Marshfield, W. G., *A. M. T. E. (H)-N. M. I., Capsize Experiments, Series 3*, A. M. T. E. (H), TM79027, 1979.

[15] Marshfield, W. G., *A. M. T. E. (H)-N. M. I., Capsize Experiments, Series 4*, A. M. T. E. (H), TR83031, 1983.

[16] Marshfield, W. G., *A. M. T. E. (H)-N. M. I., Capsize Experiments, Series 5*, A. M. T. E. (H), TR84219, 1984.

[17] Wright, J. H. G. and Marshfield, W. B., *Ship Roll Response and Capsize Behaviour in Beam Seas*, Trans. Royal Institute of Naval Architects, Vol. 122, 1980, pp. 128-149.

[18] Watanabe, Y., *On the Instability of Asymmetric Rolling at Large Angle of Inclination*, Technology in Naval, Vol. 1, No. 2, April/June, 1968, pp. 165-167.

[19] Bass, D. W., *On the Response of Biased Ships in Large Amplitude Waves*, International Shipbuilding Progress, Vol. 30 No. 341, Jan. 1983, pp. 2-9.

[20] Féat, G. and Jones, D., *Parametric Excitation and the Stability of a Ship Subjected to a Steady Heeling Moment*, International Shipbuilding Progress, Vol. 28, No. 327, 1981, pp. 263-267.

[21] Papanikolaou, A. and Zaraphonitis, G., *Computer-Aided Simulations of Large Amplitude Roll Motions of Ships in Waves and of Dynamic Stability*, International Shipbuilding Progress, Vol. 34, No 399, 1987, pp 198-206

[22] Odabasi, Yücel A. and Vince, J., *Roll Response of a Ship under the Action of a Sudden Excitation*, International Shipbuilding Progress, Vol. 29, No. 340, 1982, pp. 327-333.

[23] Flower, J. O., *The Roll Response of a Ship to a Sudden Gust of Wind*, International Shipbuilding Progress, Vol. 36, No. 407, 1989, pp. 335-349.

[24] Kobbayashi, M., *Hydrodynamic Forces and Moments Acting on Two-dimensional Asymmetrical Bodies*, International Conference on Stability of Ships and Ocean Vehicles, Glasgow, Scotland, 1975.

[25] Spouge, J. R., Ireland, N. and Collins, J. P.,*Large Amplitude Rolling Experiments Techniques*, International Conference on the Stability of Ships and Ocean Vehicles, Gdansk, Poland, 1986, pp. 95-102.

[26] Haddara, M. R. and Bennett, P., *A Study of the Angle Dependence of Roll Damping Moment*, Ocean Engineering, No. 16, 1989, pp. 411-427.

[27] Bass, D. W. and Haddara, M. R., *Roll and Sway-Roll Damping for Three Small Fishing Vessels*, International Shipbuilding Progress, Vol. 38, No. 413, 1991, pp. 51-71.

[28] Ikeda, Y., Tanaka, N. and Himeno, Y., *Effect of Hull from and Appendage on Roll Motion of Small Fishing Vessel*, Proceedings of Second International Conference on Stability of Ships and Ocean Vehicles, Tokyo, Oct, 1982, pp. 129-141.

[29] Sellars, F. *Seakeeping Characteristics of a Drifting Vessel*, Journal of Ship Research, March, 1986, pp. 26-33.

[30] Dalzell, J. F., *Model Tests of a Drifting Vessel*, Laboratory Report, SIT-DL-81-9-2204, Stevens Institute of Technology, Hoboken, N. J., June, 1981.

[31] Rogalski, W. W., *An Experimental Study of the Effect Wind-induced Drift on the Roll Response of a Hull in Beam Sea*, Thesis, Department of Naval Architecture and Marine Engineering, M. I. T., Cambridge, Mass. 1970.

[32] Roberts, J. B. and Dacunha, N. M. C., *The Distribution of Roll Amplitude for a Ship in Random Beam Waves, Comparison between theory and Experiment*, NMI Report R165, April, 1983.

[33] Zou, B., *An Experimental Study of Roll and Roll-sway Damping for Small Fishing Vessels*, Master thesis, Faculty of Engineering and Applied Science, Memorial University of Newfoundland, Canada, 1991.

[34] Peter, BloomField, *Fourier Analysis of Time Series: An Introduction*, John Wiley and Sons Inc. ISBN 0-471-082562, USA, 1976.

[35] Pawlowski, J. S., *Software for the Evalution of 2D Hydrodynamic Coefficients for Arbitrary Floating Bodies*, IMD (NRCC), 1988.